

Molecular thermodynamics of curved fluid interfaces

(Molekulare Thermodynamik gekrümmter Grenzflächen von Fluiden)

zur Erlangung des akademischen Grades eines
DOKTORS DER INGENIEURWISSENSCHAFTEN (Dr.-Ing.)
der Fakultät für Maschinenbau
der Universität Paderborn

genehmigte
DISSERTATION

von
Dipl.-Inf. Martin *Horsch*
aus Stuttgart

Tag des Kolloquiums: 10. September 2010

Referent: Prof. Dr.-Ing. Jadran *Vrabec* (Universität Paderborn)

Korreferent: Dr. rer. nat. habil. Jens *Harting* (TU Eindhoven)

Korreferent: Prof. Dr.-Ing. Hans *Hasse* (TU Kaiserslautern)

Opponent: Dr. rer. nat. Guido *Reina* (Universität Stuttgart)

Preface

The present work was composed at the Institute of Thermodynamics and Thermal Process Engineering (ITT), University of Stuttgart, and the Thermodynamics and Energy Technology Laboratory (ThEt), University of Paderborn. It is rather uncommon for such groups to grant a PhD position to a computer scientist. That this constellation remained viable is due to the confidence of Prof. Dr.-Ing. Hans *Hasse* as well as Prof. Dr.-Ing. Jadran *Vrabec*, my main supervisor. Their experience and their ideas have shaped my scientific perspective in general.

The working environment, however, depends on colleagues rather than supervisors. Dr.-Ing. Thorsten *Schnabel* served as my *Pate* in an exemplary way, communicating his perseverance in the face of apparent ups and downs. ITT nucleation research started with Jonathan *Walter's* work. His *Studienarbeit* [1] was the starting point for this project. As an auxiliary admin it was a great reassurance to work under the stewardship of Martin *Bidner*, a candid and reliable man who makes it possible to return from intricate situations to business again and again. In Paderborn I never felt out of place, thanks to the atmosphere created by the whole crew including Fiete *Dubberke*, Stefan *Eckelsbach*, «Er» or «Ich», Prof. Dr.-Ing. Dieter *Gorenflo*, Philipp *Komodromos*, Svetlana *Miroshnichenko*, Gerrit *Sonnenrein*, and Thorsten *Windmann*. Although his presence was more sporadic, Isaiah «4 litre» *Huang* surely had an impact both in Stuttgart and Paderborn. The ThEt lectures of Prof. Dr. Johann *Fischer* helped me see how the field of molecular thermodynamics emerged. I am glad to count him among my teachers.

No serious scientific publication can be accepted without a sound review process. I appreciate it very much that Dr. habil. Jens *Harting*, Prof. Dr.-Ing. Hans *Hasse*, and Prof. Dr.-Ing. Jadran *Vrabec* have accepted this task, and I thank Dr. Guido *Reina* for acting as my opponent during the thesis defense. The head of committee, Prof. Dr.-Ing. Eugeny *Kenig*, was very helpful at sorting out the formalities of my defense, and I appreciate that he has contributed corrections to the manuscript although his role did not require him to review it at all. For her important comments and suggestions I am particularly indebted to Gabriela *Guevara Carrión*.

This work cannot be ascribed to a single person by any means. Beside the people mentioned above, Dr.-Ing. Martin *Bernreuther*, Dr. Martin *Buchholz*, Dr. Calin *Dan*, Stephan *Deublein*, Dr.-Ing. Bernhard *Eckl*, Andreas *Elsner*, Sebastian *Grottel*, Martina *Heitzig*, Gerrit *Lehmann*, Zengyong *Lin*, Zheng *Liu*, Thorsten *Merker*, Azer *Nazdrajić*, Christoph *Niethammer*, Rüdiger *Pflock*, Prof. Dr.-Ing. Karlheinz *Schaber*, and Dr.-Ing. Andrea *Wix* co-authored related publications. It is impossible to detail here the contribution of the ITT students and interns David *Dylus*, Moritz *Höfert*, Vance *Hsiang*, and Nicolas *Schmidt* as well as Animesh *Agarwal*, Sahil *Madan*, Simon *Olma*, Zhongning *Wei*, Enyuan *Wu*, and Junwei *Zhang* in Paderborn. At the Imperial College I would like to thank Prof. Dr. George *Jackson* and Dr. Erich *Müller* for their hospitality and their encouragement to continue my research.

This work and this path were accessible to me from a favorable point of departure. The most sincere gratitude I therefore direct to my parents and to all those who taught me, in particular Dr. Hubert *Bisle* to whom this thesis is dedicated.

M. T. *Horsch*, Kensington (London), November 11, 2010

Dem Doktor *Bisle* gewidmet.

Per trattar del ben ch'io vi trovai, dirò de l'altre cose ch'i v'ho scorte.

Contents

List of symbols	VI
Index	VIII
Abstract	XI
1 Molecular thermodynamics	1
1.1 Ludwig <i>Boltzmann</i> and his epoch	1
1.2 Molecular modeling	8
1.3 Konrad <i>Zuse</i> and his epoch	19
1.4 Molecular simulation	28
2 Curved fluid interfaces	33
2.1 Classical nucleation theory	33
2.2 Curved interfaces in equilibrium	42
2.3 Fluid-wall contact	54
3 Direct simulation of nucleation	62
3.1 Simulation methodology	62
3.2 Carrier gas pressure effect	69
4 Conclusion	77
List of previous publications	80

List of symbols

A	<i>Helmholtz</i> energy
\mathcal{A}, \mathcal{B}	components
a, \mathbf{a}	acceleration
α, β, κ	model parameters
B	standard deviation of molecular energy
b	virial coefficient
C	condition
\mathcal{C}, \mathcal{K}	constant real numbers
Γ	interfacial excess density
c	specific heat capacity
γ	surface tension
\mathcal{D}	bond length
Δ	finite difference
d, ∂, ∇	differential operators
δ	<i>Tolman</i> length
E	empty fraction of the surface
\mathcal{E}	monomer emission rate
ε	interaction energy parameter
F	surface area
\mathbb{F}	set of molecule pairs associated with an interface
\mathcal{F}	continuous potential cutoff function
f, \mathbf{f}	force
F	specific surface energy
G	radial distribution function
\mathcal{G}	angular contribution to local structure
g	number of degrees of freedom
H	negative entropy (<i>H theorem</i>)
\mathcal{H}	Hamiltonian
h	molar enthalpy
\hbar	reduced <i>Planck</i> constant
ϑ	contact angle
i, j, k	integer numbers
J	nucleation rate, droplet formation rate
K	<i>Kolmogorov</i> complexity
\mathbb{K}	measurable space
L	channel diameter
\mathcal{L}	molecular elongation
ℓ	threshold size
λ	thermal <i>de Broglie</i> wavelength

M	polarizability
\mathcal{M}	piston mass
m	mass
μ	chemical potential
N	number of particles
\mathbb{N}	set of natural numbers
\mathcal{N}	non-isothermal factor
$\underline{\mathbf{n}}$	unit vector normal to a surface
ν	eigenfrequency of an oscillator
ξ	binary interaction coefficient
\mathcal{O}	E. <i>Landau</i> symbol
π	circumference to diameter ratio
P	partial pressure
p	pressure
$\underline{\mathbf{p}}$	momentum
ρ	density
Q	monomer acquisition enthalpy
\mathcal{Q}	order parameter
q	electric charge
R	radius
\mathbb{R}	set of real numbers
$r, \underline{\mathbf{r}}$	polar coordinate, intermolecular distance
S	supersaturation ratio
s	local structure coefficient
σ	interaction size parameter
T	temperature
\mathcal{T}	monomer transition rate
t, τ	time
U	energy
u	interaction energy, pair potential
V	volume
v	velocity
W, ω	probability
\mathcal{W}	<i>Wedekind</i> factor
Ω	transition matrix
$w, \underline{\mathbf{w}}$	dipole moment
X, Y, Z	Cartesian coordinates
x	mole fraction in the liquid phase
$\underline{\mathbf{x}}$	position
χ, ψ	angles, polar coordinates
φ, Φ	quadrupole moment
y	mole fraction in the vapor phase
v	packing fraction
\mathcal{Z}	partition function
z	<i>Zel'dovič</i> factor
ζ	reduced fluid-wall dispersive energy

Index

- Binary interaction parameter, 16
- Brownian motion, 1, 7, 21
- Buckingham potential, 11, 12

- Cluster criterion, 67
- Contact angle, VI, 54, 55, 57–59, 61
- Corresponding states, 4, 12
- Critical droplet, 37–43, 46, 48, 49, 52, 65–72, 74, 77
- Critical opalescence, 7, 26
- Critical point wetting, 59, 61
- Cutoff correction, 28

- Demon intervention, 66, 67
- Droplet formation rate, 62, 63, 65, 67, 68, 73, 74

- Embedded atom method, 16
- Energetics (natural philosophy), 1, 2, 5
- Ergodicity, 1, 21, 23, 25

- Free energy of droplet formation, 37, 39, 41, 42, 44–46, 48, 68

- Gibbs phase rule, 2
- Grand Equilibrium method, 29, 72

- Hard sphere model, 10, 32

- Kedia program, 32
- Kinetic gas theory, 1, 7
- Kolmogorov complexity, 32

- Lattice Boltzmann method, 55
- Lennard-Jones potential
 - Full, 12, 13, 15, 65
 - Truncated-shifted, 12, 13, 34–36, 49, 52, 56, 57, 59, 62, 63, 65, 67, 68, 77, 78
 - WCA potential, 13
- Ls1 project
 - Maldyn program, 28, 29, 32, 56, 65
 - Moldy program, 28, 29, 32, 65

- Massive parallelism, 20
- Materialism, 1, 2, 4, 5
- Mean first passage time (MFPT), 62, 65
- Metropolis algorithm, 25, 28–30, 32
- Monomer transition rate
 - \mathcal{E} (from liquid to vapor), 42, 78
 - \mathcal{E}_1 (from adsorbed layer to vapor), 54
 - \mathcal{T} (from vapor to liquid), 40, 42, 54
- Ms2 project, 32
- Multipole expansion, 8

- Non-isothermal factor, 40, 41, 70, 71, 77
- Nuclear armament, 19–23, 25
- Nucleation onset, 65
- Nucleation rate, 36, 38–41, 48, 62, 63, 65–68, 70, 71, 73, 74, 77
- Nucleation theorem, 46, 48
- Nucleation theory
 - Classical (CNT), 35, 37, 39–42, 49, 52, 63, 65, 66, 68–74, 77, 78
 - Laaksonen et al. (LFK), 42, 49, 52, 63, 68

- Ostwald ripening, 5

- Pairwise additivity, 11
- Perturbation theory, 10–13
- Planetary atmosphere
 - Earth, 34, 69, 72
 - Mars, 69
- Pressure effect, 37–39, 69, 71–74, 77
- Pressure tensor, 49, 52

- Radius
 - Adsorption, 43, 45, 49, 77, 78
 - Cutoff, 12, 28, 56
 - Laplace, 43, 45, 77

- Surface of tension, 43, 45, 46, 49, 52,
55, 77, 78
- Random walk, 7, 21, 63
- Reduced quantities, 12
- Science under fascism, 19–23
- Scientist
- Abrikosov*, Aleksej Alekseevič, 4
 - Allen*, Michael, 8
 - Andersen*, Hans, 13, 30
 - Arrhenius*, Svante August, 36, 40, 41
 - Banach*, Stefan, 25
 - Berendsen*, Herman Johan Christiaan,
30
 - Bernreuther*, Martin Friedrich, 32
 - Berthelot*, Daniel, 15, 16
 - Bethe*, Hans Albrecht, 19
 - Binder*, Kurt, 29
 - Blander*, Milton, 39
 - Boltzmann*, Ludwig Eduard, 1, 2, 4, 6
 - Bowles*, Richard, 27
 - Brenner*, Donald, 17
 - Brunauer*, Stephen, 54
 - Buff*, Frank, 46, 52
 - Cahn*, John Werner, 61
 - Carnahan*, Norman, 10, 11
 - Chandler*, David, 13
 - Chapman*, Sydney, 21
 - Chkonia*, Guram, 65
 - Clausius*, Rudolf Julius Emanuel, 4
 - Clerk Maxwell*, James, 4, 66
 - De Broglie*, Louis Victor, VI
 - De Coulomb*, Charles Augustin, 8
 - De Laplace*, Pierre-Simon, 77
 - Debenedetti*, Pablo Gastón, 29, 39
 - Djikaev*, Yuri, 27
 - Einstein*, Albert, 1, 7, 21, 22, 26
 - Emmett*, Paul Hugh, 54
 - Farkas*, Ladislaus, 37–42, 66, 77
 - Feder*, Jens, 40, 41, 70, 71, 77
 - Fermi*, Enrico, 25
 - Fischer*, Johann, 10, 55
 - Flood*, Håkon, 33
 - Ford*, Ian, 41
 - Frenkel*, Daan, 8, 49
 - Fuchs*, Guido, 32
 - Gallavotti*, Giovanni, 1
 - Ghiringhelli*, Luca, 17
 - Gibbs*, Josiah Willard jr., 2, 35, 43, 45,
46, 77, 78
 - Giovambattista*, Nicolás, 55, 56, 59
 - Griebel*, Michael, 8
 - Groß*, Joachim, 8, 10, 13
 - Guggenheim*, Edward Armand, 26, 35
 - Haber*, Fritz, 33
 - Hahn*, Otto, 22
 - Heisenberg*, Werner Karl, 22
 - Heitzig*, Martina, 55
 - Henderson*, Jim, 10
 - Hill*, Terrell, 35
 - Hirschfelder*, Joseph, 4
 - Iland*, Kristina, 65
 - Kashchiev*, Dimo, 48
 - Katz*, Joseph, 39
 - Kedia*, Gaurav Kumar, 32
 - Kelires*, Pantelis, 56
 - Kible*, Ralf, 73
 - Kirkwood*, John Gamble, 23, 46, 49, 52
 - Kolmogorov*, Andrej Nikolaevič, VI, 21,
32
 - Kraska*, Thomas, 62
 - Kulmala*, Markku, 41
 - Laaksonen*, Ari, 41
 - Landau*, David, 29
 - Landau*, Edmund Georg Hermann, VII
 - Landau*, Lev Davidovič, 8
 - Langmuir*, Irving, 54
 - Lee*, Jong, 42
 - Lennard-Jones*, John Edward, 12
 - Lifšic*, Evgenij Mihajlovič, 8
 - Lin*, Zengyong, 69
 - London*, Fritz Wolfgang, 11
 - Lorentz*, Hendrik Antoon, 15
 - Lotfi*, Amal, 13
 - Lovett*, Ronald, 42
 - Markov*, Andrej Andreevič, 21
 - Matsumoto*, Mitsuhiro, 62, 65, 73
 - McDonald*, James, 66, 67
 - Metropolis*, Nicholas Constantine, 25,
28–30
 - Monson*, Peter, 61
 - Napari*, Ismo, 52
 - Newton*, Isaac, 29
 - Ostwald*, Wilhelm Friedrich, 5

- Oxtoby*, David William, 48
Panagiotopoulos, Athanassios, 13
Pasta, John, 25
Planck, Max Karl Ernst Ludwig, VI
Potoff, Jeffrey, 13
Powell, Cecil Frank, 33
Preining, Othmar, 7
Römer, Frank, 62
Reguera López, David, 27, 42, 48
Reiss, Howard, 26, 27, 72
Ryckaert, Jean-Paul, 16
Sastry, Srikanth, 46
Schmelzer, Jörn, 66
Schnabel, Thorsten, 15
Smit, Berend, 8
Sokołowski, Stefan, 55
Starling, Kenneth, 10, 11
Stillinger, Frank, 65–67, 72
Stoll, Jürgen, 13, 16
Straßmann, Friedrich Wilhelm, 22
Sutherland, William, 11
Szilárd, Leó, 19, 66
Talanquer, Vicente, 68
Teletzke, Gary, 55
Teller, Ede, 19, 25, 54
Ten Wolde, Pieter Rein, 49
Thiry d'Holbach, Paul Henri, 1
Thomson, Joseph John, 1
Tildesley, Dominic, 8
Tolman, Richard Chace, VI, 23, 25, 26, 45, 46, 48, 49, 52, 57, 58, 77
Toxværd, Søren, 68
Turing, Alan Mathison, 19
Ulam, Stanisław Marcin, 25
Van Meel, Jacobus Antoon, 59
Van der Waals, Johannes Diderik jr., 5
Van der Waals, Johannes Diderik sr., 4
Vavilov, Nikolaj Ivanovič, 21
Volmer, Max, 33, 36, 38–41
Von Helmholtz, Hermann, VI
Von Helmholtz, Robert, 33
Von Neumann, János Lajos, 19, 20
Von Smoluchowski, Marian Wilhelm Teofil, 1, 7, 21, 26, 63
Von Weizsäcker, Carl Friedrich, 22
Vrabec, Jadran, 8, 10, 13, 35
Wedekind, Jan, VII, 39, 62, 65, 69–71, 74
Weeks, John, 13
Wigner, Jenő Pál, 19
Wilson, Charles Thomson Rees, 33
Yasuoka, Kenji, 62, 65, 73
Zahoransky, Richard, 65
Zel'dovič, Âkov Borisovič, VII, 77
Zuse, Konrad Ernst Otto, 19
Second law of thermodynamics, 1, 7
Supersaturation ratio, 34, 46, 48, 62, 63, 67, 68
Surface tension
 Of a droplet, 43, 46, 48, 49, 52
 Of a meniscus, 54
 Of an atomic nucleus, 22
Threshold size, 62, 63, 65–67, 74
Tolman length, 45, 46, 49, 52, 57, 58, 77, 78
Turbulent flow, 21
Umbrella sampling, 29
Vapor pressure of a droplet, 37, 46
Vapor-liquid equilibrium (VLE), 2, 13, 29, 72
Wedekind factor, VII, 70, 71, 74
Zel'dovič factor, 40, 41, 70, 71, 77

Abstract

The difference between thermophysical properties of a nanodroplet surface and a macroscopic interface, which is planar on the molecular level, can hardly be studied by experimental methods. Yet it is important for refrigeration and energy technology as well as meteorology to understand fluid interfaces with extremely high curvatures, because they characterize the initial stage of condensation and boiling processes. Curved fluid interfaces can be investigated on the nanometer length scale by molecular dynamics simulation. Thereby, droplets surrounded by a metastable vapor phase are stabilized in the canonical ensemble and sampled over an arbitrary time span. For nanodroplets of the truncated and shifted *Lennard-Jones* fluid, simulation results regarding interfacial lengths and excess quantities confirm the viability of the *Tolman* approach. The emergence of nanodroplets during nucleation is a non-equilibrium phenomenon. Both the non-steady qualities of condensation processes as well as stationary quantities relating to the nucleation in supersaturated vapors are studied here. A new method is introduced for the steady-state simulations, whereby the grand canonical ensemble is extended by demon interventions so that only nucleation in the metastable vapor is considered.

Zusammenfassung

Der Unterschied zwischen den thermophysikalischen Eigenschaften der Oberfläche eines Nanotröpfchens und einer auf molekularer Ebene planaren makroskopischen Grenzfläche ist experimentell kaum zugänglich. Dennoch ist es für die Kälte- und Energietechnik sowie die Meteorologie wichtig, extrem stark gekrümmte fluide Grenzflächen zu begreifen, da sie den Beginn von Kondensations- und Siedevorgängen charakterisieren. Die Molekulardynamik erlaubt es, gekrümmte fluide Grenzflächen auf der Nanometerskala zu untersuchen. Dabei werden von einem metastabilen Dampf umgebene Tröpfchen im kanonischen Ensemble stabilisiert und über einen beliebig langen Zeitraum ausgewertet. Simulationsergebnisse zu charakteristischen Längen und Exzessgrößen für die Oberfläche von Nanotröpfchen des stetig abgeschnittenen *Lennard-Jones*-Fluids bestätigen die Anwendbarkeit des Ansatzes von *Tolman*. Die Entstehung von Nanotröpfchen durch Nukleation ist ein Nichtgleichgewichtsphänomen. Hier werden sowohl die instationären Eigenschaften von Kondensationsprozessen als auch stationäre Größen für die Nukleation in übersättigten Dämpfen untersucht. Für die stationären Simulationen wird eine neue Methode eingeführt. Dabei wird das großkanonische Ensemble um Eingriffe eines Dämons erweitert, sodass nur die Nukleation im metastabilen Dampf berücksichtigt wird.

1 Molecular thermodynamics

1.1 Ludwig *Boltzmann* and his epoch

The molecular structure of matter



Figure 1.1: Ludwig Eduard *Boltzmann* [2].

Boltzmann is the father of molecular thermodynamics, based on the *discrete structure of matter*. He introduced many of the key notions that form the basis of physical chemistry today, among them the statistical concept of an ensemble which he called *Monode* [3]. He first formulated what is now known as the ergodic¹ hypothesis [5–7]. *Boltzmann* also developed the *H theorem* [7, 8], providing a mechanical foundation for the second law of thermodynamics under the implicit assumption of the *Stoßzahlansatz*, i.e. the separability of position and momentum coordinates. In a later article [9], he derived the *H theorem* with a different proof. However, he therein implicitly assumed the absence of long-range interactions [7]. Using the *Stoßzahlansatz*, he also obtained the *Boltzmann* equation [3, 8], which is of fundamental importance for kinetic gas theory [3, 10].

During his lifetime, *Boltzmann's* theory was opposed by a number of his colleagues, not only on the grounds of strictly thermodynamic reasoning, but also due to traditions of natural philosophy.² Around the time of his death, the molecular approach began to progress more rapidly than the competing paradigms, which included *energetics* and positivist *dynamism*.³ Within a few years it was firmly established, notably due to the impact of J. J. *Thomson's* cathode ray experiments, which proved the corpuscular nature of the electric charge, as well

¹In *Boltzmann's* own terms, it would be *isodic* rather than *ergodic*, cf. also the *Historical Note* of *Gallavotti et al.* [4].

²For instance, the encyclopedist *Thiry d'Holbach* had regarded *divisibility* as an inherent property of matter: «... de l'étendue, de la mobilité, de la divisibilité, de la solidité, de la force d'inertie. De ces propriétés générales & primitives il en découle d'autres» [11]. Against this background, *Boltzmann's* contemporaries had to be positively convinced of the superiority of a molecular paradigm.

³This development was also relevant for the philosophical discussions at that time [12, Section 5.5].

as the efforts of *Einstein* and *Smoluchowski* who had successfully applied molecular kinetics to Brownian motion.

L. E. *Boltzmann* [2, 13]:

February 20, 1844

Birth in Vienna, Austria.

1866

Dr. phil. with the dissertation *Über die mechanische Bedeutung des zweiten Hauptsatzes der mechanischen Wärmetheorie* [14] at the University of Vienna.

1869

Appointment to the new chair of Mathematical Physics at the University of Graz.

1872

Weitere Studien über das Wärmegleichgewicht unter Gasmolekülen [8].

1876 – 1890

Professorship for Experimental Physics at the University of Graz.

1877

Über die Beziehung [9].

1887

Rector of the University of Graz.

1899

Fellow of the Royal Society.

1900 – 1902

Professorship at the University of Leipzig.

September 5, 1906

Suicide in Duino near Trieste, Austria.

Phase equilibria

With great mathematical rigor, *Gibbs* conceived a theory for the phenomenological aspects of the thermodynamic ensemble, contributing to the formalization of *Boltzmann's* ideas and the field of thermodynamics as a whole [16, 17].

In his articles *on the equilibrium of heterogeneous substances* [18, 19], he put forward a general theoretical analysis of phase coexistence that covered a multitude of aspects. He derived the phase rule which states that in a system with k components and j phases coexisting in equilibrium, there are

$$g = k - j + 2, \quad (1.1)$$

thermodynamic degrees of freedom (DOF) such as composition, pressure, volume, or temperature. For instance, the vapor-liquid equilibrium (VLE), corresponding to $j = 2$, of a pure fluid ($k = 1$) has a single thermodynamic DOF ($g = 1$), which yields one-dimensional binodal lines.



Figure 1.2: Josiah Willard *Gibbs* junior [15].

The essence of the *Gibbs* approach is expressed by the notion of *axiomatic thermodynamics*. In a way similar to Euclidian geometry, it does not depend on the appearance, function, or structure of the elements it deals with. This abstractness is the reason for its independence of very basic issues with which it is objectively closely related, e.g. whether matter is continuous or atomistic. For the same reason, axiomatic thermodynamics often provides the most suitable concepts where the precise structure on the molecular level is not understood clearly. Nanoscopic fluid interfaces are an application where the theory has remained productive to the present day, and a few examples are given in this work.

J. W. *Gibbs* [2]:

February 11, 1839

Birth in New Haven, United States.

1863

Ph.D. in engineering with a dissertation *On the form of the teeth of wheels in spur gearing* [21] at Yale College.⁴

1871

Appointment to the new chair of Mathematical Physics at Yale College, where he remained until his death.

⁴*Gibbs* received the first engineering doctorate in America. His thesis was actually only published in 1947.



Figure 1.3: Johannes Diderik *van der Waals* senior [20].

1878

On the equilibrium of heterogeneous substances [18].

1897

Fellow of the Royal Society.

April 28, 1903

Death in New Haven, United States.

The equation of state

Long before molecular thermodynamics was universally accepted, *van der Waals* revealed the power inherent in its basic concepts through his general equation of state (EOS) for fluids [22]. By identifying the temperature of a liquid with its kinetic energy, he based his theory on an assumption that was still controversial at the time.⁵ The virial theorem⁶ of *Clausius* [25]

$$\frac{3}{2}pV - \frac{1}{2} \sum_{\{i,j\}} f_{ij} R_{ij} = U_{\text{kin}}, \quad (1.2)$$

could then be applied to the entire isotherm of a fluid, from a dilute gas to a dense liquid. The *van der Waals* equation [22, 23, 26]

$$\left(p + \frac{N^2 \kappa_a}{V^2} \right) (V - N\kappa_b) = NT, \quad (1.3)$$

therefore carried an immediate physical significance,⁷ since κ_a was interpreted as «the molecular pressure arising from attraction between the molecules» while $N\kappa_b$ was supposed to represent «four times the volume of the molecules» [23]. These considerations, providing a qualitatively accurate understanding of fluid phase behavior in general, were also the foundation for the theory of corresponding states [28].

Although many modern EOS are purely empirical, they all ultimately rely on molecular thermodynamics and notions introduced by *van der Waals*. His approach is still productive today, as EOS based on a sound physical reasoning are being developed and applied to an increasing number of fluid systems [29–31]. The well-known idea of a «van der Waals loop», connecting points on the spinodal line by a closed isothermal curve through the unstable regime,

⁵ *Maxwell* commented in his 1874 recension of *van der Waals*' work that for liquids «we know, as yet, nothing of the physical condition on which their temperature depends, though the researches of Boltzmann on this subject are likely to result in some valuable discoveries. M. Van der Waals seems, therefore, to be somewhat too hasty in assuming that the temperature of a substance is in every case measured by the energy of agitation of its individual molecules, though this is undoubtedly the case with substances in the gaseous state» [23].

⁶ Cf. *Hirschfelder* [24] for an in-depth discussion of relations similar in type to the *Clausius* virial theorem.

⁷ From here onwards, the convention of assigning unity value to the *Boltzmann* constant and the elementary charge is applied, i.e. the temperature 1 K is the same as an energy of the magnitude $1.3807 \cdot 10^{-23}$ J (instead of that amount of energy divided by k), and the sodium ion has a charge of +1 (instead of +1 e). Furthermore, the mole is defined to be identical with *Avogadro*'s number, i.e. $1 \text{ mol} = 6.0221 \cdot 10^{23}$. This eliminates the difference between macroscopic and molecular systems of reference, e.g. the vaporization enthalpy of water at ambient pressure is equivalently expressed by $\Delta h^v = 40.65 \text{ kJ/mol}$ or $2.448 \cdot 10^{-18} \text{ J}$ as well as 177300 K. These conventions are also employed e.g. in the textbook of *Abrikosov et al.* [27].

lacks a rigorous physical basis, since unstable states do not actually correspond to well-defined thermodynamic conditions. On the other hand, it can be successfully applied to many practically relevant systems, including vapor-liquid interfaces on the molecular level [32–34].

J. D. *van der Waals* [20]:

November 23, 1837

Birth in Leiden, Netherlands.

1873

Doctor with the dissertation *Over de continuïteit van den gas- en vloeistofoestand* [22] at the University of Leiden.

1877

Appointment to the chair of Physics (Natuurkunde)⁸ at the newly founded University of Amsterdam where he remained until 1908, succeeded by his son J. D. *van der Waals jr.*

1911 *On the value of the critical quantities* [28].

1896 – 1912

General Secretary of the Royal Netherlands Academy of Sciences.

1910

Nobel Prize in Physics.

March 8, 1923

Death in Amsterdam, Netherlands.

Phase separation



Figure 1.4: Wilhelm Friedrich *Ostwald* [35].

Ostwald ripening is the last stage of a phase transition process, where large nuclei of the emerging phase grow while the smaller ones decay due to the *Gibbs-Thomson* effect. Although the underlying thermophysical causes were understood previously, it was first independently discussed by *Ostwald* in his 1900 paper *Über die vermeintliche Isomerie* [36].

⁸Other natural sciences such as chemistry and biology are not regarded as «natuurkunde» in the Netherlands.

Over the course of several decades, *Ostwald* was also actively involved with a multitude of philosophical and political issues. For instance, he advocated progressive school reforms, radical secularism (he served as president of the anti-clerical organization *Deutscher Monistenbund*), the abolition of interest, and the development of an international auxiliary language [37–41]. *Ostwald* also argued that materialism should be replaced as the guiding philosophy of science. His own system, called *Energetik*, revolved around the conservation of energy⁹ instead of the conservation of matter which *Ostwald* presumed to be at the core of materialism [44].

Although the main shortcoming of *Ostwald*'s philosophical approach consisted in dealing with completely unrelated topics in terms of energy balances, its most relevant impact actually was that it made him an opponent of *Boltzmann*'s theoretical developments. After the success of molecular thermodynamics, which *Ostwald* eventually recognized [45], he reassigned his own scientific efforts to aesthetics and the systematization of colors [46].

W. F. *Ostwald* [13, 20]:

September 2, 1853

Birth in Riga (Pūra), Russia.

1878

Dr. chem. with the dissertation *Volumchemische und optisch-chemische Studien* [48] at the Imperial University of Dorpat (Дерпт, i.e. Tartu).

1882

Appointment to a chair of Chemistry at the Polytechnicum of Riga.

1885

Das Verdünnungsgesetz [49].

1887 – 1906

Professorship at the University of Leipzig.

1900

Über die vermeintliche Isomerie [36].

⁹*Ostwald*'s version of the categorical imperative was [41, 42]: «Vergeude keine Energie, verwerte und veredle sie!» He qualified energy with the attributes *die allgemeinste Substanz* and *das allgemeinste Akzidenz* [43].



Figure 1.5: Marian Wilhelm Teofil *Smoluchowski*, Ritter von *Smolan* [47].

1909

Nobel Prize in Chemistry.

April 3, 1932

Death in Leipzig, Germany.

Critical phenomena

By applying statistical mechanics to the density fluctuations in a homogeneous fluid, *Smoluchowski* [50] provided an explanation of critical opalescence, i.e. light scattering by fluids in the immediate vicinity of the critical point. Since in the limit of the critical point, significant density fluctuations are present on all length scales, including the wavelength of visible light, they interfere with the light, causing a *Tyndall* effect. The extent of this phenomenon was later quantified more precisely by *Einstein* [51].

Furthermore, *Smoluchowski* contributed a mathematically robust foundation for the second law of thermodynamics [52, 53] as well as Brownian motion [54–56], on the basis of the kinetic gas theory.

M. *Smoluchowski* [2, 57]:

May 28, 1872

Birth in Vorder-Brühl near Vienna, Austria.

1894

Dr. med. *sub auspiciis Imperatoris*,¹⁰ cf. *Preining* [57], with the dissertation *Akustische Untersuchungen über die Elasticität weicher Körper* [58] at the University of Vienna.

1900

Appointment as a professor of Theoretical Physics at the University of Lemberg (Львів) where *Smoluchowski* remained until 1913.

1906 – 1908

President of the Copernicus Society of Natural Scientists.

1908

Molekular-kinetische Theorie der Opaleszenz von Gasen im kritischen Zustande [50].

1914

Gültigkeitsgrenzen des zweiten Hauptsatzes der Wärmetheorie [56].

1917

Rector of the Jagiellonian University of Krakow.

September 5, 1917

Death in Krakow, Austria.

¹⁰In Austria, one dissertation per university was assigned the predicate *sub auspiciis* every year – a tradition that continues to this day, with the President replacing the Emperor. The right to award the promotion *sub auspiciis* used to rotate among the departments. This may help to explain why *Smoluchowski* received the title Dr. med. for a dissertation that was only marginally related to medicine even by 19th century standards.

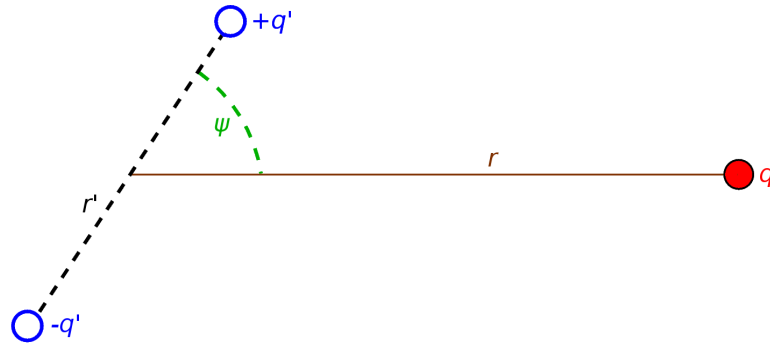


Figure 1.6: System containing a single point charge (\bullet) and a dipole composed of two opposite point charges (\circ). The angle ψ as well as the radii r and r' correspond to the system of polar coordinates used in Eqs. (1.10) and (1.11).

1.2 Molecular modeling

Intermolecular interactions operate on three length scales: short-range repulsion, short-range attraction, and long-range electrostatics which can be both attractive and repulsive.¹¹ These interactions are different manifestations of *Coulomb's law*

$$u_{qq}(r) = \mathcal{K}_C r^{-1} q_1 q_2, \quad (1.4)$$

where $\mathcal{K}_C = 167\,101 \text{ K}\text{\AA}$ is the *Coulomb constant*, q_1 and q_2 are the interacting charges, and r is the distance between the charges [63, 64]. *Coulomb's law* serves most immediately as a description of *long-range electrostatics*. Long distances, here corresponding to r above 15 \AA , permit some simplifications so that the local density of the electrons, as given by their wave functions, can usually be represented accurately enough by point charges.

Opposite charges that are situated relatively near to each other can often be treated as a single point polarity. For instance, the dipole moment

$$w = r' q', \quad (1.5)$$

is defined by the distance r' between two opposite charges $-q'$ and $+q'$. Similarly, two opposite dipoles (with a dipole moment of w) separated by a distance r'' , in the characteristic direction of the dipoles, define a quadrupole

$$\varphi = r'' w. \quad (1.6)$$

More generally, the net charge q , the dipole moment vector \underline{w} , and the quadrupole moment tensor $\underline{\Phi}$ of a body with N point charges q_i at the coordinates $\underline{x}_i = (X_{i1}/X_{i2}/X_{i3})$ are the

¹¹The reader may also want to consult, for instance, the textbooks by *Allen and Tildesley* [59], *Frenkel and Smit* [60], or *Griebel et al.* [61]. For a recapitulation of basic statistical mechanics, the reader is referred to *Landau and Lifšic* [62].

first three terms of its multipole expansion

$$q = \sum_{i=1}^N q_i, \quad (1.7)$$

$$\underline{\mathbf{w}} = \sum_{i=1}^N q_i \underline{\mathbf{x}}_i, \quad (1.8)$$

$$(\Phi)_{jk} = \begin{cases} \sum_{i=1}^N 3q_i X_{ij} X_{ik}, & \text{for } j \neq k, \\ \sum_{i=1}^N q_i (3X_{ij}^2 - \underline{\mathbf{x}}_i^2), & \text{for } j = k, \end{cases} \quad (1.9)$$

corresponding to the scalar values $w = |\underline{\mathbf{w}}|$ and $\varphi = |\Phi|$. Thereby, only the magnitude of the *highest-order non-zero multipole moment* does not depend on the choice of the coordinate axes. This is most obvious for a single point charge at the position $\underline{\mathbf{x}} = (X/Y/Z)$ with respect to the origin of the multipole expansion, which has an invariant charge q , but a coordinate system dependent dipole vector $\underline{\mathbf{w}} = q\underline{\mathbf{x}}$ and the quadrupole tensor

$$\Phi = q \begin{pmatrix} 3X^2 - \underline{\mathbf{x}}^2 & 3XY & 3XZ \\ 3XY & 3Y^2 - \underline{\mathbf{x}}^2 & 3YZ \\ 3XZ & 3YZ & 3Z^2 - \underline{\mathbf{x}}^2 \end{pmatrix}.$$

Thus, the higher-order polarities disappear only if the multipole expansion is developed around the position of the single point charge itself.¹² A system consisting of a dipole w and a relatively remote single point charge q can be expressed in a polar coordinate system such that the opposite charges are situated at $r_w^\pm = r'/2$, $\psi_w^+ = \psi$, $\psi_w^- = \psi + 180^\circ$, and $\chi_w^\pm = 0$, while the single charge has the coordinates $r_q = r$ and $\psi_q = \chi_q = 0$, cf. Fig. 1.6. The interaction energy between the single charge and the dipole is then given by

$$u_{qw}(r, r', \psi) = \frac{\mathcal{K}_C q w}{r^{1/2} (r')^{3/2}} \left(\left[\frac{r'}{4r} - \cos \psi + \frac{r}{r'} \right]^{-1/2} - \left[\frac{r'}{4r} + \cos \psi + \frac{r}{r'} \right]^{-1/2} \right), \quad (1.10)$$

which simplifies to

$$u_{qw}(r, \psi) = -\mathcal{K}_C r^{-2} q w \cos \psi, \quad (1.11)$$

in the limit $r'/r \rightarrow 0$ with a constant value of w . For the other combinations of point polarities,

¹²In the remainder of the present work, only highest-order non-zero moments will be used, i.e. polar molecules will be regarded as either dipolar or quadrupolar. There are cases where this assumption constitutes an oversimplification and several terms of the multipole expansion have to be taken into account. This regards in particular fluids that are both dipolar and significantly quadrupolar, a case which was exhaustively analyzed by *Vrabec and Gross* [65].

one analogously obtains [66]

$$u_{ww}(r, \psi_1, \psi_2, \chi) = -\mathcal{K}_C r^{-3} w_1 w_2 (2 \cos \psi_1 \cos \psi_2 - \cos \chi \sin \psi_1 \sin \psi_2), \quad (1.12)$$

$$u_{q\varphi}(r, \psi) = \frac{\mathcal{K}_C}{4} r^{-3} q \varphi (3 \cos^2 \psi - 1), \quad (1.13)$$

$$u_{w\varphi}(r, \psi_w, \psi_\varphi, \chi) = -\frac{3\mathcal{K}_C}{4} r^{-4} w \varphi (2 \cos \chi \sin \psi_w \sin \psi_\varphi \cos \psi_\varphi + [1 - 3 \cos^2 \psi_\varphi] \cos \psi_w), \quad (1.14)$$

$$u_{\varphi\varphi}(r, \psi_1, \psi_2, \chi) = \frac{3\mathcal{K}_C}{16} r^{-5} \varphi_1 \varphi_2 \left(1 - 5 [\cos^2 \psi_1 + \cos^2 \psi_2] - 15 \cos^2 \psi_1 \cos^2 \psi_2 + 2 [\cos \chi \sin \psi_1 \sin \psi_2 - 4 \cos \psi_1 \cos \psi_2]^2 \right), \quad (1.15)$$

where q , w , and φ represent point charges, dipoles, and quadrupoles, respectively, and ψ as well as χ are angles in the system of polar coordinates with the reference axis (the direction for which ψ becomes zero) given by the line connecting both point polarities. These angles describe the characteristic direction of the corresponding point multipole with respect to the reference axis: ψ is the deviation from this axis and χ is the angle between the two planes defined by the axis and one of the characteristic directions.

By applying the point polarity approximation, the computational effort for handling electrostatics is minimized while sufficient accuracy is maintained for the full arsenal of thermophysical properties that can be studied on the basis of molecular modeling [67, 68]. This is even the case if the same approximation is used for intermolecular distances below 15 Å.

The short-range *repulsive interaction* is due to the overlap between orbitals belonging to different molecules and is therefore ultimately caused by the repulsion between the electrons. At small distances between the respective atomic nuclei, the orbitals begin to overlap significantly, an unavoidable effect in all cases where *Pauli* exclusion applies.¹³ Repulsion decreases exponentially with the radius. Even on the molecular length scale, it only has a significant influence over an extremely short range of distances. Therefore, it can for many purposes be treated by the perturbation theory [69],¹⁴ based on the hard sphere model [72],¹⁵ for which the *Carnahan-Starling* [74, 75] EOS

$$\frac{p}{\rho T} = \frac{1 + v + v^2 - v^3}{(1 - v)^3}, \quad (1.16)$$

is empirically known to hold in terms of the packing fraction $v = \pi \sigma_h^3 \rho / 6$, i.e. the fraction of the volume occupied by the hard spheres, where ρ is the fluid density and σ_h is the hard

¹³For orbitals containing a single electron or in case of bosonic systems, the small distance does not necessarily lead to an overlap between orbitals.

¹⁴The relevance of the perturbation theory for modern thermodynamics is discussed by *Fischer* in *Ausgewählte Kapitel der Molekularen Thermodynamik* [70]. For its application to curved fluid interfaces, the reader is referred to *Henderson* and *Schofield* [71].

¹⁵The viability of the hard sphere model for real fluids was asserted by *Sutherland* who commented in 1893 that «with the natural gases the variation of viscosity with temperature is more rapid than was asserted by theory; ... molecular force causes the spheres to behave as regards collisions as if they were larger spheres devoid of force ... Hence, in the theory of viscosity as worked out for forceless molecules, we need only increase the square of the molecular sphere-diameter» [73].

sphere diameter. Equivalently, the *Carnahan-Starling* EOS can be denoted as a Leiden form virial expansion

$$\frac{p}{T} = \sum_{k \in \mathbb{N}} b_k \rho^k, \quad (1.17)$$

where the k -th virial coefficient is given by

$$b_k = (\pi \sigma_h^3 / 6)^{k-1} (k^2 + k - 2), \quad (1.18)$$

except for the first virial coefficient which is of course 1. Two of the peculiarities of this EOS, namely the temperature independence of the virial coefficients and the divergence of p for $v \rightarrow 1$, are due to characteristics of the hard-sphere model. In fact, any exponential decay of b_k in terms of k leads to an unphysical divergence of pressure and energy at a finite density. Nonetheless, these issues are hardly relevant in the present context, since a realistic temperature dependence can be introduced by perturbation terms and the densities for which the *Carnahan-Starling* EOS predicts an infinite pressure do not correspond to fluid phases.

The short-range *dispersive interaction* is due to the *London* force [76], i.e. the derivative of

$$u(r) = \frac{3\pi \hbar M_i M_j}{(\nu_i^{-1} + \nu_j^{-1}) r^6} + \mathcal{O}(r^{-7}), \quad (1.19)$$

wherein \hbar is the reduced *Planck* constant. Here, M and ν represent the polarizabilities as well as the eigenfrequencies, respectively, of the effective oscillators corresponding to the electrons of the molecules i and j that contribute to the dispersion. Although temporary (dispersive) and permanent (electrostatic) polarities cannot be completely separated in theory, molecular modeling usually relies on that approximation. Accordingly, the static charge distribution is described by point charges or point polarities, while effective pair potentials are used for the repulsive and *London* forces. These two contributions to the potential energy are then treated independently, and the influence of permanent polarities on the dispersive interaction is tacitly considered by adjusting the parameters of the pair potential so that experimentally available fluid properties can be reproduced by simulation. Generally, this approach also permits the assumption of *pairwise additivity*

$$U = \sum_i U_{\text{kin}}(i) + \sum_{\{i,j\}} u(i,j), \quad (1.20)$$

which is exact for *Coulomb*'s law and the kinetic part, a good approximation for the dispersive interaction,¹⁶ and inherently valid for repulsion with the exception of extremely high densities, since simultaneous repulsions between more than two molecules are relatively rare.

The exponential decay of the repulsion and the r^{-6} scaling of *London* dispersion are accounted for by the *Buckingham* [78] potential, given by

$$\frac{u(r)}{\varepsilon_B} = \frac{\beta_B^6}{(6/\alpha_B - 1) r^6} + \frac{\exp(\alpha_B [1 - r/\beta_B])}{\alpha_B/6 - 1}, \quad (1.21)$$

¹⁶ «the formula ... has the peculiarity of additivity; this means that if three molecules act simultaneously upon each other, the three interaction potentials between the three pairs ... are simply to be added, and that any influence of a third molecule upon the interaction between the first two is only a small perturbation effect» [77].

an effective pair potential with three parameters: α_B is a dimensionless value that determines the decay of the repulsive interaction, and ε_B as well as β_B are the magnitude of the potential energy minimum and the distance where the minimum is located, respectively. Additionally, the *Buckingham* potential is shielded at small distances by a hard core.

In Eq. (1.21), which accounts for both repulsive and attractive short-range effects, the energy only occurs as a multiple of ε_B while the distance is always divided by β_B . While the acceleration \underline{a} of a particle due to the interaction depends on its mass m , the force \underline{f} experienced by it is immediately given by the gradient of the potential energy. Evidently, if the acceleration multiplied with the molecular mass is considered, m cancels out and only \underline{f} remains. Since the potential energy is given as a multiple of ε_B and the derivative is taken with respect to the Cartesian coordinates that appear as multiples of β_B in Eq. (1.21), all model parameters cancel out, analogously, if \underline{a} is *reduced* (i.e. divided) by the reference acceleration

$$a_{\text{ref}} = \frac{\varepsilon_B}{\beta_B m}. \quad (1.22)$$

This reasoning permits the general introduction of reduced quantities, expressed in a system of units based on the parameters β_B , ε_B , m , and \mathcal{K}_C if electrostatic long-range interactions are present.

Such a reduction clarifies the extent of generality for a molecular modeling approach: In case of the *Buckingham* potential, only α_B remains truly variable in the sense that it has a non-linear influence, e.g. on the shape of the vapor-liquid binodal. The size and energy parameters (and also the molecular mass), however, are qualitatively eliminated, because their contribution is limited to quantitative scaling. For instance, all binodals that can be obtained by changing β_B only are geometrically similar. In this way, the approach of corresponding states manifests itself for molecular modeling. Just as for an EOS, the scaling parameters can be related to the critical point of the fluid, as long as the remaining, qualitatively relevant parameters are fixed.

The *Lennard-Jones-12-6* (LJ) potential [79] approximates the repulsion by a polynomial term.¹⁷ With a size parameter σ and an energy parameter ε , it is given by

$$u_{\text{LJ}}(r) = 4\varepsilon \left[\left(\frac{\sigma}{r} \right)^{12} - \left(\frac{\sigma}{r} \right)^6 \right]. \quad (1.23)$$

In comparison with the *Buckingham* potential, this expression is computationally easier to handle and it requires only two instead of three parameters. More importantly, these two parameters only influence quantitative scaling and can be fully eliminated as described above. Thus, one can speak of *the LJ fluid* as a single well-defined fluid model. Several widespread variants of this model are defined by truncating and shifting (TS) the LJ potential at the cutoff radius r_c , yielding the LJ-TS potential [59]

$$w_{\text{TS}}(r) = \begin{cases} u_{\text{LJ}}(r) - u_{\text{LJ}}(r_c) & \text{for } r < r_c, \\ 0 & \text{for } r \geq r_c. \end{cases} \quad (1.24)$$

Most typically, the LJ-TS potential is used with $r_c = 2.5 \sigma$ [80–86], which will be referred to as *the LJ-TS fluid* throughout the present work. However, a cutoff radius of $r_c = 2^{7/6} \sigma$ is also in use [87, 88]. With a cutoff at the potential energy minimum $r_c = 2^{1/6} \sigma$, corresponding to

¹⁷The inventor of the LJ potential, Sir J. E. *Lennard-Jones*, was still known under the name of *Jones* at the time of its publication in 1924.

Weeks-Chandler-Andersen (WCA) perturbation theory [89], one speaks of *the WCA potential* [90–93].

In Figs. 1.7 and 1.8, the LJ and LJ-TS potentials are compared with the more complicated HFD-B type¹⁸ Aziz-Chen potential [94]

$$u(r) = \alpha'_A \exp\left(\frac{-r}{\sigma_A} \left[\frac{r\beta_A}{\sigma_A} + \alpha_A\right]\right) - \left(\frac{\kappa_6\sigma_A^6}{r^6} + \frac{\kappa_8\sigma_A^8}{r^8} + \frac{\kappa_{10}\sigma_A^{10}}{r^{10}}\right) \exp\left(-\left[\frac{\beta'_A\sigma_A}{r} - 1\right]^2\right), \quad (1.25)$$

using the respective parameters corresponding to xenon [85, 95, 96].

Oddly enough, the full LJ potential overestimates the critical values of temperature and pressure for real fluids, whereas the LJ-TS model underpredicts both T_c and p_c .¹⁹ Table 1.1 shows the critical properties of argon, krypton, xenon, and methane, expressed in reduced units with respect to the corresponding LJ and LJ-TS parameters that were optimized to the overall reproduction of VLE data. While the LJ fluid is expected to have $T_c = (1.284 \pm 0.007) \varepsilon$ and $p_c = (0.115 \pm 0.003) \varepsilon\sigma^{-3}$ based on the values from Tab. 1.1, the actual critical properties were determined in 1992 by Lotfi *et al.* [97] as $T_c = 1.310 \varepsilon$ and $p_c = 0.126 \varepsilon\sigma^{-3}$, putting an end to a series of widely deviating predictions by various authors.²⁰ Conversely, the critical properties of noble gases and methane in reduced units are $T_c = (1.091 \pm 0.002) \varepsilon$ and $p_c = (0.0987 \pm 0.0007) \varepsilon\sigma^{-3}$ using the corresponding LJ-TS parameter values [85], whereas according to the same source, the LJ-TS fluid itself has $T_c = 1.0779 \varepsilon$ and $p_c = 0.0935 \varepsilon\sigma^{-3}$.

The rigid symmetric two-center LJ (2CLJQ) model consists of a point quadrupole φ in the center of mass and two LJ sites (with the same potential parameters σ and ε) equidistant from the center of mass, occupying opposite positions, separated by the elongation \mathcal{L} . In Tab. 1.1 it can be seen that, as expected, a higher reduced value of the quadrupole moment increases the reduced critical temperature. Surprisingly, the molecular elongation has even more influence: The molecular models for ethane, propene, perfluoroethane, and sulfur hexafluoride all have similar (reduced) elongations, while the polarity varies between a very weak and a very strong quadrupole moment. For T_c/ε , however, this only corresponds to a twenty percent variation. The same can be said as regards the comparison between oxygen, nitrogen, and ethene (the variation in T_c/ε is even smaller here). If the critical temperature of ethane, which is significantly anisotropic but only slightly quadrupolar, is contrasted with the LJ case²¹ of $\mathcal{L} = 0$, one obtains a deviation of about 58 %. By extrapolating the set of 2CLJQ values shown in Tab. 1.1 to the limit $\varphi \rightarrow 0$, it becomes clear that this deviation is almost entirely due to the molecular elongation. The overall dependence is discussed by Stoll *et al.* [99].

¹⁸In the relevant publication [94], three pair potentials are introduced and referred to as HFD-A, B, and C. Considering its context, the abbreviation HFD may e.g. stand for *Hartree-Fock* dispersion, although the authors do not clarify this.

¹⁹By implication, a LJ cutoff radius larger than 2.5σ must exist such that the truncated-shifted potential optimally reproduces the critical behavior of methane and the noble gases.

²⁰More recent studies, e.g. by Potoff and Panagiotopoulos [98] who obtained $T_c = (1.3120 \pm 0.0007) \varepsilon$ and $p_c = (0.1279 \pm 0.0006) \varepsilon\sigma^{-3}$, confirm the results of Lotfi *et al.* [97].

²¹Note that, although the critical temperature appears to be much higher for the 2CLJQ models than for the LJ fluid, with $\mathcal{L} \rightarrow 0$ the 2CLJQ model becomes a single LJ site with an energy parameter of 4ε , instead of ε , due to the $2 \cdot 2$ formal LJ interactions between a pair of 2CLJQ molecules. Since the critical temperatures are reduced by the respective energy parameters here, a factor four has to be applied in order to compare the values correctly.

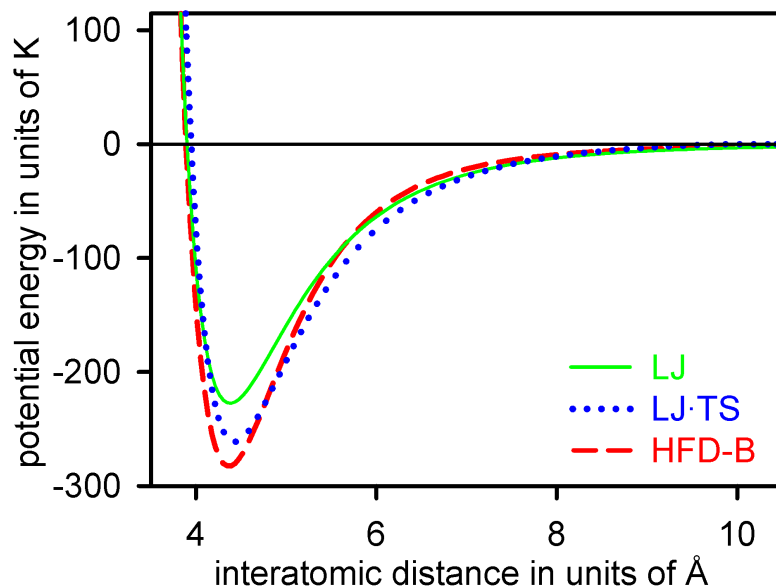


Figure 1.7: Potential energy from the pairwise interaction between xenon atoms according to (solid line) the LJ potential [96], (dotted line) the LJ-TS potential [85], and (dashed line) the HFD-B type *Aziz-Chen* potential [95], with the potential parameters corresponding to xenon.

The analogous 2CLJD approach, where the point quadrupole is replaced by a point dipole, can also be successfully applied for many dipolar molecules [100–102]. In that case, the relation between VLE data and the four potential parameters σ , ε , \mathcal{L} , and w is described by the *Gross-Vrabec* EOS [103].

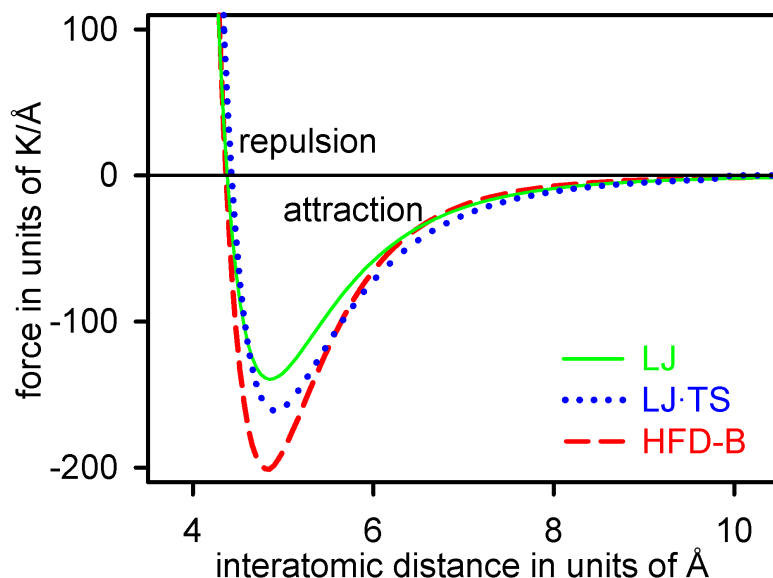


Figure 1.8: Net force from the pairwise interaction between xenon atoms according to (solid line) the LJ potential [96], (dotted line) the LJ-TS potential [85], and (dashed line) the HFD-B type *Aziz-Chen* potential [95], with the potential parameters corresponding to xenon. Positive values of the force correspond to repulsion between two atoms.

Table 1.1: LJ model parameters (top) for noble gases as well as methane [96], LJ-TS model parameters (center) for noble gases as well as methane [85], and 2CLJQ model parameters (bottom) for quadrupolar fluids [96]. The LJ size parameter σ is given in units of Å while ε is given in units of K, and further values such as the reduced molecular elongation $\mathcal{L}^* = \mathcal{L}/\sigma$, the reduced quadrupole moment $\varphi^* = \varphi/\mathcal{K}_C^{-1/2}\varepsilon^{1/2}\sigma^{5/2}$ are expressed in LJ units. Critical point properties of the respective fluids according to experimental results [104–115] are also indicated using the LJ system of units, i.e. $T_c^* = T_c/\varepsilon$ for temperature and $p_c^* = p_c/\varepsilon\sigma^{-3}$ for pressure.

Fluid	$\sigma/\text{Å}$	ε/K	\mathcal{L}^*	φ^*	T_c^*	p_c^*	
Ar	3.3952	116.79			1.290	0.1179	[105]
Kr	3.6274	162.58			1.288	0.1174	[107]
Xe	3.9011	227.55			1.273	0.1104	[108]
CH ₄	3.7281	148.55			1.283	0.1162	[114]
Ar	3.3916	137.90			1.092	0.0995	[105]
Kr	3.6233	191.52			1.094	0.0993	[107]
Xe	3.9450	265.78			1.090	0.0978	[108]
CH ₄	3.7241	175.06			1.089	0.0983	[114]
C ₂ H ₄	3.7607	76.950	0.33757	1.5320	3.669	0.2523	[112]
N ₂	3.3211	34.897	0.31508	1.0319	3.616	0.2583	[113]
O ₂	3.1062	43.183	0.31225	0.6155	3.580	0.2535	[110]
SF ₆	3.9165	118.98	0.66578	2.0000	2.679	0.1423	[106]
C ₂ F ₆	4.1282	110.19	0.66000	1.9989	2.659	0.1406	[111]
C ₃ H ₆	3.8169	150.78	0.65535	1.4461	2.420	0.1234	[104]
CO ₂	2.9847	133.22	0.81000	1.8176	2.283	0.1067	[115]
C ₂ H ₆	3.4896	138.99	0.68094	0.2646	2.229	0.1097	[109]

It is straightforward to generalize the part of a molecular model that covers long-range electrostatics to mixtures. There is no reason to assume that the simplifications which are usually made, such as point charges and point polarities, should be less valid for the unlike interaction between molecules that belong to different components than between molecules of the same species. Therefore, the *Coulomb* equation can be applied to the unlike interaction between point polarities as well, and no further modification is required.

The case is more complicated for the *London* force and the short-range repulsive interaction. In principle, the same considerations apply for mixtures as well as for pure fluids, but when the LJ potential is used as an approximation, it is not straightforward to extend it to the interactions of unlike species with the same accuracy. In practice, a number of heuristic combination rules are used, some of which even claim to have a physical foundation.²² The length scale for the unlike interaction can be quite reliably estimated from the *Lorentz* combination rule [117]

$$\sigma_{AB} = \frac{1}{2}(\sigma_A + \sigma_B), \quad (1.26)$$

which is particularly accurate for the repulsive part. *Berthelot* [118] proposed the rule

$$\varepsilon_{AB} = (\varepsilon_A \varepsilon_B)^{1/2}, \quad (1.27)$$

²²Instead of discussing a variety of structurally similar rules here, the reader is referred to *Schnabel et al.* [116].

Table 1.2: Binary interaction parameters for the modified *Berthelot* rule, cf. Eq. (1.28), adjusted to VLE data using LJ and 2CLJQ models [119–121]. No experimental results are available for binary VLE of methane, ethane or propene with oxygen while for the system CO₂ + Kr, the temperature range permitting vapor-liquid coexistence for the pure fluids do not overlap, i.e. T_c is 209.46 K for krypton [107], while T_3 is 216.58 K for carbon dioxide [122, 123]. Therefore, the corresponding ξ values could not be fitted using the *Stoll* approach [124].

Fluid	$\xi(\text{Ar})$	$\xi(\text{Kr})$	$\xi(\text{CH}_4)$	$\xi(\text{N}_2)$	$\xi(\text{O}_2)$	$\xi(\text{CO}_2)$	$\xi(\text{C}_2\text{H}_6)$
Kr	0.989						
CH ₄	0.964	0.998					
N ₂	1.010	0.989	0.958				
O ₂	0.988	1.050	—	1.007			
CO ₂	0.999	—	0.962	1.041	0.979		
C ₂ H ₆	0.978	1.023	0.997	0.974	—	0.954	
C ₃ H ₆	1.019	1.001	1.032	0.959	—	0.915	1.015

for the characteristic energy of unlike interactions. Due to the empirical nature of the LJ potential and the corresponding pure fluid parameters themselves, however, the theoretical soundness of such rules is inherently limited.

The best proof that can be given for a combination rule therefore is that it covers experimental data and adequately extends the empirical approach of molecular modeling from pure fluids to mixtures. In this sense, the *Lorentz* rule can be used together with the modified *Berthelot* combination rule [121]

$$\varepsilon_{AB} = \xi (\varepsilon_A \varepsilon_B)^{1/2}, \quad (1.28)$$

where the binary interaction parameter ξ is usually between 0.9 and 1.05, cf. Tab. 1.2. For predictive calculations, e.g. when no experimental data are available for a mixture, it is common to apply Eqs. (1.26) and (1.27) without any modification [125], which is called the *Lorentz-Berthelot* rule.

In a recent systematic study [121], covering 267 binary mixtures, 30 of the corresponding ξ values were determined to be smaller than 0.9 while six were greater than 1.05. Although this is not, at first sight, a negligible fraction, all significantly deviating values can be explained by inadequacies of the employed modeling approach. The most significant outliers correspond to mixtures where one of the simulated components is the LJ model of neon (e.g. $\xi = 0.733$ with Kr and 1.124 with CO₂), the 2CLJQ model of carbon dioxide ($\xi = 1.080$ with CO and 1.124 with Ne) as well as models for the halogenated methane refrigerants *R23*, *R30*, *R32*, and *R41* (where ξ is relatively low in several cases, e.g. $\xi = 0.775$ for CH₃F + C₂F₆ as well as $\xi = 0.790$ for CH₂F₂ + SF₆), i.e. only six out of the 78 fluid models that were considered [121]. These six models can be argued to be insufficient representations of the actual molecular structure.²³

²³Halogenated methane, for instance, is inconsistently represented by single-center (*R30*, *R30B2*, and *R32*) and two-center dipolar LJ models (all other species), without any plausible justification. The LJ model of neon is also known to perform poorly for pure fluid VLE properties [121] as well as *Henry's* law constants [126]. Carbon dioxide, finally, is better represented by a 3CLJQ model [127] than by the 2CLJQ model from Tab. 1.1, and the ξ values for mixtures containing CO₂ could well be in the typical range if that model was used instead.

Table 1.3: Parameters of the *Tersoff* potential for nitrogen [128], carbon [129], including the present optimization of this parameter set for graphite, silicon [130], and germanium [130].

	N	C (<i>Tersoff</i>)	C (graphite)	Si	Ge
α_A [\AA^{-1}]	2.7	2.2119	2.2750	1.7322	1.7047
α_R [\AA^{-1}]	5.4367	3.4879	3.5871	2.4799	2.4451
α_ψ	1.3304	0.7275	0.7275	0.7873	0.7563
β_ψ	$5.2938 \cdot 10^{-3}$	$1.5724 \cdot 10^{-7}$	$1.5724 \cdot 10^{-7}$	$1.1 \cdot 10^{-6}$	$9.0166 \cdot 10^{-7}$
ε_A [K]	$5.9387 \cdot 10^6$	$4.0233 \cdot 10^6$	$4.0233 \cdot 10^6$	$5.4678 \cdot 10^6$	$4.8650 \cdot 10^6$
ε_R [K]	$7.3899 \cdot 10^7$	$1.6172 \cdot 10^7$	$1.6172 \cdot 10^7$	$1.6024 \cdot 10^7$	$2.0528 \cdot 10^7$
κ_T	$4.1258 \cdot 10^8$	$1.4477 \cdot 10^9$	$1.4477 \cdot 10^9$	$1.0078 \cdot 10^{10}$	$1.1327 \cdot 10^{10}$
κ'_T	$6.5078 \cdot 10^2$	$1.9219 \cdot 10^1$	$1.9219 \cdot 10^1$	$2.63 \cdot 10^2$	$2.45 \cdot 10^2$
r_0 [\AA]	2.1	2.1	2.35	3.0	3.1
r_1 [\AA]	1.8	1.8	2.0	2.7	2.8
χ_T	124° 13'	124° 47'	124° 47'	126° 45'	116° 2'

For macromolecules as well as molecules with a flexible structure, e.g. hydrocarbons which can rotate around single carbon-carbon bonds, internal DOF have to be considered. The present study, however, only considers simple molecular fluids where the internal vibrational and rotational modi can either be neglected altogether or taken into account implicitly, i.e. by effective potential parameters for dispersion and repulsion.²⁴

In order to accurately describe properties of a solid material, it is usually necessary to employ multi-body potentials which have a large number of model parameters and are computationally relatively expensive. For metals, a reliable approximation of actual material properties can be obtained by applying the embedded atom method where the *Coulomb* interaction between the atomic nuclei is combined with a functional of the local electron density [132]. The latter depends on the local structure on the atomic level and thereby causes multi-body effects.

For carbon, semiconductors, and ceramics, multi-body effects arise as well. However, these cannot simply be explained in terms of a local electron density, since electrons are not delocalized in such materials. Instead, interatomic bonds have to be considered explicitly. Under certain conditions, these bonds can simply be represented by harmonic oscillators (cf. Section 2.3), i.e. without multi-body terms. In a more general setting, e.g. for amorphous structures or configurations involving the coexistence of different solid phases such as graphite and diamond [133], the influence of bond angles has to be taken into account as well, since at unfavourable geometries, no molecular orbital can be formed and thus no attraction between the atoms is present. A suitable model for such systems therefore needs to evaluate all the angles formed by triples of neighboring atoms.

The *Tersoff* potential

$$U_{\text{pot}} = \frac{1}{2} \sum_{i \neq j} \mathcal{F}(r_{ij}) u_T^{i,j}, \quad (1.29)$$

²⁴The reader is referred to *Ryckaert et al.* [131] for a discussion of modeling and simulation of fluid systems with significant internal DOF.

with [130]

$$\mathcal{F}(r) = \begin{cases} 0, & \text{for } r \geq r_0, \\ \frac{1}{2} \left(1 + \cos \left[\frac{\pi(r-r_1)}{r_0-r_1} \right] \right), & \text{for } r_1 < r < r_0, \\ 1, & \text{for } r \leq r_1, \end{cases}$$

$$u_{\text{T}}^{\iota,j} = [\varepsilon_{\text{R}} \exp(-\alpha_{\text{R}} r_{\iota j}) - s_{\iota j} \cdot \varepsilon_{\text{A}} \exp(-\alpha_{\text{A}} r_{\iota j})], \quad (1.30)$$

wherein ι and j are atoms, considers these effects and can be applied to all hybridization states of carbon, but also to germanium [129] as well as silicon [130] and ceramics [128, 134], cf. Tab. 1.3.²⁵ The multi-body effects are covered by a local structure coefficient

$$s_{\iota j} = \left(1 + \left[\beta_{\psi} \sum_{k \notin \{\iota, j\}} \mathcal{F}(r_{\iota k}) \mathcal{G}(\iota-j, \iota-k) \right]^{\alpha_{\psi}} \right)^{-1/2\alpha_{\psi}}, \quad (1.31)$$

specified in terms of angular contributions corresponding to bond pairs $(\iota-j, \iota-k)$ with

$$\mathcal{G}(\iota-j, \iota-k) = 1 + \frac{\kappa_{\text{T}}}{\kappa'_{\text{T}}} - \frac{\kappa_{\text{T}}}{[\cos \psi(\iota-j, \iota-k) - \cos \chi_{\text{T}}]^2 + \kappa'_{\text{T}}}, \quad (1.32)$$

taking into account all neighbors k of ι and the respective angles $\psi(\iota-j, \iota-k)$ formed with the bond between ι and j .

However, the *Tersoff* potential deviates by about 3% from the actual bond length in graphite [137], i.e. $\mathcal{D} = 1.421 \text{ \AA}$ [138], a result that is confirmed by present molecular simulations,²⁶ cf. Tab. 1.4. For the purpose of simulating graphite, a different parameter set is proposed here, cf. Tab. 1.3. In Fig. 1.9, the new parameter set is compared with the standard potential, regarding the radial distribution function (RDF)

$$G(R) = \frac{1}{4\pi(R\rho)^2} \frac{d}{dR} \left| \{(\iota, j) \mid r_{\iota j} \leq R\} \right|, \quad (1.33)$$

within a single graphene layer. It should be noted that due to its small cutoff radius, the *Tersoff* potential does not reproduce any interlayer interaction in graphite.²⁷

Table 1.4: Potential energy contribution (per atom) of the original *Tersoff* model for carbon [129], for a graphite structure in dependence of the bond length \mathcal{D} in the initial configuration. Large values of \mathcal{D} lead to a permanent tension within the solid, whereas rippling of the layers is caused by small values [140].

\mathcal{D} [Å]	1.4574	1.4595	1.4605	1.4616	1.4626	1.4648
U_{pot}/N [K]	-84,796.2	-84,802.8	-84,808.2	-84,806.9	-84,805.7	-84,803.5

²⁵More elaborate potentials (requiring a slightly larger computational effort) were proposed by *Brenner* [135] as well as *Ghiringhelli et al.* [136].

²⁶The energy values shown in Tab. 1.4 are huge in relation to typical pair potentials, e.g. as shown in Fig. 1.7. The large values assigned to the energy parameters ε_{A} and ε_{R} of the *Tersoff* potential, cf. Tab. 1.3, reflect the fact that the forces acting on atomic nuclei in a solid material are of a different order of magnitude than the intermolecular interactions present in fluid systems.

²⁷However, effective LJ parameters are available as a model for the interlayer dispersion in graphite [139].

1.3 Konrad Zuse and his epoch

The general purpose electronic computing machine

World War II brought not only the greatest extent of destruction ever witnessed, but also a corresponding development in military technology, required as a means of maximizing the destructive capacities commonly known as *defense*. While *Turing* developed various special purpose computers for breaking the German military encryption, the United States accomplished a revolution in both nuclear technology and computing at Los Alamos. There, it was particularly *von Neumann* who contributed to the design of the ENIAC general purpose computer, presented to the public in 1946.

German research efforts were less successful with respect to the atomic bomb,²⁸ the first

²⁸ Many of the eminent contributors to the nuclear research of the Manhattan project had previously studied and worked in Germany [142–144]. Most notably, *Bethe* had been scientifically active in Frankfurt, München, Stuttgart, and Tübingen [145], 1924–1933, *Szilárd* in Berlin [146], 1920–1933, *Teller* in Karlsruhe, München, Leipzig, and Göttingen [147], 1926–1934, *von Neumann* in Berlin [148, 149], 1926–1930, and *Wigner* in

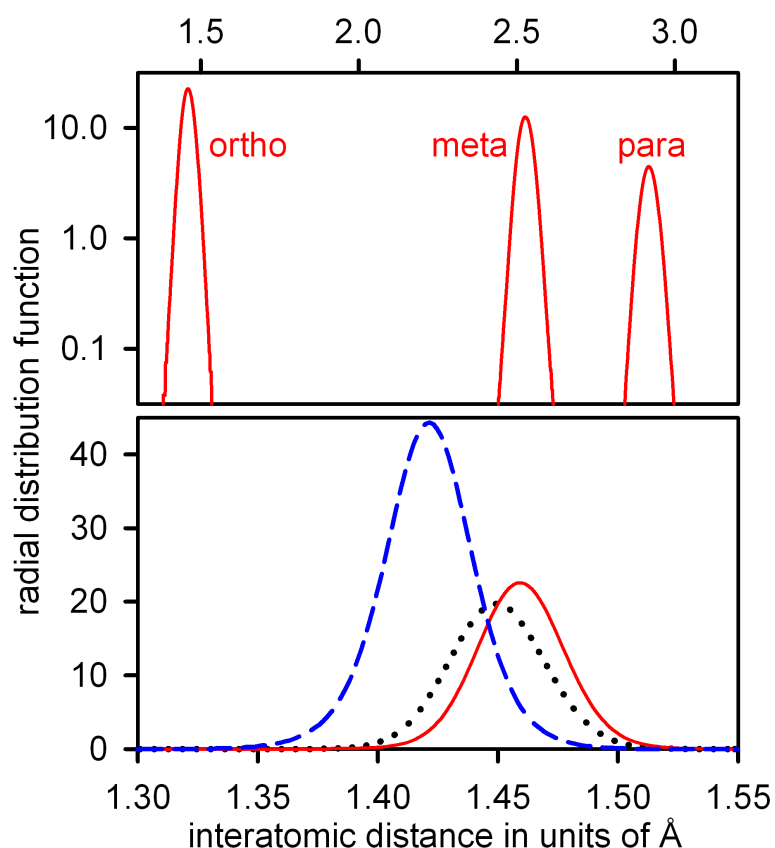


Figure 1.9: Top: RDF for the *Tersoff* model [129, 130] from molecular simulation using an initial configuration corresponding to planar graphite layers with a bond length of $\mathcal{D} = 1.455 \text{ \AA}$, indicating the distance between neighbors in *ortho*, *meta*, and *para* position; bottom: comparison between the *ortho* peak of the carbon-carbon RDF for the *Tersoff* potential with an initial interatomic distance of $\mathcal{D} = 1.413$ (dotted line) and 1.455 \AA (solid line) as well as the rescaled *Tersoff* potential (dashed line), cf. Tab. 1.3, using the actual bond length in graphite ($\mathcal{D} = 1.421 \text{ \AA}$).



Figure 1.10: Konrad Ernst Otto Zuse [141].

Turing complete electronic computer, however, was Zuse's Z3, operative in Berlin from 1941 to 1943. Its inventor regarded computers as having the intelligence of *humans with super-dimensional brains*²⁹ and while he did perceive their potential application for scientific computing, Zuse's ambition went far beyond this. Anticipating the spread of electronic data processing, he developed the first higher level programming language, the *Plankalkül* [151], a logical formalism based on lambda calculus. In the same spirit, Zuse dedicated an essay to the potential use of computing equipment to replace bureaucratic structures in the administration of planned economies [152].

Although high level programming languages are commonly used today, Zuse's approach proved to be ahead of its time, while the *von Neumann* design became the standard for computer architecture. Again, the relevance of Zuse's ideas can only be correctly assessed in hindsight, e.g. his 1958 invention of the vector computer makes him a pioneer of massive parallelism [153]. After moderate successes in business, Zuse retired relatively early and dedicated himself to painting.

K. E. O. Zuse [2, 141]:

June 22, 1910

Birth in Berlin, Germany.

1936

The patents *Rechenmaschine* [154] and *Mechanisches Schaltglied* [155] are registered in Germany.

1936 – 1941

In Berlin-Kreuzberg, Zuse constructs the mechanical computer *Z1* and the first electronic computer *Z3*.

1948

Über den Allgemeinen Plankalkül [151].

Berlin as well as Göttingen [20], 1920–1930. Thus it can be argued that it was fascist research that failed, while German science actually won the war.

²⁹With this justification, Zuse regarded computers as a necessity for modern scientific work even in 1948: «Die Theorie der Atomphysik ist heute zu einer Wissenschaft geworden, welche fast alle Gebiete der Mathematik erfasst. Wer gelegentlich einen kleinen Einblick in diese nur wenigen zugängliche Welt genommen hat, wird den Eindruck bekommen, daß es sich hier um eine Materie handelt, welche nur von Menschen mit überdimensionierten Gehirnen beherrscht werden kann» [150].

1949

The enterprise *Zuse KG* is founded in Neukirchen (between Fulda and Kassel).

1956

Dr.-Ing. h.c. at the Technical University of Berlin.

1964 – 1969

Zuse works for *Siemens AG* as a consultant.

December 18, 1995

Death in Hünfeld near Fulda, Germany.

Time-continuous stochastic processes



Figure 1.11: Andrej Nikolaevič *Kolmogorov* [2].

The theory of random walks had proven to be physically significant by *Smoluchowski's* and *Einstein's* work on Brownian motion. It was formalized by *Markov* (Марков) who investigated series of mutually independent variables [156], known today as *Markov* chains. For many stochastic processes, however, it is crucial to apply a time-continuous modeling approach instead of a series of discrete events. *Kolmogorov* (Колмогоров) made relevant breakthroughs in that direction [157–159], including the *Chapman-Kolmogorov* equation, which for an enumerable state space can be denoted as

$$\Omega(t + \tau) = \Omega(t)\Omega(\tau), \quad (1.34)$$

for a transition matrix $\Omega(t)$ describing the transition probability between states within a time interval of t , as well as the *Kolmogorov forward* and *backward* equations [157], describing the temporal evolution of a continuous-time *Markov* process over a set of real variables.

In practice, even continuous order parameters are often discretized (e.g. in case of forward flux sampling), so that Eq. (1.34) is more generally applicable than it might seem. The version of the theorem corresponding to a continuous state space \mathbb{K}^g , defined over a finite number g of variables Q_1 to Q_g , is

$$\int_{\mathbb{K}} W(Q_1 = X_1 \wedge \cdots \wedge Q_g = X_g) dX_g = W(Q_1 = X_1 \wedge \cdots \wedge Q_{g-1} = X_{g-1}), \quad (1.35)$$

where the probability of a condition C is given by $W(C)$.

Kolmogorov's contributions also transformed other areas of science that are of a certain importance in the present context [160], including the theory of turbulent flow [161], ergodic theory [162], and information theory [163]. When the principles of scientific honesty came under attack, it was also *Kolmogorov* who could be relied upon for a valiant defense.³⁰

A. N. *Kolmogorov* [2, 160, 167]:

April 25, 1903

Birth in Tambov (Тамбов), Russia.

1929

Promotion at the Moscow State University.

1930

Appointment as a professor at the Moscow State University.

1931

Über die analytischen Methoden in der Wahrscheinlichkeitsrechnung [157].

1938 – 1958

Department head at the *Steklov* Institute in Moscow.

1954

Théorie générale des systèmes dynamiques [162].

1980

Wolf Prize in mathematics.

October 20, 1987

Death in Moscow, Soviet Union.

The stability limit for nuclei

Von Weizsäcker, beside *Hahn*, *Heisenberg*, and *Straßmann*, was a key figure for the development of nuclear research in Germany which had both scientific and political reasons.³¹ For the present study it is particularly relevant that he introduced the *droplet model* of the atomic nucleus [169, 170], where the theoretical bond energy of the nucleus is described by

$$U_{\text{th}} = U_F + U_V + U_C + U_A, \quad (1.36)$$

³⁰His 1940 intervention in favor of genetics [164] was based on a rigorous statistical re-evaluation of available data that had previously been interpreted as a confirmation of the artificial vernalization method advocated by *Lysenko* (Лысенко). To this criticism, *Lysenko* publicly replied that «нас, биологов, и не интересуют математические выкладки, подтверждающие практически бесполезные статистические формулы менделистов» [165, 166]. This did surprisingly little to diminish the degree of official support for *Kolmogorov's* work, considering that the eminent «mendelist» geneticist *Vavilov* (Вавилов) was imprisoned at the same time. In 1941, *Kolmogorov* even received the «Stalin» USSR State Prize.

³¹In *Einstein's* August 1939 letter to President *Roosevelt*, a crucial contribution to the inception of the Manhattan project, he adverted to the fact «that the son of the German Under-Secretary of State, von Weizsäcker, is attached to the Kaiser-Wilhelm-Institut in Berlin where some of the American work on uranium is now being repeated» [168].

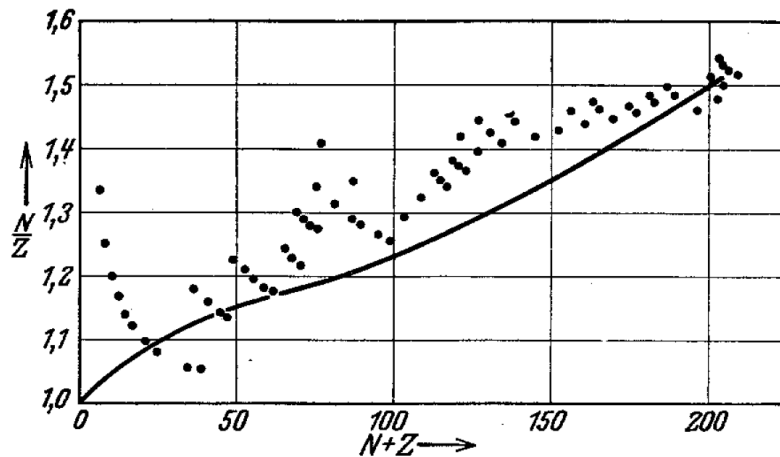


Figure 1.12: Nucleus stability limit according to the droplet model (solid line) along with the isotopes known to be stable in 1935 (●), scanned from *von Weizsäcker's* article [169]. In his notation, N and Z are the number of neutrons and protons in the nucleus, respectively. The two significantly anomalous cases correspond to the stable isotopes Cl_{17}^{35} (regular chlorine) and K_{19}^{39} (regular potassium).

which includes a surface contribution U_F , mediated by an effective surface tension γ , and a volume contribution U_V . The last two terms represent the *Coulomb* interaction U_C and a perturbation U_A due to the asymmetry between the number of protons and neutrons in the nucleus.

This development suddenly carried the spherical fluid phase boundary and the question of stability and instability of droplets into the spotlight of contemporary nuclear physics.³² Since atomic nuclei are particularly small bodies, it also prompted the issue of understanding the curvature influence on interface properties. Therefore, it is not surprising that *Tolman*, a former contributor to the Manhattan project who served as an advisor to the UN Atomic Energy Commission, developed the first effective theory of molecular-level curvature effects on the surface tension.³³ Previously, this question had not been systematically considered by the physico-chemical community.

Von Weizsäcker himself was deeply concerned by the existential threat for humanity caused by nuclear weapons.³⁴ He instigated the *Erklärung der achtzehn Atomwissenschaftler* [176] of 1957, opposing the inclusion of the atomic bomb in the arsenal of the West German military, and devoted most of his subsequent work to the investigation of the social impact of scientific innovations.

C. F. *von Weizsäcker* [178]:

³²This analogy is also the probable origin of the terms *critical nucleus* and *nucleation*, called *charakteristisches Tröpfchen* [171] or *Keim* [172] and *Keimbildung* [171–173], respectively, in earlier German works.

³³The article *The effect of droplet size on surface tension* [174], published posthumously in 1949, was the last scientific contribution of R. C. *Tolman* (1881 – 1948). It was actually submitted to the journal by *Kirkwood* two weeks after *Tolman's* death [175].

³⁴He considered himself lucky not to have met any significant success with his wartime research: «Im Krieg blieb den deutschen Physikern die letzte Härte der Entscheidung erspart. Wir erkannten, daß wir keine Bomben machen konnten. Wir waren glücklich darüber» [176]. However, as explained above, only those scientists who had previously chosen to serve the fascist state were later spared that decision, not German physicists in general.



Figure 1.13: Carl Friedrich *Freiherr von Weizsäcker* [177].

June 28, 1912

Birth in Kiel, Germany.

1916

King *Wilhelm II.* of Württemberg elevates the *von Weizsäcker* family to the higher nobility.

1933

Dr. rer. nat. with the dissertation *Durchgang schneller Korpuskularstrahlen durch ein Ferromagnetikum* [179] at the University of Leipzig.

1935

Zur Theorie der Kernmassen [169].

1946 – 1957

Professor at the University of Göttingen affiliated to the Max Planck Institute of Physics.

1957

Die Verantwortung der Wissenschaft im Atomzeitalter [176].

1970 – 1980

Director of the Max Planck Institute for the Research of Living Conditions in the Modern World.



Figure 1.14: Stanisław Marcin *Ulam* [2].

1979

Proposed as Federal President by W. Brandt.³⁵

April 28, 2007

Death in Starnberg, Germany.

Monte Carlo simulation

Although Stanisław *Ulam* was a student of the great mathematician Stefan *Banach* and obtained various notable results in pure mathematics,³⁶ his research on technical applications ultimately turned out to have a larger impact.

Most notoriously, he contributed to the *Teller-Ulam* design of nuclear weapons, which was a crucial step to the development of the hydrogen bomb. However, *Ulam* is also, together with Nicholas *Metropolis*, the inventor of Monte Carlo (MC) simulation [181]. The *Fermi-Pasta-Ulam* «experiment» of 1955 was the first systematic investigation of the statistical mechanical properties – in particular ergodicity – for an idealized model by computer simulation [182].

S. M. *Ulam* [2]:

April 13, 1909

Birth in Lemberg (Львів), Austria.

1933

Promotion at the Polytechnic Institute of Lwów (Львів).

³⁵His brother Richard, who was eventually elected in 1984, had already been the CDU presidential candidate in 1974. This may help to explain why C. F. von Weizsäcker declined the SPD nomination.

³⁶The spirit of the Lwów school of mathematics and of *Ulam*'s own contributions is captured by the group's notebook of open problems, the *Księga Szkołka* (named for a café), which *Ulam* eventually published [180].

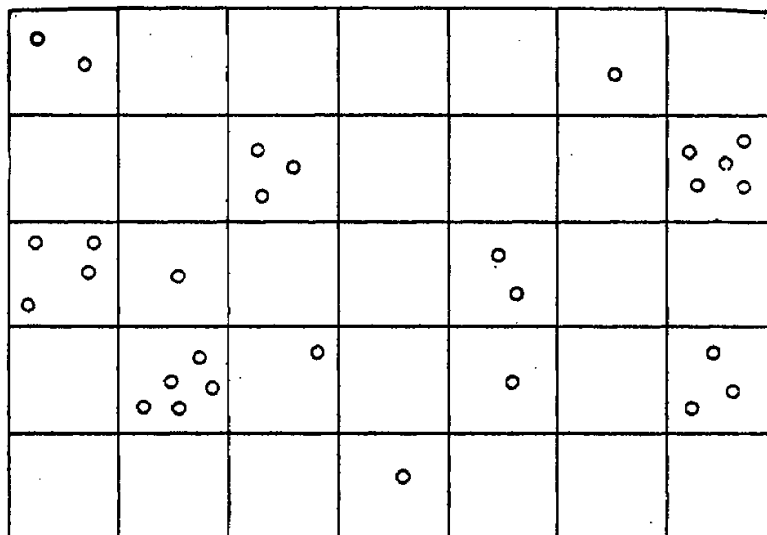


Figure 1.15: Illustration of the *liquid drop model* [183]. *Reiss* proposed to separate the system into nanoscopic subvolumes «enclosed by a shell whose walls are permeable to molecular force fields, but impermeable to molecules themselves» [183].

1943 – 1965

Research scientist at Los Alamos National Laboratory.

1949

The Monte Carlo method [181].

1955

Fermi-Pasta-Ulam experiment [182].

1965

Appointment to a chair of Mathematics at the University of Colorado, Boulder.

May 13, 1984

Death in Santa Fe, United States.

Molecular thermodynamics of nanodroplets

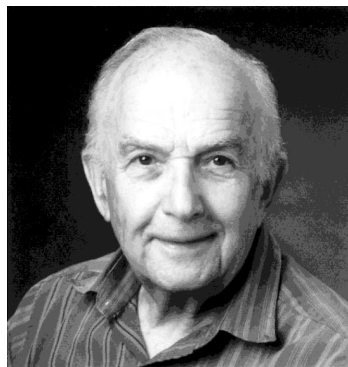


Figure 1.16: Howard Reiss [184].

Beginning in the 1930s and 1940s with the work of *Verschaffelt* [185] and *Guggenheim* [186], researchers concerned with interfacial thermodynamics increasingly looked beyond the picture of a postulated discrete phase boundary. In 1948 and the subsequent years, this led to the theoretical developments of *Tolman* [174, 187] and further authors [188–190], which were mostly still based on effective radii and hence on a formal discretization, while certain aspects of these theories also relied explicitly on the continuity of the interface.³⁷

A perspective on nucleation entirely based on molecular thermodynamics was introduced by *Reiss* a few years after *Tolman's* work. Similar to *Tolman* himself, *Reiss* had worked on the Manhattan project and subsequently directed his research towards nucleation. According to his *liquid drop model* [183, 191], the formation of a nanoscopic droplet is considered as a process occurring within a characteristic volume which is of the same order of magnitude as the droplet, cf. Fig. 1.15. This approach had various features distinguishing it from previous contributions to nucleation theory. For instance, the depletion occurring in the vapor surrounding a growing droplet was qualitatively covered. More importantly, however, the concepts that

³⁷For instance, the *Tolman* length is the difference between two effective radii (for discretized spherical phase boundaries), yet it was used by *Tolman* [174] precisely to describe the non-discreteness of interfaces.

Smoluchowski and *Einstein* applied to the critical opalescence occurring in stationary homogeneous systems were now also recognized as a viable tool for discussing the non-stationary emergence of heterogeneity by phase separation.

Further early work of *Reiss* dealt with nucleation in binary systems [192], the evaporation of nanodroplets [193], and the surface tension as well as other thermophysical properties of ionic liquids [194, 195]. More recently, he has focused on the rigorous evaluation and implementation of methods for the molecular simulation of homogeneous nucleation processes [196, 197]. Together with *Reguera*, *Bowles*, and *Djikaev*, he proposed an *extended modified liquid drop model* (EMLD), reconsidering basic ideas of the theoretical approach that *Reiss* introduced in the 1950s [198].

H. *Reiss* [184, 199]:

1922

Birth in New York City, United States.

1949

Ph.D. at Columbia University.

1952

Theory of the liquid drop model [183].

1963 – 1968

Director of the North American Aviation Science Center in Thousand Oaks, CA.³⁸

1965

Methods of thermodynamics [202].

1968 – present

Professor for Physical Chemistry at the University of California, Los Angeles.

1969

Founding editor-in-chief of the *Journal of Statistical Physics*.

1973

Tolman medal of the American Chemical Society.

1977

Member of the U.S. National Academy of Sciences.

³⁸In this function, *Reiss* was also promoted to a vice presidency of North American Aviation, a company that had supplied the Royal Air Force with fighter aircraft during World War II and constructed the first Californian nuclear reactor [199, 200]. Throughout the 1960s, North American Aviation focused on the U.S. space program, e.g. as the principal contractor for the ill-fated *Apollo I* mission [201].

1.4 Molecular simulation

Molecular simulation methods are mainly used today for calculating ensemble averages of thermophysical quantities based on potential models (although many further aspects of nanoscopic systems can be dealt with as well). A common property of the simulated systems is that, although they usually contain as many particles as the respective program permits on the available hardware, they are still extremely small. At best, a micron is reached in one or two of the box dimensions.³⁹ They are therefore often too small and too large at the same time: too small to completely neglect interactions over distances that exceed the system size, too large to permit a full computation of the interactions between all pairs of particles inside the box.

The number of explicitly computed pairwise interactions is therefore in practice restricted by a cutoff radius r_c and, archaically,⁴⁰ the minimum image convention whenever the periodic boundary condition is used. Beyond the cutoff radius, the potential energy and the virial are corrected [59, 66], e.g. by assuming for the LJ contributions that the RDF is unity for $r > r_c$ and by applying the reaction field method [204] for point polarities as well as methods based on *Ewald* summation for point charges that do not cancel out locally [61].

The main two ways of obtaining thermophysical results on the basis of molecular models are MC algorithms, where the phase space is sampled probabilistically, and molecular dynamics (MD), i.e. the numerical integration of the classical Newtonian equations of motion.

The *Metropolis et al.* [205] algorithm has become almost synonymous of MC simulation. According to this approach, only configurations are sampled. The kinetic energy of the system is macroscopically given by the temperature (in case of the NVT , NpT , and μVT ensembles). The microscopic momentum coordinates of individual particles are not computed at all.⁴¹ In each step, a single particle j is moved at random (this movement is understood to include the internal DOF as well), corresponding to the test transition

$$\underline{\mathbf{x}} = (X_{11}, \dots, X_{j1}, \dots, X_{jg}, \dots, X_{Ng}) \Rightarrow \underline{\mathbf{x}}' = (X_{11}, \dots, X'_{j1}, \dots, X'_{jg}, \dots, X_{Ng}), \quad (1.37)$$

wherein g translational, rotational, or internal DOF pertaining to a single particle are simultaneously varied. Since a constant total kinetic energy is assumed, it is possible to evaluate the internal energy difference $U' - U = \Delta U_j^{\text{pot}}$ by considering the potential energy of the particle j only. The relative probability of the configurations in the canonical ensemble is

$$\frac{\omega(\underline{\mathbf{x}}')}{\omega(\underline{\mathbf{x}})} = \exp\left(\frac{-\Delta U_j^{\text{pot}}}{T}\right). \quad (1.38)$$

Thus, only the interaction potentials involving the particle j have to be considered. If the algorithm ensures that from configuration $\underline{\mathbf{x}}'$, a test transition to $\underline{\mathbf{x}}$ is equally probable as vice versa, the canonical ensemble is sampled by applying the acceptance probability

$$W(\underline{\mathbf{x}} \Rightarrow \underline{\mathbf{x}}') = \max\left(1, \frac{\omega(\underline{\mathbf{x}}')}{\omega(\underline{\mathbf{x}})}\right). \quad (1.39)$$

³⁹In case of the present simulations conducted with the programs related to the *ls1* project, all systems contained between 2^{14} and 2^{24} particles. For typical fluid densities and a cubic simulation box, this corresponds to a box length from 100 up to 2 000 Å, although for specific purposes an anisotropic shape was chosen here which also permits the direct investigation of surface areas up to a square micron.

⁴⁰The minimum image convention consists in neglecting, for a given pair of particles i and j , all periodically reproduced images i' and j' except for the pair with the smallest distance [203]. However, for every reasonably sized simulation box, the distance between the second-to-next periodic neighbors necessarily exceeds r_c . If that is not the case, the system is either too small or the cutoff radius is too large.

⁴¹For this purpose, however, a *Maxwell* distribution can be assumed.

If the test transition is rejected, configuration \underline{x} is restored and \underline{x}' is not included in the statistical evaluation. With the exception of the microcanonical case, Eq. (1.39) can be applied to the other ensembles as well, if the corresponding expression for the probability densities is used instead of Eq. (1.38). A strictly microcanonical ensemble can only be simulated if a kinetic term is introduced for every DOF, although that implies giving up some of the inherent advantages of MC simulation. It can also be approximated by the ensemble with constant N , V , and U_{pot} , which requires an equilibrated starting configuration [60].

Umbrella sampling [206], a variant of this algorithm, can also be efficiently applied to obtain free energy profiles with respect to a specified order parameter. Thereby, the relative probabilities of the configurations are modified by a factor that only depends on the respective value of the order parameter. In this way, a sufficient statistical basis can be obtained even for energetically unfavorable values. This makes umbrella sampling a suitable approach for studying rare events, in particular nucleation [87, 88, 207–209], since free energy differences can be determined over a specified range of the relevant order parameter.

Beginning with the 1970s, a variant of umbrella sampling called *temperature scaling MC simulation* was also applied for the calculation of phase equilibria [210, 211] as well as the critical point [211]. Since then, however, it has been superseded by more specific methods:

- Histogram reweighting [212], based on recording the probability distribution (histogram) for the number of particles in the grand canonical ensemble. This approach also has the advantage of permitting immediate access to the critical point [98].
- *Gibbs* ensemble simulation [213], where the phase coexistence is reproduced by directly enforcing the thermal, mechanical, and chemical equilibrium.
- The NpT plus test particle method [66, 204, 214–216], which extrapolates the results of two independent simulation runs to determine the intersection between the curves corresponding to the coexisting phases in the μ - p diagram, cf. Fig. 1.17.
- The Grand Equilibrium method [217], improving the NpT plus test particle method such that the extrapolation is carried out on the fly during the second simulation run.

Interestingly, D. Landau and Binder begin their *Guide to Monte Carlo simulations* [218] with the words: «In a Monte Carlo simulation we attempt to follow the \langle time dependence \rangle of a model for which change, or growth, does not proceed in some predefined fashion (e.g. according to Newton's equations of motion) but rather in a stochastic manner which depends on a sequence of random numbers.»⁴² Actually, MC simulation cannot be immediately applied to determine quantities related to time, such as diffusion coefficients or the frequency of rare events, although dynamic MC algorithms that facilitate this have been proposed as well [219, 220]. The widespread use of MC simulation, however, is rather due to its viability for exploring the phase space stochastically.

MD simulation, on the other hand, does describe the evolution of a system over time and can therefore be applied immediately to dynamic properties. It constructs an approximate trajectory of a multi-particle system by integrating the classical equations of motion

$$\dot{\underline{p}} = -\nabla_{\underline{x}}\mathcal{H}, \quad (1.40)$$

$$\dot{\underline{x}} = +\nabla_{\underline{p}}\mathcal{H}, \quad (1.41)$$

⁴²Cf. the opening section [218], which is entitled «What is a Monte Carlo simulation?». This understanding, however, restricts the applicability of MC simulation to an unreasonable extent, since all real systems actually «proceed in some predefined fashion» even where the underlying laws are probabilistic.

applying Hamiltonian mechanics to the momentum coordinate vector $\underline{\mathbf{p}}$ and the position coordinate vector $\underline{\mathbf{x}}$. Since this system of equations is energy preserving for the Hamiltonian $\mathcal{H} = U$, nothing more than a well-defined force field (e.g. a set of pairwise contributions to the potential energy) and an initial configuration with the corresponding values of N , V , and U is required for simulating the *microcanonical* ensemble.

For other ensembles, the respective boundary conditions have to be imposed artificially. In the *canonical* case, it is for most purposes sufficient to rescale the translational as well as the rotational momenta of all particles by a normalizing factor to keep the kinetic energy constant [216]. This is known as isokinetic rescaling or as a *Berendsen* thermostat, where the first term usually suggests that the kinetic energy is kept exactly constant, while *Berendsen et al.* [225] applied a coupling constant, which still allows the kinetic energy to vary. The *Andersen* thermostat [203] achieves the same objective by introducing stochastic collisions with virtual particles from an external reservoir. The *Nosé-Hoover* thermostat [226, 227], which introduces a single additional DOF that is coupled to the total kinetic energy, is widely regarded as the most realistic representation of the fluctuations in a small system.⁴³

The *isothermal-isobaric* ensemble is usually simulated with the *Andersen* barostat [66, 203, 216], i.e. a simulation box that expands or contracts in dependence of the instantaneous pressure as determined from the intermolecular interactions. For this purpose, the coordinate system is reduced by the cubic root of the volume

$$(\underline{\mathbf{p}}', \underline{\mathbf{x}}') = V^{-1/3}(\underline{\mathbf{p}}, \underline{\mathbf{x}}), \quad (1.42)$$

⁴³In certain cases, however, the *Nosé-Hoover* thermostat can lead to periodic «undulations in the instantaneous kinetic temperature» [228]. These artefacts are obviously due to the harmonic oscillator coupled to the kinetic energy of the system; they can similarly arise, for the same reason, with structurally analogous methods such as the *Andersen* barostat [66].

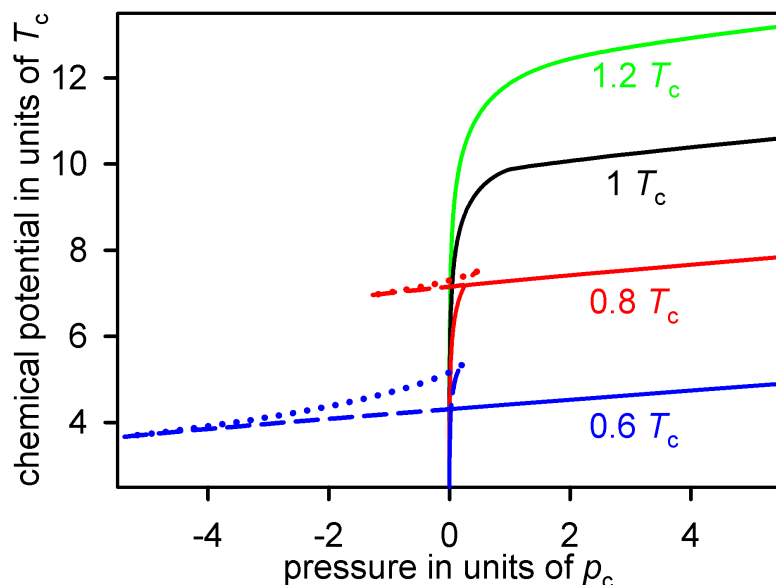


Figure 1.17: $\mu - p$ diagram for a non-polar fluid including the stable (solid lines), metastable (dashed lines), and unstable regime (dotted lines) according to the *Redlich-Kwong-Soave* [221, 222] EOS with an acentric factor [223] of zero at temperatures of 0.6, 0.8, 1, and 1.2 T_c . Properties of the $\mu - p$ diagram are discussed in more detail by *Debenedetti* [224].

and the extended Hamiltonian

$$\mathcal{H} = U_{\text{kin}}(V^{1/3}\underline{\mathbf{p}}') + U_{\text{pot}}(V^{1/3}\underline{\mathbf{x}}') + \frac{\mathcal{M}\dot{V}^2}{2} + pV, \quad (1.43)$$

is applied to the reduced coordinates as well as the volume [203]. Therein, the volume contribution to the potential energy is given immediately by the virial for the configuration $\underline{\mathbf{x}}'$, whereas the kinetic energy⁴⁴ is proportional to $V^{2/3}$. The last two terms of Eq. (1.43) are effective kinetic and potential energy contributions, respectively, for V which is formally treated as an additional DOF of the reduced system. The magnitude of the response \dot{V} to fluctuations of the virial is regulated by the quantity \mathcal{M} , which is sometimes referred to as the piston mass although the *Andersen* barostat does not use a piston and

\mathcal{M} is not really a mass.

As a combination of MD with the *Metropolis* algorithm, *grand canonical* molecular dynamics (GCMD) alternates between regular integration time steps as well as the stochastic insertion and deletion of particles [229, 230], such as to maintain a constant value of the chemical potential for one or several components. Thereby, a random particle is removed for a test deletion, while for a test insertion the coordinates of an additional particle are chosen at random. The acceptance criterion is defined probabilistically by

$$W = \min\left(\rho\lambda^3 \exp\left[\frac{-\mu - \Delta U_{\text{pot}}}{T}\right], 1\right), \quad (1.44)$$

a variant of Eq. (1.39), in case of deletions, and analogously for insertions [59]. The same version of Eq. (1.39) is also used for MC simulation of the grand canonical ensemble. In Eq. (1.44), ρ is the density⁴⁵ and $\lambda = \hbar(2\pi/mT)^{1/2}$ is the thermal *de Broglie* wavelength, while the potential energy associated with the deleted particle corresponds to $-\Delta U_{\text{pot}}$.

Briefly comparing the two major simulation approaches, MD has one definite advantage over MC simulation: it permits to access properties of typical trajectories as well as the evolution of non-equilibrium systems. While such systems do, strictly speaking, usually belong to a well-defined statistical ensemble, in case of non-equilibrium properties one is not interested in the ensemble average but rather in the realistic behavior of a control volume involved in an irreversible process. On the other hand, MC simulation can more easily be parallelized. It is less prone to numerical errors – for instance, configurations with extreme repulsion between molecules are mostly rejected due to the energetic acceptance criterion. Even when they occur, the extreme velocities corresponding to such configurations do not have to be handled numerically,⁴⁶ since MC does not compute the momentum coordinates. The core of an MD

⁴⁴For the NpT ensemble, evidently, a thermostat is required as well to keep the kinetic energy constant or approximately constant. The intervention of the thermostat, however, either occurs by means of an additional microscopic DOF, as in case of the *Nosé-Hoover* thermostat, or it has to be regarded as formally external to the equations of motion so that the dependence of U_{kin} on V is not distorted.

⁴⁵In the present work, the term *density* and the symbol ρ always refer to the number per volume (i.e. number density) instead of the mass per volume (i.e. mass density).

⁴⁶In principle, MD simulation in the microcanonical, canonical, or isothermal-isobaric ensemble can handle such events as well by increasing the temporal resolution for the integration of particle collisions. In case of the grand canonical ensemble, the problem is more intricate, because collisions can also occur there by insertion of a new particle (even if the acceptance probability for such configurations is relatively low). This leads to a sudden increase in the local internal energy, whereas in the other ensembles kinetic and potential energy are only transformed. If it is desired to avoid this artifact, gradual insertion and excluded volume approaches have to be employed.

application is the computation of forces, whereas MC is based on the potential energy. In certain cases, where the derivative of the potential is more involved than the potential itself, this also contributes to the efficiency of MC simulation.⁴⁷

Modern hardware is sufficiently developed to liberate the programmer of the concerns that troubled the first developers of molecular simulation programs.⁴⁸ Without much optimization it is possible to explore the phase space for systems of thousands of particles in the typically acceptable time span of a few days on a cluster of workstations or even a single workstation.

Similarly, no challenges are present from the usual algorithmic point of view, which disregards constant prefactors on the consumed resources and merely considers asymptotic behavior: all of the required algorithms require linear space and, at worst, $\mathcal{O}(N^2)$ time. For short-range interactions this can be improved to $\mathcal{O}(N \log N)$.⁴⁹ Therefore, if molecular simulation is considered a typical application for high performance computing, this is by no means due to the inherent complexity of the problem, but rather the opposite: it is precisely because efficient algorithms are not only known but also easy to implement that molecular simulation has become so widespread, at least in the scientific community, while the systems under consideration become larger and larger.

For the same reason, the standard criticisms made of the algorithmic approach, namely that it neglects constant prefactors and focuses on atypically large instances of a problem, are invalid here. When a problem is theoretically hard, the studied instances are usually small, and the most practical algorithm in these cases may not exhibit the optimal asymptotic scaling. When asymptotically efficient algorithms are really available, however, the obverse of this fact can be experienced: the instances are often extremely large, so that using the theoretically optimal algorithm becomes crucial.

This may serve to explain why several molecular simulation programs were used for the present work, and how they differ from each other: on the one extreme of the range, the *Kedia* program was entirely developed by engineers (mainly G. K. *Kedia* and G. *Fuchs*) and focuses on a particular functionality while it is only suitable for small systems. The programs that belong to the *ls1* project were partly developed and heavily optimized by scientific computing professionals [232, 233] in an ongoing effort under the leadership of M. F. *Bernreuther*. Their functionality is relatively restricted, but the implemented algorithms are more efficient when applied to large systems and can be parallelized with a relatively small effort required for inter-process communication. Finally, the *ms2* project corresponds to a compromise between these approaches [234].

⁴⁷One such case is the *Tersoff* potential. For hard sphere systems, this distinction becomes even more significant: from an MC point of view, there are only forbidden configurations *with* and permitted configurations *without* overlap, where the latter are all equally probable. To implement MD in such a case all collisions have to be detected accurately and in their correct temporal order. This becomes particularly expensive when polyhedra are regarded instead of spheres. While such operations can, of course, be efficiently handled by graphics processing units, it is still clearly more reasonable to run an MC simulation in these cases unless dynamic properties are explicitly of interest. Since the *Metropolis* criterion only requires the detection of overlaps, it can be handled by a graphical coprocessor just as well.

⁴⁸As *Ng et al.* [210] expressed it in 1979: «To prevent the resulting cost from becoming prohibitive we studied a system containing only 32 independent particles.» The present world record was established by a *trillion-atom molecular dynamics* simulation [231] at the Los Alamos and *Lawrence Livermore National Laboratories* in 2008.

⁴⁹This means $\mathcal{O}(N \log N)$ with respect to the number of particles N . If the system size is measured in terms of the *Kolmogorov* complexity K of a typical configuration [163], this corresponds to linear time scaling $\mathcal{O}(K)$.

2 Curved fluid interfaces

2.1 Classical nucleation theory

Homogeneous nucleation is the first step of a first-order phase transition in the bulk of a metastable phase. Real condensation processes, e.g. in the atmosphere, are usually heterogeneous [235–237], so that the liquid phase starts to form at preferred sites such as ions or solid aerosols. Often there is a complex mechanism of nucleation [238], but qualitatively, such cases are mostly analogous to nucleation in the homogeneous bulk vapor. They differ by providing special locations where the free energy barrier of the condensation process is lower than in the bulk. Therefore, understanding homogeneous nucleation in supersaturated vapors is essential for more complex processes as well. And despite its general importance and apparent simplicity, it is not yet fully captured on the theoretical level.

Condensation occurring above the saturated vapor pressure was discovered experimentally during the nineteenth century. It was for instance discussed by R. von Helmholtz [239] who developed a method for measuring the humidity of air by adiabatic expansion. He observed the presence of supersaturated states as well as the contribution of aerosol particles to nucleation. Although by that time, in principle, the theory of thermodynamics was sufficiently developed to account for the observations, R. von Helmholtz was apparently surprised by the results of his measurements.¹ Moreover, he came to conclusions that were qualitatively wrong and ascribed nucleation exclusively to the heterogeneity of the system.² At the turn of the century, Wilson [240] corrected the imperfect understanding of metastability that had prevailed before, both on an experimental and a theoretical level, by demonstrating that all supersaturated states eventually break down and that a certain maximal supersaturation ratio can never be exceeded, even in the perfectly homogeneous case.

Among German chemical engineers, an interest in nucleation as an independent phenomenon was raised in 1922 when Haber, the chemistry Nobel laureate of 1918, published a study on the freezing of supercooled melts [173]. He claimed that in a melt which is supercooled by ΔT , an emerging crystal is stable if its radius R exceeds the value given by [173]

$$\frac{R\Delta T}{T} = \frac{2F}{N^{-1}\Delta\tilde{N}h\rho^\diamond}, \quad (2.1)$$

where F is the specific surface energy of the crystal, $N^{-1}\Delta\tilde{N}h$ is the melting heat, and ρ^\diamond is the density of the solid phase. In the subsequent years, Volmer and Weber [171] as well

¹«Nach den theoretischen Erörterungen und der allgemein verbreiteten Anschauung müsste gesättigte Luft bei der kleinsten, ja bei einer unendlich kleinen Depression Nebel erzeugen. ... Schon die ersten Versuche zeigten aber, dass dies nicht der Fall ist» [239].

²«Es kommt nun aber noch ein zweiter, sehr wichtiger Factor in Betracht ..., das ist der „Dunstgehalt“ der Luft. ... Wenn dieselbe von „Dunst“ – wie Kiessling alle heterogenen Bestandteile zusammen nennt – befreit ist, so kann man sie nach diesen Untersuchungen bis zu einem beliebigen Grade übersättigen, ohne daß eine Spur von Nebelbildung auftritt» [239]. For R. von Helmholtz, supersaturation was an undesired effect, so he did not attempt to determine its maximal attainable value.

as *Farkas* [172] developed the foundations of CNT, and *Powell* [241] as well as *Volmer* and *Flood* [242] provided reliable experimental data for the onset of nucleation, corresponding to the maximal attainable supersaturation ratio in a homogeneous system.

The driving force of a phase transition is the difference between the chemical potential μ of the metastable phase and the saturated chemical potential $\mu_s(T)$. By applying the *Gibbs-Duhem* equation, it can be determined from an integral over the metastable part of the pressure isotherm

$$\Delta\mu = \mu - \mu_s(T) = \int_{p_s(T)}^p \frac{dp}{\rho}, \quad (2.2)$$

between the saturated pressure $p_s(T)$ and the pressure p of the metastable phase. For the vapor phase, the saturated state with the chemical potential $\mu_s(T)$ and the vapor density $\rho''(T)$ refers to the vapor-liquid equilibrium or, below the triple point temperature T_3 , the vapor-solid equilibrium. A pure metastable vapor is usually described by the supersaturation ratio

$$S_\rho = \rho/\rho''(T), \quad (2.3)$$

$$S_p = p/p_s(T), \quad (2.4)$$

$$S_\mu = \exp(\Delta\mu/T), \quad (2.5)$$

in terms of density, pressure, or chemical potential. The chemical potential supersaturation ratio S_μ appears directly in many thermodynamic expressions, but only S_ρ and S_p can be measured in experiments – and even this is complicated because of the rapidly changing temperature in most experimental settings [243, 244]. For supersaturated vapors of a real fluid

$$S_p > S_\rho > S_\mu > 1, \quad (2.6)$$

generally holds. The deviation between these measures of the supersaturation can be very significant, as shown in Fig. 2.1 for the LJ-TS fluid.³

Mixtures can be characterized in a very similar way whenever the emerging condensed phase contains overwhelmingly a single high-boiling component. Then the supersaturation ratio refers to the condensing component only, i.e. the component that undergoes a phase transition, while the other components are regarded as an inert carrier gas. This approach can for instance be applied to water in the earth's atmosphere.

For an ideal gas, the three supersaturation ratios are equal, $S_\rho = S_p = S_\mu$, and this approximation is often used for the sake of simplicity.⁴ This is typically done implicitly, e.g. by defining the supersaturation ratio as $S = S_p$ [250–254] or $S = S_\rho$ [255] and inserting it in thermodynamic expressions where S_μ should be used from a more rigorous point of view. At low temperatures, in particular below the triple point temperature T_3 , where most experiments are conducted, the ideal gas law is a good approximation and the three expressions for the supersaturation ratio lead to similar absolute values.

In case of the present study, however, MD simulation results for small systems were used to obtain the dependence of the metastable pressure on fluid density at constant temperature.

³The plots shown in the figure correspond to cubic interpolations between MD simulation results. For the full LJ fluid, there is also an EOS that is known to accurately describe metastable vapor states [245], confirmed by related simulation results [246–249].

⁴Of course, this only makes sense if one assumes an *ideal gas* vapor that can be condensed to a *non-ideal* liquid phase.

Table 2.1: Virial coefficients for the LJ-TS fluid as determined from a fit to the MD simulation results shown in Fig. 2.2 and to the saturated vapor and liquid densities determined in a previous study [85]. The spinodal densities $\rho'^{\#}$ and $\rho''^{\#}$ for liquid and vapor, respectively, were determined from the fifth-order virial expansion, cf. Eq. (1.17), with $b_k = 0$ for $k \geq 6$.

T	$-b_2$	b_3	$-b_4$	b_5	ρ'	ρ''	$\rho'^{\#}$	$\rho''^{\#}$
0.65	11.7675	44.5866	96.9625	71.4351	0.813	0.00406	0.660	0.0592
0.7	9.77572	34.176	76.4866	59.4954	0.787	0.00728	0.636	0.0740
0.75	8.43697	27.7315	62.373	50.3464	0.759	0.0124	0.613	0.0886
0.8	7.33394	21.854	41.1349	40.3329	0.730	0.0198	0.588	0.103
0.85	6.48592	18.3318	40.0252	34.6962	0.699	0.0304	0.564	0.119
0.9	5.44587	12.3036	25.0989	23.6305	0.664	0.0446	0.532	0.134
0.95	4.97043	10.0411	17.1387	16.0653	0.622	0.0648	0.499	0.149
1	4.67665	9.83155	15.6063	13.8778	0.571	0.0962	0.466	0.174

For the LJ-TS fluid, the isotherms shown in Fig. 2.2 were also correlated by a fifth-order virial expansion in Leiden form, cf. Eq. (1.17), with the temperature dependent virial coefficients given in Tab. 2.1. Note that the b_k values obtained from the fit are approximately linear in $1/T$.

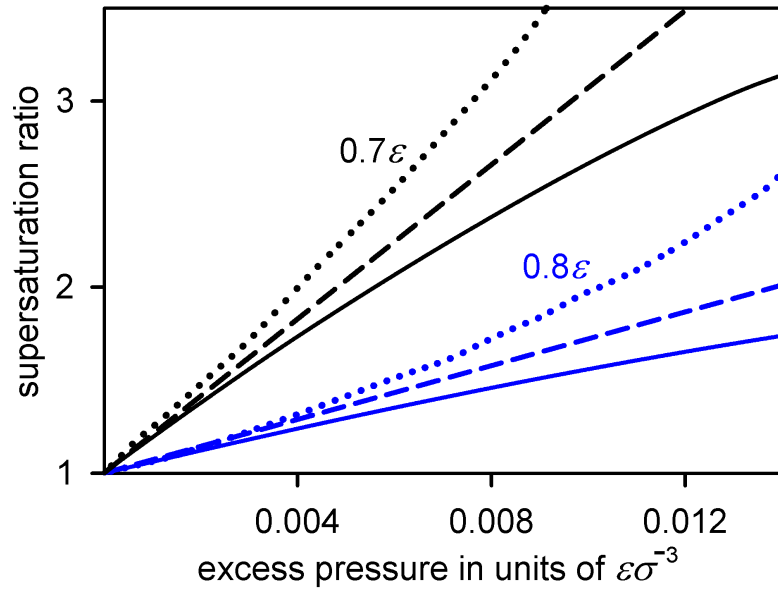


Figure 2.1: Supersaturation ratio in terms of chemical potential (solid lines), pressure (dashed lines), and density (dotted lines) over the excess pressure $p - p_s$ for the LJ-TS fluid at temperatures of 0.7ε and 0.8ε .

The key properties of vapor to liquid nucleation in a closed system at constant volume and temperature are the nucleation rate J and the magnitude ΔA^* of the free energy barrier that must be overcome to form stable droplets. The usual approach, classical nucleation theory (CNT), is based on the treatment of the spherical vapor-liquid phase boundary by *Gibbs* [18, 19]. CNT uses the capillarity approximation, i.e. it assumes that in many aspects, small droplets behave exactly like the bulk liquid. Within the framework of CNT, for instance, the differential

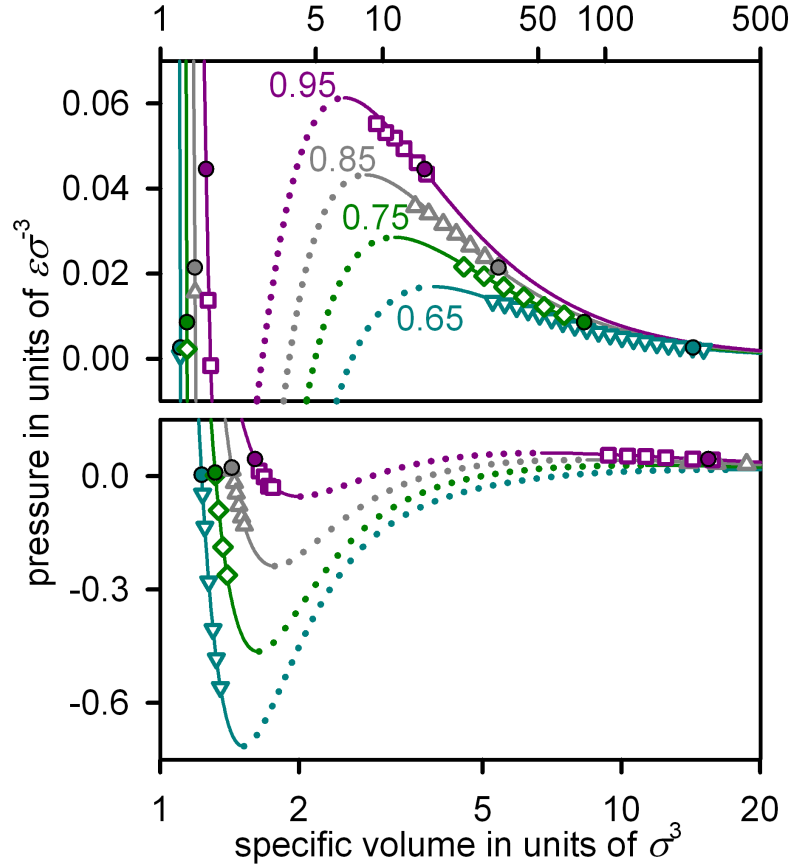


Figure 2.2: Isotherms in a pressure-volume diagram for the LJ-TS fluid as determined by MD simulation of small systems at temperatures of 0.65 (∇), 0.75 (\diamond), 0.85 (\triangle), and 0.95 ε (\square) as well as the saturated states (\bullet) according to *Vrabec et al.* [85] in comparison with the fifth-order virial expansion, cf. Tab. 2.1 and Eq. (1.17), which was correlated to the present simulation data. Results in the vicinity of the spinodal line are not shown here, and no such values were used for adjusting the virial coefficients, to ensure that only states unperturbed by nucleation were considered.

droplet density,⁵ defined by

$$\rho_i = \left(\frac{\partial V_i}{\partial i} \right)_{T, S_\mu}, \quad (2.7)$$

is assigned the same value as the saturated liquid density $\rho'(T)$. Note that V_i refers to the volume occupied by a liquid droplet in an equilibrium configuration, which depends on the number of molecules i inside the droplet.

The foundations for CNT were established by *Volmer* and *Weber* [171] who, following the approach of *Arrhenius*, proposed the approximation

$$J \sim \exp(-\Delta A^*/T), \quad (2.8)$$

for the nucleation rate. On the basis of this relation, they argued that nucleation occurs when ΔA^* and T are of similar magnitude,⁶ however, without discussing the precise value of the

⁵A discussion of axiomatic thermodynamics that elaborates on the deviation between properties expressed in integral quantities versus differential quantities, regarding the molecular length scale, is given by *Hill* [256].

⁶«Beobachtbar ist die Keimbildung nur, wenn W sich der Größenordnung von kT nähert» [171].

proportionality constant in Eq. (2.8).

They also introduced the notion of a droplet that corresponds to a given supersaturated vapor pressure p , defined by a straightforward condition: the droplet and the surrounding vapor must be in thermodynamic equilibrium. For the nucleation process at the pressure p , this criterion defines the *critical droplet*. When such a droplet is formed, the metastability of the supersaturated phase breaks down.⁷ Thus, the vapor pressure of the critical droplet is the same as the supersaturated pressure of the surrounding vapor

$$p_s(\iota^*, T) = p. \quad (2.9)$$

With increasing droplet size, the curvature of the droplet surface decreases and its vapor pressure approaches the saturated vapor pressure

$$\lim_{\iota \rightarrow \infty} p_s(\iota, T) = p_s(T), \quad (2.10)$$

since $p_s(T)$ corresponds to vapor-liquid coexistence with a planar phase boundary. Critical droplet formation is the activation barrier for the condensation process. Smaller droplets evaporate on average, $p(\iota, T) > p$, and larger droplets grow, $p(\iota, T) < p$. In between, at the critical size, evaporation of the droplet and condensation from the surrounding vapor cancel out, leading to the equilibrium as given by Eq. (2.9).

Equivalently, the condition $\iota = \iota^*(T, S_\mu)$ is characterized by an extremum of the free energy. The free energy due to the presence of a droplet is composed of the surface contribution A_F as well as the volume contributions A' and A'' of the droplet and the surrounding vapor, respectively,

$$dA = dA' + dA'' + dA_F. \quad (2.11)$$

In a closed isothermal system with thermal equilibrium between both phases and a constant volume, this evaluates to

$$\left(\frac{\partial A_F}{\partial \iota} \right)_{N,V,T} = \gamma \left(\frac{\partial F}{\partial \iota} \right)_{N,V,T}, \quad (2.12)$$

for the surface contribution with a droplet surface tension γ which is defined by

$$\gamma = \left(\frac{\partial A_F}{\partial F} \right)_{N,V,T} = \left(\frac{\partial A}{\partial F} \right)_{\iota, N, V, T}, \quad (2.13)$$

and approximated by the surface tension γ_∞ of the planar phase boundary within CNT. The vapor-liquid interface area F is assumed to be

$$\left(\frac{\partial F}{\partial \iota} \right)^3 \approx \frac{2\pi}{3\iota} \left[\frac{4}{\rho'(T)} \right]^2, \quad (2.14)$$

based on the approximation of a spherical droplet with $\rho_\iota = \rho'$.

The assumption $\gamma = \gamma_\infty$ can only be explained historically. At the time when CNT was developed, neither the experimental nor the theoretical methods were sufficiently advanced to

⁷ «Jedem Druck ... ist ein kugeliges Tröpfchen der Phase b ... zugeordnet, welches mit diesem Druck gerade im Gleichgewicht steht. Hat man ein Tröpfchen von dieser charakteristischen Größe erzeugt, so genügt eine unendlich kleine Arbeit, um die Phase a völlig instabil zu machen» [171].

understand the curvature dependence of the surface tension. However, it was clear even to the first proponents of the theory that substantial deviations could be expected.⁸

The volume contributions to the free energy are

$$\frac{\partial A'}{\partial v} = -p_i \frac{\partial V_i}{\partial v} + \mu_i \approx -\frac{p_i}{\rho'} + \mu_i, \quad (2.15)$$

for a liquid droplet with the volume V_i , the pressure p_i , and the chemical potential μ_i , as well as

$$\frac{\partial A''}{\partial v} = p \frac{\partial V_i}{\partial v} - \mu \approx \frac{p}{\rho'} - \mu, \quad (2.16)$$

for the supersaturated vapor that contains the remaining $N - i$ particles and occupies the rest of the volume $V - V_i$. It is assumed here that a single component condenses and μ is the chemical potential of this particular component in the supersaturated vapor. For the free energy dependence on the droplet size this adds up to

$$\frac{\partial A}{\partial v} = \gamma \frac{\partial F}{\partial v} + (\mu_i - \mu) - \frac{p_i - p}{\rho_i}, \quad (2.17)$$

applying the definition of the differential droplet density, cf. Eq. (2.7). This free energy expression contains a positive contribution proportional to the *surface area* differential ∂F , and contributions due to the chemical potential difference and the pressure difference, respectively, which are proportional to ∂v and hence to the *droplet volume* differential. Therein, the pressure difference term is always negative in a supersaturated system, while the chemical potential difference is positive for $v < v^*$ and negative for $v > v^*$.

Based on the approximation of an incompressible liquid phase, the chemical potential inside the droplet is given by

$$\mu_i - \mu_s(T) = \int_{p_s(T)}^{p_i} \frac{dp}{\rho_i(T, p)} \approx \frac{p_i - p_s(T)}{\rho'}. \quad (2.18)$$

The density in the denominator of course refers to the (compressed) liquid here, while μ_s and p_s are saturation properties of the component that undergoes a phase transition – as opposed to the pressure p of the supersaturated vapor which can include a carrier gas. Combining the simplifications and assumptions outlined above leads to

$$\frac{\partial A}{\partial v} \approx \gamma_\infty \left(\left[\frac{4}{\rho'} \right]^2 \frac{2\pi}{3v} \right)^{1/3} - T \ln S_\mu + \frac{p - p_s}{\rho'}, \quad (2.19)$$

a version of Eq. (2.17) occasionally used to evaluate CNT [254]. More frequently, however, the term $(p - p_s)/\rho'$ is also omitted [250, 251, 255, 257], leading to the approximation

$$\frac{\partial A}{\partial v} \approx \gamma_\infty \left(\left[\frac{4}{\rho'} \right]^2 \frac{2\pi}{3v} \right)^{1/3} - T \ln S_\mu. \quad (2.20)$$

⁸As *Farkas* acknowledged in 1927 with respect to his derivation of CNT: «Bei dieser Ableitung ist angenommen, dass die Oberflächenspannung σ unabhängig von x ist, was aber sicher nicht der Fall ist, wenn man zu so kleinen Tröpfchen übergeht» [172]. Therein, x is the droplet radius.

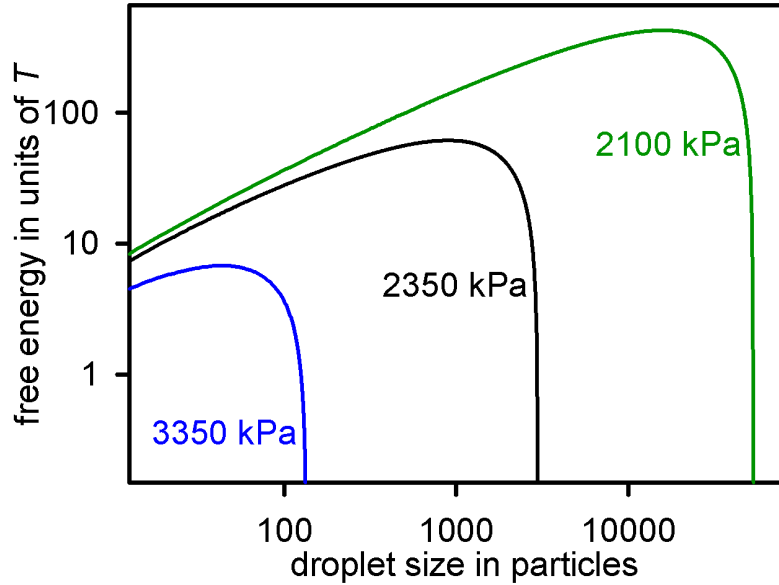


Figure 2.3: Free energy of droplet formation in supersaturated carbon dioxide at 253 K for pressures of 2100, 2350, and 3350 kPa according to CNT without the pressure effect, in the thermodynamic limit (i.e. assuming an infinitely large system so that the supersaturated vapor pressure does not depend on the droplet size).

According to CNT, the critical droplet size evaluates to

$$i^* = \frac{32\pi}{3\rho'^2} \left(\frac{\gamma_\infty}{\Delta\mu_e} \right)^3, \quad (2.21)$$

wherein

$$\Delta\mu_e = \Delta\mu + \frac{p_s - p}{\rho'}, \quad (2.22)$$

is called the effective chemical potential difference by *Wedekind et al.* [254].

The deviation between $\Delta\mu_e$ and $\Delta\mu$ accounts for the pressure effect. For the sake of clarity, the theory based on Eq. (2.19) will be referred to as CNT and the version that uses Eq. (2.20) as *CNT without the pressure effect*, or *CNT $^{\Delta\mu}$* , considering that it uses $\Delta\mu$ in lieu of $\Delta\mu_e$.

Following the «internally consistent» approach of *Blander and Katz* [258] no difference is made between vapor monomers and single-particle droplets. Hence, the free energy of formation is defined as zero for a single-particle droplet and can be obtained by integration

$$A_i = \int_1^i \left(\frac{\partial A}{\partial i} \right)_{N,V,T} di, \quad (2.23)$$

for a droplet containing i particles, cf. Fig. 2.3.

The discussion of other ensembles is more complicated but eventually leads to the same result. This is necessarily the case, because in the thermodynamic limit, where the relation between system and droplet size approaches infinity, the distinction between the canonical and other ensembles disappears. The difficulty lies in the precise definition of, e.g., the isothermal-isobaric or the grand canonical ensemble for a multi-phase system, and in characterizing them

by a thermodynamic potential. For the ensemble defined by constant supersaturated vapor pressure and temperature, Eq. (2.17) with the corresponding free energy⁹ replacing A was derived by *Debenedetti* [224].

The kinetic aspect, beyond the straightforward application of an *Arrhenius* equation, was investigated by *Farkas* [172] who elaborated on the basic thermodynamic considerations of *Volmer* and *Weber*. He obtained an equation for the nucleation rate that can be expressed as

$$J = \mathcal{C}\mathcal{T} \cdot \frac{N' Z_{\text{F}} F^*}{V \sqrt{2\pi}} \exp\left(\frac{-\Delta A^*}{T}\right), \quad (2.24)$$

for a system containing N' vapor monomers. Therein, \mathcal{T} is the transition rate of gas molecules through a surface, i.e. the number of transition events per surface area and time, which is given by the *Hertz-Knudsen* equation [259]

$$\mathcal{T} = (2\pi m T)^{-1/2} p. \quad (2.25)$$

The surface area of a critical droplet is F^* , and the factor \mathcal{C} was introduced by *Farkas* [172] to cover the curvature effect on the surface tension of nanoscopic droplets.¹⁰ The factor Z_{F} in Eq. (2.24) is related to the size dependence of the droplet vapor pressure $p_{\text{s}}(\iota, T)$, i.e. the pressure of a supersaturated vapor in equilibrium with the droplet, in the vicinity of the critical droplet size ι^* . It is defined by

$$-Z_{\text{F}}^2 = \frac{\partial}{\partial \iota} \ln \frac{p_{\text{s}}(\iota, T)}{p} \Big|_{\iota=\iota^*}. \quad (2.26)$$

Equivalently, it can be expressed by the *Zel'dovič* (Зельдович) factor [264]

$$z = \sqrt{\frac{-\partial^2 A}{2\pi T \partial \iota^2}} \Big|_{\iota=\iota^*} \approx \frac{Z_{\text{F}}}{\sqrt{2\pi}}. \quad (2.27)$$

Even if a constant temperature is assumed for the supersaturated bulk vapor, the question remains how fast the latent heat released during condensation is carried away from the surface of a growing droplet. *Feder et al.* [261] incorporated heat transfer effects into CNT by introducing the non-isothermal factor \mathcal{N} into the expression for J . The heat transferred to a droplet when it acquires an additional particle is

$$Q(\iota) = \Delta h^{\text{v}} - \frac{T}{2} - \gamma \left(\frac{\partial F}{\partial \iota} \right), \quad (2.28)$$

taking into account the enthalpy of vaporization Δh^{v} as well as the free energy needed to extend the surface area. The standard deviation of the energy of vapor molecules that collide with a droplet is, again according to *Feder et al.* [261], given by

$$B = T \sqrt{c_{\text{v}} + \frac{1}{2}}, \quad (2.29)$$

⁹The thermodynamic potential for this ensemble is similar but not equal to the *Gibbs* free energy, because the system to which it applies includes the droplet which has a higher pressure than the surrounding vapor.

¹⁰As mentioned above, *Farkas* assumed that the surface tension could depend on the droplet radius. However, the nature of this dependence was unknown to him, and he only stated in very general terms: «Um die Differentialgleichung zu integrieren, müssen wir $p(n)$... von dem entsprechenden Radius x kennen. ... Die Konstante vor der e -Potenz wird als unbekannt beibehalten, da man die übliche Integration nicht anwenden kann, weil die Formel in einem wesentlichen Teil des Bereiches nicht gültig ist» [172]. Authors subsequent to *Farkas* were usually less scrupulous and omitted the factor \mathcal{C} altogether [260–263].

where c_v is the isochoric heat capacity of the supersaturated vapor. The combination of these effects reduces the nucleation rate by the factor [261]

$$\mathcal{N} = \left[\left(\frac{Q(i^*)}{B} \right)^2 + 1 \right]^{-1}. \quad (2.30)$$

Thus, the CNT expression for the nucleation rate ¹¹ can be summarized as

$$J = \mathcal{C}\mathcal{N}\mathcal{T} \cdot \frac{N'zF^*}{V} \exp\left(\frac{-\Delta A^*}{T}\right). \quad (2.31)$$

Deviations of more than ten orders of magnitude between actual nucleation rates and the CNT predictions were observed under certain conditions experimentally [265] and from MD simulation [266], in particular for vapor to solid nucleation of metals. Such inaccuracies can be plausibly attributed to the unrealistic treatment of the smallest clusters, consisting of a few particles only, where the surface tension is known to be much smaller than for the planar interface [85, 267, 268], cf. Section 2.2.

The nucleation theory of *Laaksonen, Ford, and Kulmala* (LFK) acknowledges a curvature dependence of the specific surface energy F , i.e. [269]

$$F_i = \gamma_\infty \left(1 + \alpha_L i^{-1/3} + \alpha'_L i^{-2/3} \right). \quad (2.32)$$

The parameter values α_L and α'_L are defined by comparing the *Fisher* [270] EOS

$$pV = N'T \sum_i \exp(-\Delta A_i/T), \quad (2.33)$$

$$N = N' \sum_i i \exp(-\Delta A_i/T), \quad (2.34)$$

to a virial-type expansion of the second order. *Laaksonen et al.* [269] represent this as

$$N' = \frac{pV}{T} \left(1 + \frac{b'p}{T} \right) = \frac{1}{N} \left(\frac{pV}{T} \right)^2, \quad (2.35)$$

where the effective second virial coefficient is, in this case, defined as

$$b' = \frac{V}{N} - \frac{T}{p}. \quad (2.36)$$

Note that the specific surface energy F from Eq. (2.32) is multiplied with the surface area F for all free energy expressions, and F is assumed to scale with $i^{2/3}$. Thus, the value of α'_L only influences a constant summand which cancels out for the free energy of formation and, by consequence, does not affect the values of i^* and J . On the basis of the considerations outlined above, the remaining parameter evaluates to

$$\alpha_L = \frac{-p_s(T)i^{2/3}}{\gamma_\infty F_i} b'. \quad (2.37)$$

Depending on the thermodynamic conditions, the LFK approach can imply an unphysically increased value of F for small droplets, cf. Fig. 2.4.

¹¹In the remainder of this work, CNT will mostly be evaluated with $\mathcal{C} = 1$ (for the LJ-TS fluid at high supersaturation ratios, however, a value of $\mathcal{C} = 200$ will be shown to be appropriate empirically), whereas the isochoric heat capacity c_v of the saturated vapor will be used to determine \mathcal{N} .

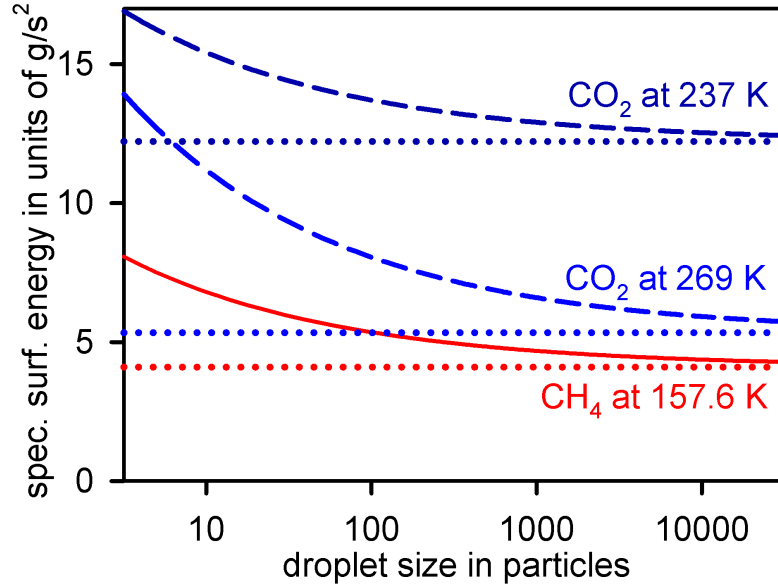


Figure 2.4: Dependence of the specific surface energy F_s on the droplet size v for methane (solid lines) and carbon dioxide (dashed lines) at a chemical potential supersaturation ratio $S_\mu = 1.2$ for different temperatures, according to LFK theory; dotted lines: surface tension of the planar interface, used in CNT and $\text{CNT}^{\Delta\mu}$ to approximate the specific surface energy.

2.2 Curved interfaces in equilibrium

Phase coexistence methods are an established approach for obtaining equilibrium data from molecular simulation [271]. As *Farkas* [172] pointed out, for a system with N particles composed of a droplet containing v and a supersaturated vapor containing $N - v$ particles, an equilibrium between the droplet and the supersaturated vapor corresponds to the condition $v = v^*(T, S_\mu)$.

Thus, the equilibrium droplet is a critical droplet. This consideration can be applied to obtain properties of the critical droplet based on CNT [272].¹² It is also of central relevance for the EMLD model¹³ of *Reguera et al.* [198] and its application to nucleation theory [273, 274]. In equilibrium, the transition rate \mathcal{T} of vapor monomers through the droplet surface per interface area equals the monomer emission rate \mathcal{E} of the droplet [263]

$$\mathcal{T}(T, S_\mu) = \mathcal{E}(T, v^*). \quad (2.38)$$

On the basis of this condition, the monomer emission rate can be obtained directly from the kinetic gas theory once the size of the critical droplet is known, without introducing any assumptions about the internal structure of the droplet and the shape of its surface [275].

¹²Note that for the more common versions of the classical approach, which neglect the pressure effect, this would necessarily lead to inaccurate and inconsistent conclusions. On the basis of the present considerations, it can for instance be deduced from $\text{CNT}^{\Delta\mu}$ that the critical droplet has a different chemical potential than the surrounding supersaturated vapor, although both phases are also known to be in equilibrium under these conditions.

¹³*Reguera et al.* [198] remark that «a stable cluster in a N, V, T system corresponds to the critical cluster in an open (μ, V, T) system at the corresponding supersaturation. . . in a confined system, since the total number of molecules N is fixed, the growth of the droplet causes depletion of vapor molecules . . . Eventually the drop assumes an equilibrium size and coexists with the vapor in accordance with the Kelvin relation».

However, the same configuration of a system that includes a curved vapor-liquid interface can be in a stable or an unstable equilibrium, depending on the boundary conditions. As pointed out by Lovett [276], the fact that a critical droplet «can only be in (stable) equilibrium with a supersaturated vapour in a system with a finite (small) volume» makes these small systems, where «the thermodynamic analysis is straightforward and the configurations are easily simulated», an attractive topic for molecular simulation. Beginning with the work of Lee *et al.* [277], who investigated the free energy of formation for LJ clusters by MC simulation, the scenario of a droplet surrounded by supersaturated vapor is often found in the literature and the emphasis usually lies on equilibrium conditions [85, 87, 197, 278, 279].

Such an approach leads to more accurate data on the critical droplet, e.g. its size l^* or surface tension γ^* , than observing growth and decay of droplets by non-equilibrium MD simulation [280, 281]. It permits sampling critical droplet properties over a large number of time steps so that any desired level of accuracy is eventually reached. Simulation of critical droplets in equilibrium is also computationally efficient since only small systems have to be considered.

According to the *Gibbs* approach to phase coexistence [18, 19], the entire volume is discretely divided between the two phases. The sub-volumes are separated by the dividing surface, a *formal* interface that does not occupy any volume.¹⁴ The thermodynamic properties of the entire system are composed by the respective bulk contributions, corresponding to the homogeneous phases, and an excess term that *formally* characterizes the surface contribution, e.g.

$$N_A = V' \rho'_A + V'' \rho''_A + N_A^F, \quad (2.39)$$

which defines the excess number of particles N_A^F belonging to component \mathcal{A} that are adsorbed to the interface. The *Gibbs* adsorption (or equimolar) radius R_ρ is defined by a sphere around the center of mass of the droplet which divides the system into volumes $V' = 4\pi R_\rho^3/3$ and $V'' = V - V'$ such that the excess number of particles becomes zero

$$3(N - V\rho'') = 4\pi R_\rho^3(\rho' - \rho''). \quad (2.40)$$

The approximation

$$R_\rho \approx \left(\frac{3l}{4\pi\rho'} \right)^{1/3}, \quad (2.41)$$

can be applied with high accuracy in this case to obtain the adsorption radius. Furthermore, the surface of tension radius R_γ can for the present purposes be defined by

$$R_\gamma = \frac{2}{\rho_i} \left(\frac{\partial l}{\partial F} \right)_{N,V,T}, \quad (2.42)$$

while the *Laplace* equation

$$\gamma = \frac{1}{2} R_{\mathcal{L}} (p_i - p), \quad (2.43)$$

can also be understood as the definition of a characteristic radius [85]: the *Laplace* radius $R_{\mathcal{L}}$.

If the condition that defines the formal dividing surface is varied, the more general *Kondo* equation [190]

$$\gamma_C + \frac{\partial \gamma_C / \partial C}{2 \partial \ln R_C / \partial C} = \frac{1}{2} R_C (p_i - p), \quad (2.44)$$

¹⁴ «Let us take some point in or very near to the physical surface of discontinuity, and imagine a geometrical surface to pass through this point and all other points which are similarly situated» [18].

has to be applied instead of the *Laplace* equation. Therein, C is the *condition* defining a radius R_C as well as an interfacial area with

$$F_C \sim R_C^2. \quad (2.45)$$

Accordingly, the surface tension γ_C is obtained by

$$\gamma_C = \left(\frac{\partial A_F}{\partial F_C} \right)_C. \quad (2.46)$$

The condition C must be defined over a closed subset of \mathbb{R} and all excess properties related to the formal dividing surface must be differentiable with respect to C so that the partial derivatives¹⁵ $\partial\gamma_C/\partial C$ as well as $\partial R_C/\partial C$ are well-defined. Furthermore, C must be sufficiently realistic to permit the definition of γ_C by the partial derivative from Eq. (2.46).¹⁶

The evident similarity of the *Laplace* equation and the *Kondo* equation, cf. Eqs. (2.43) and (2.44), suggests a comparison of these expressions for the special case of $R_C = R_{\mathcal{L}}$ with $\gamma_C = \gamma$. This apparently yields

$$\left(\frac{\partial \gamma_C}{\partial C} \right) = 0, \quad (2.47)$$

which might be interpreted as proving that the formal surface tension γ_C , defined by Eq. (2.46), becomes minimal if the *Laplace* equation is chosen as the condition defining the radius of the formal dividing surface [190, 282, 283].

However, apart from the obvious condition for the second partial derivative which can also be proven using that approach [190], this conclusion relies on a further implicit assumption. Note that for the special case under consideration, i.e. $\gamma_C = \gamma$, a relation between the *surface tension* and the interface area of the corresponding *surface of tension* is already given by the thermodynamic definition of the surface tension, cf. Eq. (2.13). This is now combined with the *Laplace* equation, which relates the *radius* to the *surface tension*, cf. Eq. (2.43). Hence, the relation between the *radius* and the *surface of tension* is no longer a matter of choice, i.e. it cannot simply be declared proportional to R_C^2 , cf. Eq. (2.45).

The validity of Eq. (2.47) therefore actually depends on an additional non-trivial precondition, namely

$$\frac{1}{F} \left(\frac{\partial F}{\partial i} \right)_{N,V,T} = \frac{2}{R_{\mathcal{L}}} \left(\frac{\partial R_{\mathcal{L}}}{\partial i} \right)_{N,V,T}, \quad (2.48)$$

i.e. the differential form of Eq. (2.45), which merits a brief but independent discussion in its own right. The free energy of formation for a droplet can be expressed as

$$\left(\frac{\partial A}{\partial i} \right)_{N,V,T} = \left(\frac{\partial A_F}{\partial i} \right)_{N,V,T} + (\mu_i - \mu) - \frac{\Delta p}{\rho_i}, \quad (2.49)$$

according to Eqs. (2.12) and (2.17), with $\Delta p = p_i - p$, while from the definition of the surface of tension radius, cf. Eq. (2.42), an additional relation, i.e.

$$\left(\frac{\partial A_F}{\partial i} \right)_{N,V,T} = \frac{2\gamma}{R_{\gamma\rho_i}}, \quad (2.50)$$

¹⁵Note that these derivatives are taken only with respect to the condition C defining the surface, i.e. without changes in the actual physical configuration. The present remark applies to Eq. (2.47) as well.

¹⁶In the referenced article [190], these demands are met informally by applying a bijection between C and R_C so that in all cases, the radius can be varied instead of the condition defining the radius.

follows for the surface contribution to the free energy. For a droplet in equilibrium with a supersaturated vapor, the chemical potential must be invariant across the phase boundary. This is obvious for stable equilibria, and since a stable equilibrium can be converted to an unstable equilibrium by increasing N and V at constant density, pressure, and chemical potential of the vapor as well as the droplet, it must be valid for critical droplets in general. In particular, this implies that μ is the same as μ^* , i.e. the value of μ_i for $i = i^*(T, \mu)$.

By inserting Eqs. (2.43), (2.49), and (2.50) into the equilibrium criterion $\partial A/\partial i = 0$, it follows¹⁷ that the *Laplace* radius and the surface of tension radius are equal

$$\begin{aligned} \frac{2\gamma}{R_\gamma \rho_i} - \frac{2\gamma}{R_{\mathcal{L}} \rho_i} &= 0, \\ R_\gamma &= R_{\mathcal{L}}, \end{aligned} \quad (2.51)$$

whereby it is established that Eq. (2.42) actually *is* a viable definition of the surface of tension radius. By applying the definitions of the differential droplet density, cf. Eq. (2.7), as well as the surface of tension radius, cf. Eq. (2.42), the ratio

$$\frac{R_{\mathcal{L}}}{F} \frac{\partial F/\partial i}{\partial R_{\mathcal{L}}/\partial i} = \frac{2}{F} \left(\frac{\partial V_i}{\partial R_{\mathcal{L}}} \right)_{N,V,T}, \quad (2.52)$$

is obtained, while it would have to be 2 if Eq. (2.48) was valid.¹⁸ This would, however, imply

$$F \partial R_\gamma = \partial V_i \approx F \partial R_\rho, \quad (2.53)$$

a proposition which is contradicted by the known deviation between the surface of tension radius R_γ and the equimolar radius R_ρ on the molecular length scale [174]. In fact, the *Tolman* length [174], defined by

$$\delta = R_\rho - R_\gamma, \quad (2.54)$$

is often understood as the characteristic dimension of a phase boundary with respect to the direction normal to the interface. The present preliminary discussion can therefore be summarized by the following statements:

- A) The *Laplace* radius is not proportional to the square root of the surface of tension F , and therefore Eqs. (2.45) and (2.48) do not hold, for systems with a non-zero *Tolman* length.
- B) A condition C which defines R_C by $R_{\mathcal{L}}$, i.e. according to Eq. (2.43), while the surface tension $\gamma_C = \gamma$ is related to the surface area $F_C = F$ by Eq. (2.13), does not generally yield the lowest possible value of γ_C .

The corresponding results claimed by previous authors [190, 282, 283], cf. Eqs. (2.44) and (2.47), can be shown to rely on Eq. (2.48) which is not valid in most cases.

- C) The *Laplace* radius $R_{\mathcal{L}}$ is, however, identical with the surface of tension radius R_γ as defined by Eq. (2.42).

¹⁷Formally, this conclusion is only valid for vapor-liquid interfaces in equilibrium. However, it should be noted that the *Laplace* equation is itself derived from an equilibrium of forces so that it cannot be applied to non-equilibrium states, neither as a definition of $R_{\mathcal{L}}$ nor for other purposes. From a methodological point of view, it is therefore more adequate to view R_γ , defined according to Eq. (2.42), as a *generalization* of the *Laplace* radius.

¹⁸Here it is expedient to point out that V_i is the volume of the droplet whereas V refers to the whole system.

D) The actual relation between $R_{\mathcal{L}}$ and the interfacial area of the surface of tension F can be obtained by integrating Eq. (2.52).

The *Tolman* [174, 187] approach to curved interfaces is based on the application of axiomatic thermodynamics to excess quantities of an effective dividing surface as discussed by *Gibbs*. Thereby, the *Laplace* equation, cf. Eq. (2.43), is combined with the *Gibbs-Duhem* equation, cf. Eq. (2.2), for both coexisting phases, as well as the *Gibbs* adsorption equation

$$d\gamma = -\Gamma d\mu, \quad (2.55)$$

where Γ represents the interfacial excess density associated with the surface of tension, i.e. a quantity that is expressed in units of mol/m² or σ^{-2} . That yields [174]

$$\left(\frac{\partial 2\gamma}{\partial \gamma R_{\gamma}} \right)_T = -\frac{\Delta\rho}{\Gamma}, \quad (2.56)$$

in terms of the density difference $\Delta\rho$ between the coexisting phases, which leads to

$$\left[\left(\frac{\partial \ln R_{\gamma}}{\partial \ln \gamma} \right)_T - 1 \right]^{-1} = \frac{2\delta}{R_{\gamma}} + \frac{2\delta^2}{R_{\gamma}^2} + \frac{2\delta^3}{3R_{\gamma}^3}, \quad (2.57)$$

by further algebraic transformations. The *Tolman* length δ , related to the interfacial excess density by [174]

$$\frac{\Gamma}{\delta\Delta\rho} = 1 + \frac{\delta}{R_{\gamma}} + \frac{1}{3} \left(\frac{\delta}{R_{\gamma}} \right)^2, \quad (2.58)$$

is known to be positive for the surface of a droplet, because the pressure decay occurs further inside the droplet than the density decay [85]. The *Tolman* equation

$$\frac{\gamma_{\infty}}{\gamma} = 1 + \frac{2\delta}{R_{\gamma}} + \mathcal{O}(R_{\gamma}^{-2}), \quad (2.59)$$

is a simplification of Eq. (2.57) which relates δ to the curvature dependence of the surface tension, in accordance with the considerations of *Kirkwood* and *Buff* [188, 282, 284].

Although *Tolman* [174] considered the possibility that δ could itself depend on the droplet radius, he proposed to disregard this dependence.¹⁹ Since the *Tolman* equation is an expansion in terms of the curvature, describing the deviation from the zero curvature surface tension, the accurate value for δ to be consistently used is the planar interface *Tolman* length δ_{∞} which is reached in the limit $R_{\gamma} \rightarrow \infty$.²⁰ By applying the capillarity approximation, cf. Eq. (2.41), *Tolman's* first-order curvature expansion then transforms to

$$\frac{\gamma}{(3\nu/4\pi\rho')^{1/3} - \delta_{\infty}} = \frac{\gamma_{\infty}}{(3\nu/4\pi\rho')^{1/3} + \delta_{\infty}}, \quad (2.60)$$

if the higher-order terms are neglected.

¹⁹«In the application . . . , we shall . . . treat δ as a constant. At the present stage of theory, we could hardly hope to make a reliable computation of the dependence of δ on droplet size, but can conclude that δ will be reasonably constant over a wide range of droplet sizes since it measures the distance between two surfaces whose separation is presumably closely connected with intermolecular distances in the liquid» [174].

²⁰For this observation, the author is indebted to *Srikanth Sastry* (Bengalūru).

Regarding the dependence of the critical quantities on the chemical potential of the super-saturated vapor, the identity

$$\left(\frac{\partial i^*}{\partial \mu}\right)_T = \left(\frac{\partial i}{\partial \mu_i}\right)_T \Big|_{\mu_i=\mu} = \left(\frac{i \partial i}{V_i \partial p_i}\right)_T \Big|_{p_i=p}, \quad (2.61)$$

follows immediately from the *Gibbs-Duhem* equation, cf. Eq. (2.18), as well as the equality of the chemical potential in equilibrium. If the *Laplace* equation is also applied, it follows that

$$\left(\frac{\partial \mu}{\partial i^*}\right)_T = \frac{V_i}{i} \left(\frac{\partial}{\partial i} \left[p_s(i, T) + \frac{2\gamma_i}{R_{\mathcal{L}}} \right]\right)_T \Big|_{i=i^*}, \quad (2.62)$$

and by inverting the *Gibbs-Duhem* integration for the contribution of the vapor pressure $p_s(i^*, T) = p$, one finally obtains

$$\left(\frac{\partial i^*}{\partial \mu}\right)_T = 2 \left(\frac{\partial \gamma_i}{\partial i R_{\mathcal{L}}}\right)_T^{-1} \left(1 - \frac{\rho V_i}{i}\right) \Big|_{i=i^*}. \quad (2.63)$$

The free energy barrier in the thermodynamic limit formally depends on μ according to the expression

$$\begin{aligned} \left(\frac{\partial A^*}{\partial \mu}\right)_T &= \left(\frac{\partial A_i}{\partial \mu}\right)_T \Big|_{i=i^*} \\ &+ \left(\frac{\partial A_i}{\partial i}\right)_{\mu, T} \Big|_{i=i^*} \left(\frac{\partial i^*}{\partial \mu}\right)_T. \end{aligned} \quad (2.64)$$

The second contribution disappears since $\partial A/\partial i = 0$ at the critical droplet size, and with Eqs. (2.23), (2.49), and (2.50) it follows that²¹

$$\frac{\partial A^*}{\partial \mu} = \frac{\partial}{\partial \mu} \int_1^{i^*} \left(\frac{\partial A_i}{\partial i}\right)_{\mu} di \quad (2.65)$$

$$= \int_1^{i^*} \frac{\partial}{\partial \mu} \left[\frac{2\gamma}{\rho_i R_{\mathcal{L}}} - \frac{\Delta p}{\rho_i} + \mu_i - \mu \right] di, \quad (2.66)$$

holds for a constant temperature. Using *Gibbs-Duhem* integration and the *Laplace* equation, the partial derivative for the chemical potential inside the droplet μ_i becomes

$$\frac{\partial \mu_i}{\partial \mu} = \frac{\partial(p + \Delta p)}{\rho_i \partial \mu}, \quad (2.67)$$

so that Δp cancels out in Eq. (2.66). One can then insert $(\partial p/\partial \mu)_T = \rho$ and by neglecting the supersaturation dependence of the surface energy, i.e. in the present context by assuming for $i = i^*$ that

$$\left| \frac{\partial A_F(i)}{\partial \mu} \right| \ll \left| \frac{\partial A^*}{\partial \mu} \right|, \quad (2.68)$$

²¹The free energy of formation can be integrated at constant chemical potential of the vapor because it was assumed above that the critical droplet is formed in the thermodynamic limit of a relatively large system where droplet growth does not affect the properties of the bulk vapor.

cf. Eq. (2.50), the expression for the free energy barrier from Eq. (2.66) simplifies to

$$\left(\frac{\partial A^*}{\partial \mu}\right)_T = \left(1 - \frac{1}{v^*}\right) (\rho V_i - v^*). \quad (2.69)$$

This equation is called the *nucleation theorem*. It relates the critical droplet size to the supersaturation dependence of the free energy barrier. Various forms of the nucleation theorem were presented by *Oxtoby* and *Kashchiev* [285] as well as subsequent authors [286–289]. The most popular variants also neglect the pre-exponential contribution to the nucleation rate, relating it only to the free energy barrier [290]. This permits the determination of the critical droplet size from the slope of J over S_μ in a double-logarithmic plot

$$v^* \approx \left(\frac{\partial \ln J}{\partial \ln S_\mu}\right)_T \left(1 - \frac{\rho}{\rho'}\right)^{-1} + 1. \quad (2.70)$$

Note that CNT and its usual modifications assume the surface energy to be entirely independent of the supersaturation [261, 269] so that Eq. (2.68) and therefore the nucleation theorem as given by Eq. (2.69) should actually be valid in most cases.

Less confidence can be placed in Eq. (2.70) and similar variants of the nucleation theorem in the vicinity of the spinodal line, because there can be a significant pre-exponential contribution to $(\partial \ln J / \partial \ln S)_T$. However, this remark does not extend to experimental results far from the spinodal line, where that approximation is in fact sufficiently accurate. The actual difficulty in these cases rather consists in obtaining reliable values for both the derivative of $\ln J$ and the supersaturation with respect to the chemical potential.

For the simulation of vapor-droplet equilibria it is crucial to choose the relation of the

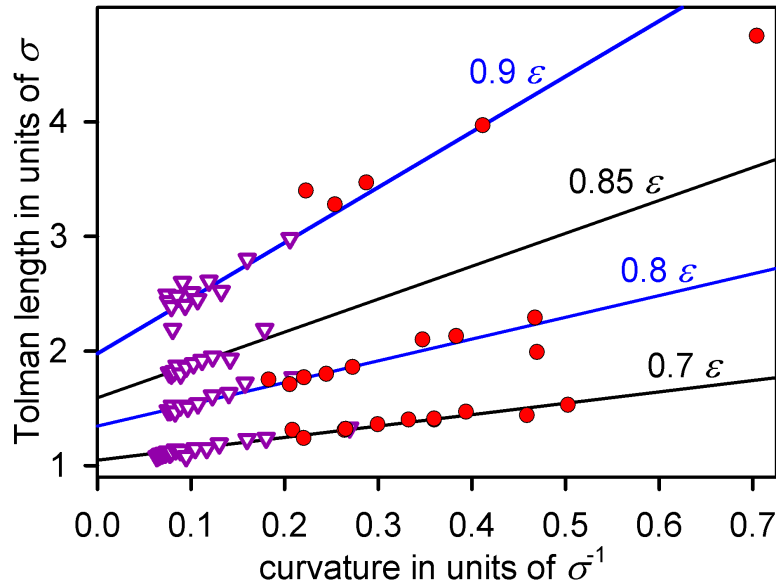


Figure 2.5: Tolman length δ of droplets over the curvature of the surface of tension R_γ^{-1} determined by canonical ensemble equilibrium MD simulation of the LJ-TS fluid, (●) from the present work and (▽) from a previous study [85], in comparison with a linear correlation (solid lines), cf. Eqs. (2.71) and (2.72).

number of particles in the droplet to the total number of particles in the system appropriately.²² The liquid fraction must be relatively large so that changes in droplet size significantly affect the density of the surrounding vapor and the droplet cannot evaporate completely due to the increase of the vapor density.

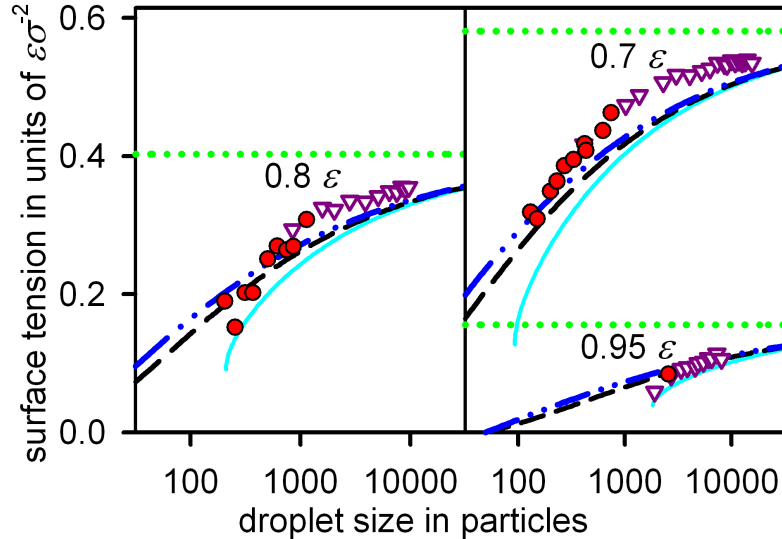


Figure 2.6: Surface tension of the LJ-TS fluid over droplet size determined by canonical ensemble equilibrium MD simulation with the *Irving-Kirkwood* pressure tensor [189], (●) from the present work and (▽) from a previous study [85]. The horizontal dotted lines represent the surface tension of the planar vapor-liquid interface which is also the droplet surface tension assumed by CNT. Furthermore, three variants of the *Tolman* equation are compared with the simulation results: the full relation between curvature and surface tension, cf. Eq. (2.57), where Eqs. (2.71) and (2.72) are used to correlate δ (solid lines); the full relation, cf. Eq. (2.57), with the *Tolman* length approximated by $\delta = \delta_\infty(T)$ as proposed by *Tolman* [174], using Eq. (2.71) to correlate δ_∞ (dashed lines). The *Tolman* equation truncated after its first-order contribution in terms of the curvature, cf. Eq. (2.60), using the planar interface *Tolman* length (dashed-dotted lines). For the present purpose, the equimolar radius R_ρ is related to the number of particles ν in the droplet by Eq. (2.41) and to the surface of tension radius R_γ by Eq. (2.54).

Complementing data from a previous study [85], vapor-droplet equilibrium MD simulations were conducted for small systems (total number of particles $N < 2 \cdot 10^4$) here to obtain properties of the critical droplet at moderate supersaturation ratios. Droplets with $10^2 < \nu < 10^4$ particles were inserted into saturated or moderately supersaturated vapor phases. The droplet size was evaluated by applying a version of the cluster criterion of *ten Wolde* and *Frenkel* [291] cluster criterion with a connectivity radius of $R_\ell = 1.5 \sigma$ and $j = 4$ required neighbors. These parameter values were chosen in order to remain consistent with previous results [85].

A «reliable computation» [174] of δ , while hard to achieve in 1949, can now easily be conducted by molecular simulation. By sampling curved vapor-liquid interfaces in equilibrium, the *Tolman* length was found to depend linearly on curvature down to extremely small droplet sizes, cf. Fig. 2.5. By extrapolation, the planar interface value of δ for the LJ-TS fluid can be

²² *Reguera et al.* [198] noted «that beyond a particular volume, which can be called the *evaporation boundary* ... the coexistence equation no longer has a solution. This means that we cannot have a droplet coexisting with its vapor in a big closed container.»

Table 2.2: Supersaturation dependence of the surface tension γ^* (in units of $\varepsilon\sigma^{-2}$) and the size i^* (in number of particles) of the critical droplet from canonical ensemble equilibrium MD simulation of the LJ-TS fluid, applying the *Irving-Kirkwood* pressure tensor [189] at temperatures of 0.65, 0.85, and 0.95 ε , in comparison with theoretical predictions for i^* on the basis of full CNT as described above and CNT without the pressure effect as well as LFK theory. The supersaturation is given in terms of the chemical potential supersaturation ratio S_μ . The approach used to fit the density and normal pressure profiles [85] could not be consistently applied to the MD simulation run corresponding to the results shown in the last line, so that in this case no value can be given for the surface tension.

$T\varepsilon^{-1}$	S_μ	γ^*	i^*	$i^*(\text{CNT})$	$i^*(\text{CNT}^{\Delta\mu})$	$i^*(\text{LFK})$
0.65	1.436	0.590	1270	1250	1230	1240
	1.453	0.572	1080	1130	1110	1120
	1.483	0.578	1030	968	949	956
	1.559	0.553	689	677	664	667
	1.563	0.563	720	665	652	655
	1.758	0.501	342	331	324	325
	1.797	0.527	246	295	289	290
0.85	1.122	0.222	2220	2710	2340	2980
	1.179	0.202	839	933	800	1060
	1.198	0.224	1320	708	606	814
	1.201	0.187	992	680	582	783
	1.206	0.157	676	636	544	734
	1.261	0.127	449	337	287	399
	1.302	0.031	17.0	230	236	276
	1.318	0.072	253	201	170	243
0.95	1.067	0.084	2550	2100	1450	2820
	1.070	0.059	1900	1850	1280	2510
	1.087	—	1060	996	682	1420

correlated using the expression

$$\delta_\infty(T) = 0.22 + \frac{0.29\sigma}{1 - T/T_c}, \quad (2.71)$$

while the curvature dependence is described by

$$\frac{[\delta(T, R_\gamma) - \delta_\infty(T)] R_\gamma}{0.110\sigma^2} = \left(1 - \frac{T}{T_c}\right)^{-2.10}. \quad (2.72)$$

Surface tension and size of the critical droplet were determined for six temperatures in the range between 0.65 and 0.95 ε . The surface tension was computed here by following a virial route, based on the *Irving-Kirkwood* pressure tensor [189] which was first applied to (spherical) interfaces by *Buff* [282]. Its normal component is given by [189, 293]

$$p_n(r) = T\rho(r) + \sum_{\{i,j\} \in \mathbb{F}(r)} -\frac{du_{ij}}{dr_{ij}} \frac{|\mathbf{x} \cdot \mathbf{r}_{ij}|}{4\pi r^3 r_{ij}}, \quad (2.73)$$

Table 2.3: Supersaturation dependence of the size ι^* (in number of particles), the surface of tension radius R_γ (in units of σ), the *Tolman* length δ (in units of σ), and the surface tension γ^* (in units of $\varepsilon\sigma^{-2}$) of the critical droplet from canonical ensemble equilibrium MD simulation of the LJ-TS fluid at temperatures of 0.7, 0.8, and 0.9 ε . The quantities R_γ , δ , and γ^* are obtained by evaluating the normal pressure following the *Irving-Kirkwood* approach [189]. The surface tension is also evaluated according to the *Tolman* equation truncated after its first term, cf. Eq. (2.59), using the actual value of δ as well as the correlated value for the *Tolman* length of the planar vapor-liquid interface δ_∞ . The supersaturation is given in terms of the chemical potential supersaturation ratio S_μ .

$T\varepsilon^{-1}$	S_μ	ι^*	R_γ	δ	γ^*	$\gamma^*(\delta)$	$\gamma^*(\delta_\infty)$
0.7	1.432	739	4.81	1.31	0.463	0.379	0.408
	1.446	621	4.54	1.24	0.437	0.378	0.400
	1.524	232	2.78	1.40	0.364	0.292	0.334
	1.530	422	3.76	1.32	0.418	0.344	0.376
	1.543	329	3.33	1.36	0.395	0.322	0.359
	1.561	425	3.79	1.31	0.408	0.346	0.377
	1.644	274	3.01	1.40	0.386	0.303	0.345
	1.647	229	2.78	1.41	0.363	0.290	0.334
	1.726	134	1.99	1.53	0.319	0.231	0.285
	1.757	201	2.54	1.47	0.349	0.271	0.321
1.770	147	2.18	1.44	0.309	0.252	0.298	
0.8	1.212	1130	5.47	1.75	0.308	0.246	0.270
	1.249	856	4.87	1.71	0.269	0.237	0.260
	1.249	750	4.53	1.77	0.264	0.226	0.253
	1.289	612	4.10	1.80	0.270	0.215	0.244
	1.300	503	3.66	1.86	0.251	0.200	0.233
	1.372	367	2.88	2.10	0.202	0.164	0.209
	1.372	205	2.13	1.99	0.190	0.140	0.178
	1.394	313	2.62	2.13	0.202	0.154	0.199
	1.415	254	2.15	2.29	0.152	0.129	0.179
	1.415	254	2.15	2.29	0.152	0.129	0.179
0.9	1.134	1370	4.49	3.40	0.132	0.0935	0.125
	1.145	932	3.48	3.47	0.118	0.0785	0.110
	1.147	1040	3.94	3.28	0.139	0.0882	0.117
	1.162	650	1.42	4.75	0.0328	0.0306	0.0621
	1.179	744	2.43	3.97	0.0869	0.0551	0.0895

where $\rho(r)$ is the local density and the summation covers the set $\mathbb{F}(r)$ containing all unordered pairs of molecules i and j that are connected by a line intersecting the sphere of radius r around the center of mass. Intersection coordinates (relative to the center of mass of the liquid drop) are given by \underline{x} and the distance between the molecules is expressed by r_{ij} as well as \underline{r}_{ij} , while $-du_{ij}/dr_{ij}$ is the force acting between i and j . On this basis, the surface tension was determined as [293]

$$(2\gamma)^3 = -\Delta p^2 \int_{r=0}^{r=\infty} dp_n(r) r^3. \quad (2.74)$$

The results are shown in Tabs. 2.2 and 2.3 as well as in Figs. 2.6 and 2.7. The planar interface surface tension γ_∞ of the LJ-TS fluid [85]

$$\frac{\gamma_\infty \sigma^2}{\varepsilon} = 2.08 \left(1 - \frac{T}{T_c}\right)^{1.21}, \quad (2.75)$$

with $T_c = 1.0779 \varepsilon$, is represented by horizontal lines in Fig. 2.6. Clearly, the surface tension is significantly reduced for small droplets when compared to γ_∞ . This contradicts the results of several studies based on density functional theory where a maximum of γ over the droplet size was obtained [294–296].

Concerning the virial route to the surface tension, however, various issues remain to be settled as well:

- It is not clear to what extent the spherical average of the pressure tensor succeeds in accounting for the free energy contribution of capillary waves, i.e. the excited vibrational modi of the interface [297, 298].
- *Irving and Kirkwood* originally proposed their expression for the special case of «a single component, single phase system» [189]. Its derivation relies on truncating an expansion

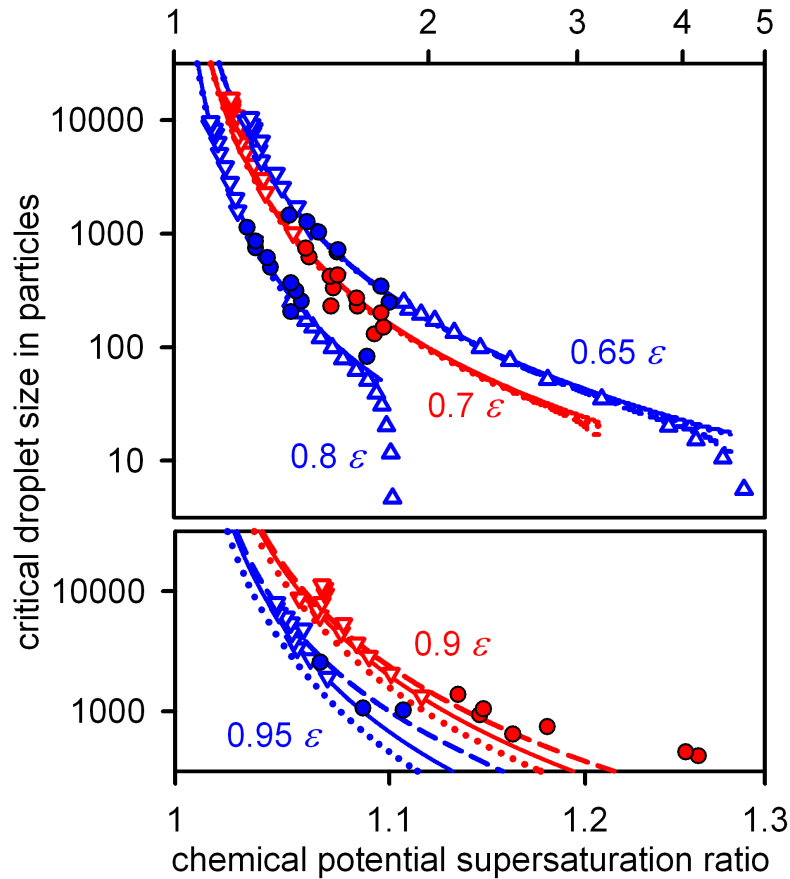


Figure 2.7: Critical droplet size v^* of the LJ-TS fluid over the supersaturation ratio S_μ in terms of the chemical potential, (\bullet) from the present work, (∇) from a previous study [85], (\triangle) according to *Napari et al.* [292], and following CNT (solid lines), CNT without the pressure effect (dotted lines) as well as LFK theory (dashed lines).

in terms of derivatives of the pairwise density $\rho^{(2)}$ after the first term, which is equal to $\rho^{(2)}$, thereby disregarding the density gradient completely. For a droplet, this can lead to inaccuracies: «at a boundary or interface . . . neglecting terms beyond the first may not be justified» [189].

- By construction, the virial route cannot be separated from the assumption of a mechanical equilibrium that underlies both the basic approach and the derivation of the pressure tensor. For nanoscopic droplets, however, configurations deviating from the equilibrium shape correspond to a significant fraction of the partition function.

Inserting the δ_∞ values from Eq. (2.71) into Eq. (2.60) leads to a theoretical description that excellently matches the simulation results on the curvature dependence of γ , cf. Tab. 2.3 and Fig. 2.6, considering that therein, no parameters were adjusted to the surface tension of droplets at all. This underlines the internal consistency of the *Tolman* approach.

2.3 Fluid-wall contact

The interaction between a solid wall and a fluid in immediate contact with the wall affects static and dynamic properties of the fluid in several ways. For instance, a local ordering with density minima and maxima at characteristic distances from the wall is induced, leading to *adsorption*, i.e. a change of the total number of fluid molecules which is proportional to the surface area, cf. Eq. (2.39). If there is a free energy difference between a section of the surface area covered by liquid and a section covered by vapor, the *contact angle* between the wall and a vapor-liquid interface is not rectangular. Instead, the area of the vapor-liquid phase boundary is increased such that the overall free energy of the system reaches a minimum. By MD simulation, these phenomena can be reliably investigated on a molecular basis.

Adsorption has a high technical relevance, since it can e.g. be used for drying and purification [125, 299–301]. Micro- and nanoporous adsorbents such as activated carbon are of particular interest here because of their relatively large surface area. For relevant technical applications, the regeneration of the adsorbent by desorption is as important as adsorption itself, and it is crucial to know the adsorption isotherms to optimize these processes. A molecular theory of adsorption was first proposed by *Langmuir* [302] who assumed that a single layer of vapor monomers can be adsorbed on a solid surface. The rate at which monomers are adsorbed is $E\mathcal{T}\alpha_{\text{ad}}$, where E is the empty fraction of the surface, \mathcal{T} is the monomer transition rate given by the *Hertz-Knudsen* equation, cf. Eq. (2.25), and α_{ad} is the *Langmuir* adsorption constant, which is usually assumed to be pressure independent. The monomer emission rate from the solid surface is assumed to be proportional to $1 - E$, reaching a magnitude of \mathcal{E}_1 for a fully covered surface. In equilibrium, therefore [302]

$$E\mathcal{T}\alpha_{\text{ad}} = (1 - E)\mathcal{E}_1, \quad (2.76)$$

holds while

$$\frac{1}{E} = \frac{\mathcal{T}\alpha_{\text{ad}}}{\mathcal{E}_1} + 1, \quad (2.77)$$

characterizes the vacant fraction of the surface. Both α_{ad} and \mathcal{E}_1 are temperature-dependent quantities. The *Langmuir* adsorption constant is always smaller than 1 and decreases somewhat with increasing T , but the major contribution to the temperature dependence is due to \mathcal{E}_1 which is roughly proportional to the saturated vapor pressure of the fluid as long as no substantial changes occur to the surface structure or the interaction between the fluid and the solid. At high pressures, multi-layer adsorption can also occur, which is qualitatively covered by the *Brunauer-Emmett-Teller* theory [303].

In the present study, fluid-wall contact is considered for pure fluids only, which eliminates the main technical application of adsorption and desorption. However, vapors in contact with a solid often exhibit one or more adsorbed layers, and all fluids are locally ordered in the vicinity of a wall. Therefore, adsorption as a basic effect is of preeminent importance here as well.

For the three-phase contact between a vapor-liquid interface and a planar substrate, i.e. a solid wall, the contact angle ϑ is given by the *Young* equation [304]

$$\cos \vartheta = \frac{\Delta\gamma_s}{\gamma}, \quad (2.78)$$

wherein γ is the surface tension acting at the interface between the vapor and the liquid phase, while $\Delta\gamma_s$ indicates the difference between the specific surface energies of the substrate when it

is in contact with the vapor and the liquid, respectively. The sign of $\Delta\gamma_s$ is positive, i.e. partial or perfect wetting occurs, if the surface tension between the solid and the vapor exceeds the specific surface energy for the sections of the substrate covered by liquid.²³

Using the density functional theory, *Teletzke et al.* [305] examined the dependence of wetting and drying transitions on characteristic size and energy parameters of the fluid-wall dispersive interaction. Subsequently, *Sokołowski and Fischer* [306] as well as *Giovambattista et al.* [307] investigated fluid density profiles in extremely narrow channels for several values of the fluid-wall dispersive energy and surface polarity, respectively. On the microscopic and nanoscopic level, the statics and dynamics of fluids under confinement and the corresponding three-phase contact lines can for instance be studied using the lattice *Boltzmann* method [308, 309].

MD simulation can be applied to this problem as well, leading to a consistent molecular approach.²⁴ A suitable way of calculating the contact angle of a fluid on a solid substrate by MD simulation regards a liquid slab between two parallel planes, in coexistence with its own vapor. This has the advantage that at least for a contact angle of 90° the curvature of the fluid phase boundary is zero, whereas for a bubble or a droplet the surface of tension radius is necessarily limited by the simulated droplet volume, leading to an extremely high curvature and a corresponding modification of interface properties. Moreover, by applying a periodic boundary condition to obtain a cylindrically shaped interface, cf. Fig. 2.8, one of the curvature radii can be extended to infinity.

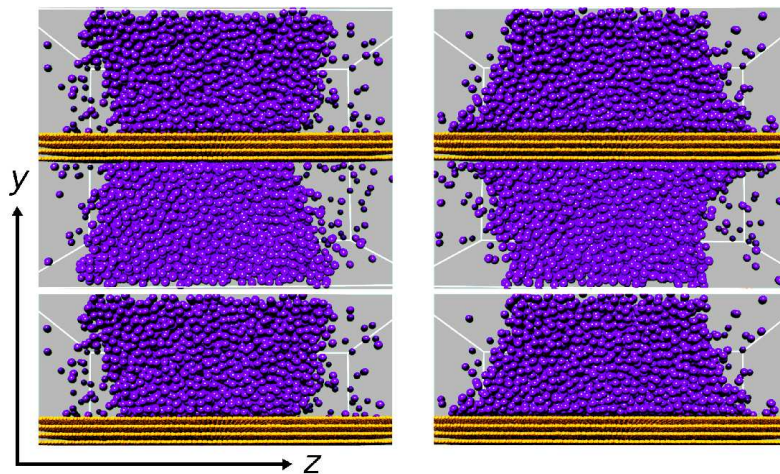


Figure 2.8: Simulation snapshots for the reduced fluid-wall dispersive energy ζ of 0.09 (left) and 0.16 (right) at a temperature of 0.73ε . The upper half is reproduced in the bottom to illustrate the effect of the periodic boundary condition.

A layered wall was represented here by a comparably straightforward system of coupled harmonic oscillators, using different spring constants for the transverse vibration with respect

²³Note that since only planar substrates are considered here, the specific surface energy (which is an integral quantity) and the surface tension (a differential quantity) are the same as far as sections of the wall are concerned. For the discussion of curved surfaces, which is restricted to the contact between fluid phases in the present treatment, this is of course not the case and γ cannot be equated with F , since a growth of the surface area in these cases does not occur at a constant surface of tension radius.

²⁴The author would like to thank Martina *Heitzig* for carrying out the simulation work discussed here.

to the layers

$$u_i^Y(Y_i) = \frac{\kappa^Y}{2}(Y_i - Y_i^\circ)^2, \quad (2.79)$$

wherein Y_i° is the equilibrium value of the Y coordinate, and longitudinal oscillations,

$$u_{ij}^{XZ}(r_{ij}) = \frac{\kappa^{XZ}}{2}(r_{ij} - \mathcal{D})^2, \quad (2.80)$$

with respect to the equilibrium bond length \mathcal{D} between neighboring wall atoms i and j . The fluid under investigation was the LJ-TS model, and the fluid-wall interaction was represented by the LJ-TS potential with $\sigma_{\text{fw}} = \sigma$, while

$$\varepsilon_{\text{fw}} = \zeta\varepsilon, \quad (2.81)$$

was systematically varied, whereby the same cutoff radius $r_c = 2.5\sigma$ was used for the fluid-fluid and the fluid-wall interaction.

The model parameters were chosen to represent the structure and density relations of graphite and methane. Accordingly, the spring constant $\kappa^{XZ} = 15600$ N/m, corresponding to sp^2 bonds, was adjusted to the carbon-carbon (C-C) RDF obtained from simulations with the rescaled *Terstoff* potential, cf. Section 1.2. In agreement with the relation between the C-C bond energy (4.3 eV) and the interaction energy between adjacent graphite layers (0.07 eV) as given by *Cotton et al.* [310], the interlayer spring constant was specified as $\kappa^Y = \kappa^{XZ}/60$. Applying the LJ-TS parameter values for methane, the reduced C-C bond length was $\mathcal{D} = 0.3816\sigma$.

Massively parallel canonical ensemble MD simulations were conducted with the *ls1 mardyn* program. For all simulation runs, the integration time step was set to 1 fs. Vapor and liquid were independently equilibrated in homogeneous simulations for 10 ps. This was followed by 200 ps of equilibration for the combined system, i.e. a cylindrically curved liquid slab surrounded by vapor, with a wall consisting of four to seven layers, cf. Fig. 2.8. The periodic boundary condition was applied to the system, leaving a channel for the fluid with a height of $L = 27.4\sigma$ between the wall and its periodic image.

During the MD simulations, the density profiles were averaged via binning over at least 800 ps after equilibration and the arithmetic mean of the saturated vapor and liquid densities was applied to define the position of the phase boundary. In the immediate vicinity of the wall, the fluid is affected by short-range ordering effects [308, 311, 312]. The influence of this phenomenon was minimized by taking density averages over a bin size of about 1σ , following *Giovambattista et al.* [313].

A circle was adjusted to the interface at distances between 2 and 11σ from the wall, cf. Fig. 2.9, and the tangent to this circle at a distance of 1σ from the wall was consistently used to determine the contact angle. Due to the finite size of the channel, an interface curvature up to

$$R_{\text{min}}^{-1} = \left(\frac{L}{2} - \sigma\right)^{-1} = 0.0788\sigma^{-1}, \quad (2.82)$$

was reached in the limit of perfect wetting and drying, while no curvature was present for $\vartheta = 90^\circ$ and²⁵

$$R^{-1} = R_{\text{min}}^{-1} \cos \vartheta, \quad (2.83)$$

follows in case of partial wetting or drying.

Since for the present system, R_{\min}^{-1} is not a negligible value even on the molecular length scale, the curvature influence on the tension of the meniscus has to be considered explicitly, taking the cylindrical shape of the interface into account. The *Laplace* equation becomes

$$\gamma = R_{\mathcal{L}}\Delta p, \quad (2.84)$$

cf. Eq. (2.43), when one of the characteristic radii of curvature is infinite. On this basis, *Tolman's* discussion of curved interfaces [174] mostly carries over to the present case. Its further preconditions, the *Gibbs-Duhem* equation and the *Gibbs* adsorption equation, cf. Eqs. (2.2) and (2.55), apply to systems with a cylindrical phase boundary as well. In full analogy with the spherical case, the surface tension of a cylindrical vapor-liquid phase boundary can be related to the interfacial excess density by

$$\left(\frac{\partial \gamma}{\partial R_{\mathcal{L}}}\right)_T = -\frac{\Delta\rho}{\Gamma}, \quad (2.85)$$

cf. Eq. (2.56), from which one obtains the exact *Tolman* relation

$$\left[\left(\frac{\partial \ln R_{\mathcal{L}}}{\partial \ln \gamma}\right)_T - 1\right]^{-1} = \frac{\delta}{R_{\mathcal{L}}} + \frac{\delta^2}{2R_{\mathcal{L}}^2}, \quad (2.86)$$

cf. Eq. (2.57), by comparison with the dividing surface for which Γ is equal to zero. The relation between the *Tolman* length and the interfacial excess density is

$$\frac{\Gamma}{\delta\Delta\rho} = 1 + \frac{\delta}{2R_{\mathcal{L}}}, \quad (2.87)$$

²⁵According to the convention employed here, the curvature has a negative sign for a concave meniscus, corresponding to wetting, while it is positive for drying.

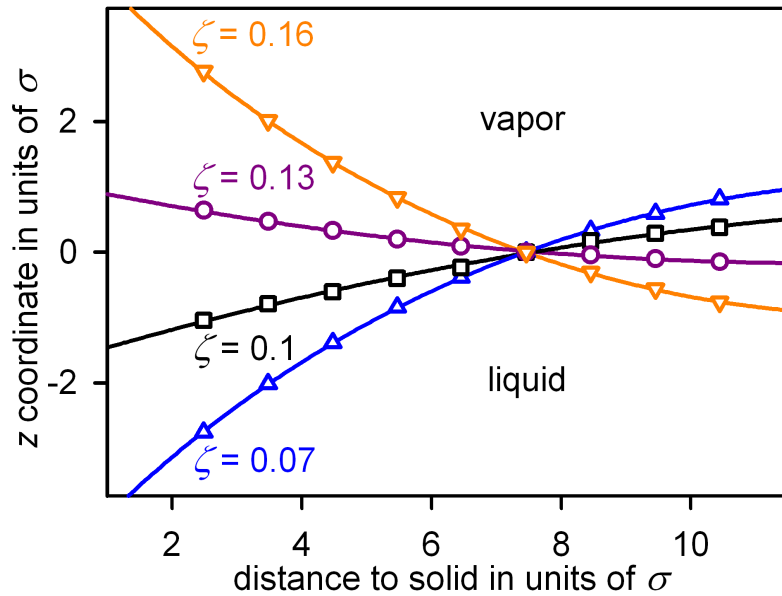


Figure 2.9: Vapor-liquid interface profiles for the reduced fluid-wall dispersive energy ζ of 0.07 (upward triangles), 0.10 (squares), 0.13 (circles), and 0.16 (downward triangles) at a temperature of 0.82ε .

cf. Eq. (2.58), for the system under consideration. As shown in Fig. 2.10, this can be approximated by the corresponding version of the *Tolman* equation

$$\frac{\gamma_\infty}{\gamma} = 1 + \frac{\delta}{R_{\mathcal{L}}} + \mathcal{O}(R_{\mathcal{L}}^{-2}), \quad (2.88)$$

cf. Eq. (2.59), neglecting the higher-order contributions and applying the approximation $\delta \approx \delta_\infty(T)$ as correlated by Eq. (2.71).

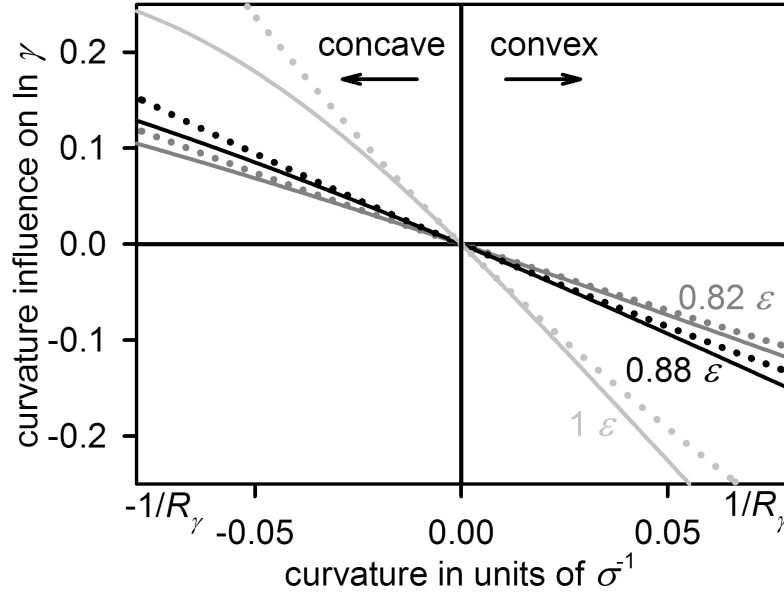


Figure 2.10: Curvature influence $\ln \gamma/\gamma_\infty(T)$ on the surface tension of cylindrical vapor-liquid menisci for the LJ-TS fluid at temperatures of 0.82, 0.88, and 1 ε according to the full *Tolman* relation (solid lines), cf. Eq. (2.86), and the *Tolman* equation (dotted lines), cf. Eq. (2.88), neglecting higher-order contributions, over curvature in terms of the inverse *Laplace* radius $R_{\mathcal{L}}^{-1}$. The left and right limits of the figure correspond to the curvature reached for the limits of perfect wetting and drying, respectively, in case of the present contact angle simulations. The *Tolman* length is approximated by its value for the planar phase boundary as correlated by Eq. (2.71).

Although a certain deviation does arise between the full and the truncated expressions, the present results for droplets, cf. Figs. 2.5 and 2.6, show that the main inaccuracy consists in using the *Tolman* length of the planar interface. This is probably the case for a cylindrical curvature as well, and since quantifying the dependence of δ on $R_{\mathcal{L}}$ for these systems must be left to future studies, Eq. (2.88) will be used here as the most adequate available approximation.

By combining the *Young* equation, cf. Eq. (2.78), with the *Tolman* equation as well as Eq. (2.83), the relation between the contact angle in a slit-like nanopore and the surface tension values for the respective planar interfaces is obtained as

$$\cos \vartheta = \left(\frac{\gamma_\infty}{\Delta\gamma_s} + \frac{\delta_\infty}{R_{\min}} \right)^{-1}, \quad (2.89)$$

i.e. the *Young-Tolman* equation for cylindrical menisci, wherein R_{\min} is half the effective channel diameter.

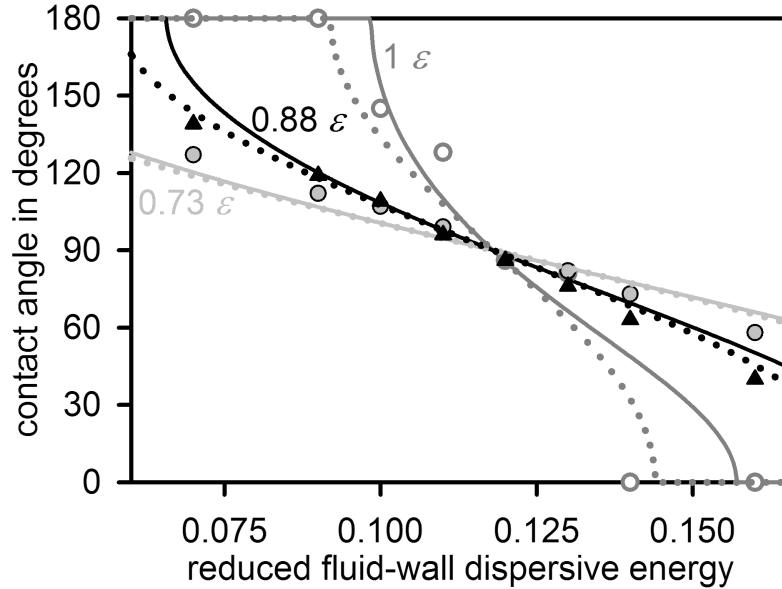


Figure 2.11: MD simulation results for the contact angle in dependence of the reduced fluid-wall dispersive energy at temperatures of $T = 0.73$ (\bullet), 0.88 (\blacktriangle), and 1ε (\circ) in comparison with the *Young-Tolman* equation (solid lines), cf. Eq. (2.78), and the *Young* equation (dotted lines), cf. Eq. (2.89), with $\zeta_0 = 0.118$ and a reduced fluid-wall surface energy difference of $\mathcal{K}_\gamma = 7 \sigma \varepsilon$.

The present MD simulation results are shown in Tab. 2.4 as well as Figs. 2.11 and 2.12. Note that the triple point temperature of the LJ-TS fluid is about 0.65ε according to *van Meel et al.* [314] while the critical temperature is 1.0779ε as mentioned above [85] so that the entire regime of vapor-liquid coexistence was covered here.²⁶

High values of ζ correspond to a strong attraction between fluid particles and wall atoms. This leads to a contact angle below 90° , i.e. to partial ($\vartheta > 0^\circ$) or perfect ($\vartheta = 0^\circ$) wetting of the surface. As expected, with increasing fluid-wall dispersive energy, the extent of wetting grows, cf. Fig. 2.11. As can be seen in Fig. 2.12, a transition from obtuse to acute contact angles occurs at ζ values between 0.11, where the contact angle cosine is negative over the whole studied temperature range, and 0.13, where the cosine becomes positive.

Figure 2.11 shows that for high temperatures, the range of ζ values leading to the formation of a contact angle, as opposed to perfect wetting or drying, is quite narrow. The present plots agree qualitatively with those determined by *Giovambattista et al.* [313] for the influence of the polarity of hydroxylated silica surfaces on the contact angle formed with water. In Fig. 2.12, it can be seen clearly that the extent of wetting or drying, respectively, increases as the temperature approaches T_c , eventually leading to critical point wetting. Furthermore, the following tendencies can be observed immediately:

- A) The absolute magnitude of $(\partial \cos \vartheta / \partial T)_\zeta$ increases as perfect wetting or drying is approached, i.e. the plots shown in Fig. 2.12 become steeper.

²⁶Due to nanoscopic confinement, the effective triple point temperature is probably somewhat elevated for the present system while the critical temperature is lower than for the bulk fluid [315–317]. During simulations at $T = 0.75 \varepsilon$ with $\zeta = 0.3978$, for instance, the emergence of a vapor-solid equilibrium can be found, although this is a relatively extreme case because of the comparably high ζ value.

Table 2.4: Contact angle of the LJ-TS fluid from MD simulation of vapor-liquid menisci in a planar channel with a height of 27.4σ and walls composed of hexagonal layers with a bond length of 0.3816σ as well as an interlayer distance of 0.8996σ in dependence of T and ζ .

$\zeta \backslash T/\varepsilon$	0.73	0.82	0.88	1
0.07	127°	134°	139°	180°
0.09	112°	116°	119°	180°
0.10	107°	106°	109°	145°
0.11	99°	95°	96°	128°
0.12	—	—	86°	86°
0.13	82°	79°	76°	81°
0.14	73°	67°	63°	0°
0.16	58°	45°	40°	0°

- B) In the vicinity of the critical temperature, small temperature changes lead to a much more significant variation of ϑ than for $T \ll T_c$.
- C) The contact angle dependence on ζ is approximately linear in the range $60^\circ < \vartheta < 120^\circ$.
- D) The ϑ - ζ diagram is approximately symmetric with respect to a temperature invariant value $\zeta_0 \approx 0.118$ of the reduced fluid-wall dispersive energy for which the contact angle becomes rectangular.

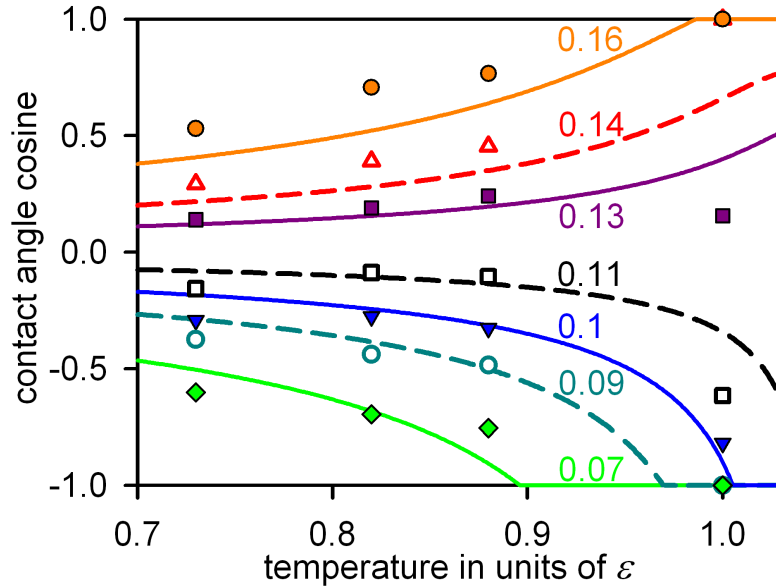


Figure 2.12: MD simulation results for the contact angle over temperature with a reduced fluid-wall dispersive energy of $\zeta = 0.07$ (\blacklozenge), 0.09 (\circ), 0.1 (\blacktriangledown), 0.11 (\square), 0.13 (\blacksquare), 0.14 (\triangle), and 0.16 (\bullet) in comparison with the *Young-Tolman* equation (solid and dashed lines), cf. Eq. (2.89), with $\zeta_0 = 0.118$ and a reduced fluid-wall surface energy difference of $\mathcal{K}_\gamma = 7 \sigma \varepsilon$.

Observation A suggests a first-order transition between partial and perfect wetting or drying, respectively, for the present system, as described by *Cahn* [318]. For a second-order wetting transition, $(\partial \cos \vartheta / \partial T)_\zeta$ would converge to zero in the limit of perfect wetting, a tendency that is not supported at all by the present simulation results. Observation D corroborates *Monson* [319] who obtained the same symmetry based on mean-field DFT calculations.

The physical causes at work behind the dependence of ϑ on the temperature and the reduced fluid-wall dispersive energy can be theoretically understood, at least qualitatively, by considering the specific surface energy difference $\Delta\gamma_s$ between the coexisting fluid phases in contact with the substrate. If $\Delta\gamma_s$ is reduced by the density difference $\Delta\rho$ between the fluid phases as well as the deviation of ζ from the value where the solid prefers none of the fluid phases, i.e. $\Delta\zeta = \zeta - \zeta_0$, the quantity

$$\mathcal{K}_\gamma = \frac{\Delta\gamma_s}{\Delta\rho \Delta\zeta}, \quad (2.90)$$

is obtained. Applying the correlations for the LJ-TS fluid regarding the fluid phase density difference [85]

$$\frac{\Delta\rho}{\rho_c} = -0.1014 T_b^{3/2} - 0.2751 T_b + 3.631 T_b^{1/3}, \quad (2.91)$$

with $T_b = (1 - T/T_c)$, as well as the *Tolman* length and the vapor-liquid surface tension in the zero-curvature limit, cf. Eqs. (2.71) and (2.75), the *Young-Tolman* equation, cf. Eq. (2.89), can be used to obtain the contact angle for a given magnitude of the reduced fluid-wall surface energy difference \mathcal{K}_γ . As shown in Figs. 2.11 and 2.12, this straightforward theoretical approach captures the qualitative behavior of the considered system. A good quantitative agreement is reached for a constant value $\mathcal{K}_\gamma = 7 \sigma\varepsilon$, although there is of course no reason to assume that \mathcal{K}_γ should be entirely independent of both ζ and T .

Figure 2.11 indicates both the results of the *Young-Tolman* equation for the actual channel diameter and the respective contact angles from the *Young* equation, corresponding to the macroscopic case where no significant curvature effects are present for the fluid phase boundary. It can be seen that the difference between the contact angle in the simulated system and the macroscopically observable value is negligible in most of the cases, while it becomes quite influential at high temperatures and large deviations from 90° .

3 Direct simulation of nucleation

3.1 Simulation methodology

Experimental methods for studying homogeneous nucleation face considerable challenges: In practice, a homogeneous system without walls or other irregularities can at best be approximated, a difficulty that is absent in molecular simulation. Furthermore, the experimentally accessible range of the nucleation rate J is limited to comparably slow processes that are relatively far from the spinodal [320].

In molecular simulation, homogeneous nucleation can be studied straightforwardly, e.g. by a direct method where a supersaturated vapor is sampled, the emerging droplets are counted, and the number of relatively large droplets is evaluated over time. The droplet formation rate J_ℓ is the number of droplets exceeding a threshold size ℓ formed per volume and time in a supersaturated vapor

$$J_\ell = \Sigma_{i>\ell} \frac{dN_i}{V dt}, \quad (3.1)$$

once the metastable state is established, i.e. after a relaxation time depending on the initial conditions. Therein, N_i is the number of droplets containing i particles. That is the basis of the *Yasuoka-Matsumoto* (YM) approach of obtaining nucleation rates by direct molecular simulation [255], which has found widespread acceptance [266, 321–326], along with mean first passage time (MFPT) analysis as introduced by *Wedekind et al.* [327, 328], which is based on the repetitive simulation of even smaller systems.

Experimentally, the nucleation rate J is also determined as a droplet formation rate, but with a threshold size many orders of magnitude larger than the critical droplet size. Due to restrictions in computing power, however, a size on the nanometer scale must be chosen as the threshold in molecular simulation. Under such conditions, the choice of ℓ may influence the result and it must be indicated explicitly, i.e. as J_ℓ instead of J .

For simulation in the canonical ensemble, it has to be taken into account that as the condensation proceeds, the density of the remaining vapor decreases and the pressure in the vapor is reduced significantly.¹ This causes larger droplets to be formed at a lower rate, cf. Figure 3.1. In the present work, the droplet formation rate is therefore given together with pressure values or supersaturation ratios determined in the center of an interval during which $\Sigma_{i>\ell} dN_i/dt$ was obtained by linear approximation.

With the presently available computational resources, MD simulations of volumes $V \approx 10^{-21} \text{ m}^3$ can be conducted for a time span of a few nanoseconds with an acceptable computational effort. Thus with the direct approach, which requires several stable droplets to emerge in the system, only nucleation rates sufficiently above $10^{30} \text{ m}^{-3}\text{s}^{-1}$ are accessible unless correspondingly larger computational resources are employed. Hence, the direct approach can currently only be applied to vapors at extreme supersaturation ratios, i.e. in the vicinity of the spinodal line. This still leaves about six orders of magnitude that neither can be covered by

¹In case of expanding systems, as simulated by *Römer and Kraska* [326], this effect is of course even stronger.

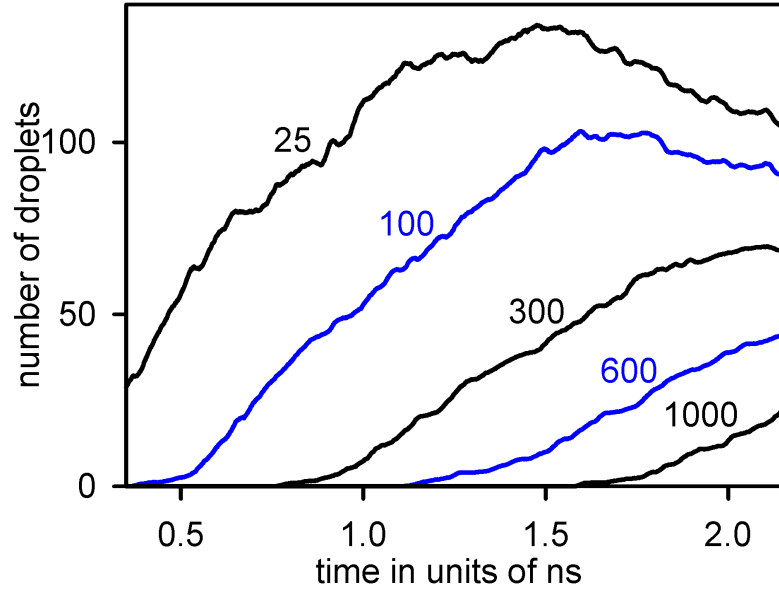


Figure 3.1: Number of droplets containing at least 25, 100, 300, 600, and 1000 particles, respectively, over simulation time in a volume of $(63.7 \text{ nm})^3$ filled with methane at 130 K and 1.606 mol/l.

experiment nor by molecular simulation [320] so that a sound theoretical model or interpolation between simulation and experiment is required.

The size evolution of any given droplet can be analyzed in terms of a random walk over the order parameter ι , changing only by relatively small amounts $\Delta\iota$, usually by the absorption or emission of monomers, i.e. single vapor particles [329]. As outlined by *Smoluchowski* [50, 52], the probabilities for the growth and decay transitions are proportional to the respective values of the partition function \mathcal{Z} , resulting in

$$W^+(\iota) = \frac{1}{2} + \frac{(d\mathcal{Z}/d\iota)\Delta\iota}{2\mathcal{Z} + \mathcal{O}(\Delta\iota^2)} + \mathcal{O}(\Delta\iota^2), \quad (3.2)$$

and

$$W^-(\iota) = \frac{1}{2} - \frac{(d\mathcal{Z}/d\iota)\Delta\iota}{2\mathcal{Z} + \mathcal{O}(\Delta\iota^2)} + \mathcal{O}(\Delta\iota^2). \quad (3.3)$$

The probability $W^F(\iota)$ that a certain size is *eventually* reached (at any time during the random walk), given that the current size is ι , has the property

$$W^F(\iota) = W^+(\iota)W^F(\iota + \Delta\iota) + W^-(\iota)W^F(\iota - \Delta\iota). \quad (3.4)$$

By substituting

$$W^F(\iota \pm \Delta\iota) = W^F(\iota) \pm \frac{dW^F}{d\iota}\Delta\iota + \frac{d^2W^F}{2d\iota^2}\Delta\iota^2 + \mathcal{O}(\Delta\iota^3), \quad (3.5)$$

it follows for small $\Delta\iota$, neglecting terms of third order and higher, that

$$\frac{d\mathcal{Z}}{\mathcal{Z}d\iota} = \frac{-d(dW^F/d\iota)}{2(dW^F/d\iota)d\iota}. \quad (3.6)$$

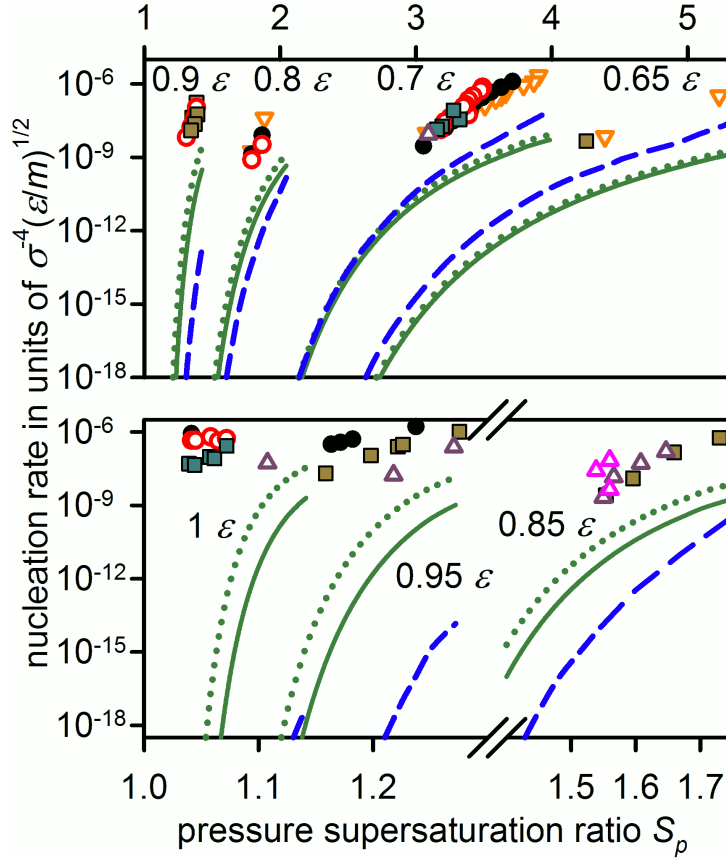


Figure 3.2: Droplet formation rate for the LJ-TS fluid from the present direct simulations over pressure supersaturation ratio S_p for threshold values ℓ of (∇) 25, (\bullet) 50, (\circ) 75, (\blacksquare) $100 \leq \ell \leq 150$, as well as (\triangle) $\ell \geq 300$ particles, and nucleation rate following CNT (solid lines), CNT without the pressure effect (dotted lines) as well as LFK theory (dashed lines).

Using the partition function for the canonical ensemble, the derivative of the probability is given by

$$\frac{dW^F}{d\ell} = \alpha' \exp(2\Delta A_\ell/T), \quad (3.7)$$

where α' is an integration constant. Obtaining the two remaining parameters from the boundary conditions

$$\mathcal{Q}(1) = 0, \quad (3.8)$$

$$\lim_{\ell \rightarrow \infty} \mathcal{Q}(\ell) = 1, \quad (3.9)$$

the committor function $\mathcal{Q}(\ell)$, i.e. the probability for a droplet containing ℓ particles of eventually reaching macroscopic size, is

$$\mathcal{Q}(\ell) = \frac{\int_1^\ell \exp(2\Delta A_i/T) di}{\int_1^\infty \exp(2\Delta A_i/T) di}. \quad (3.10)$$

The droplet formation rate J_ℓ is related to the nucleation rate J by

$$J = J_\ell \mathcal{Q}(\ell), \quad (3.11)$$

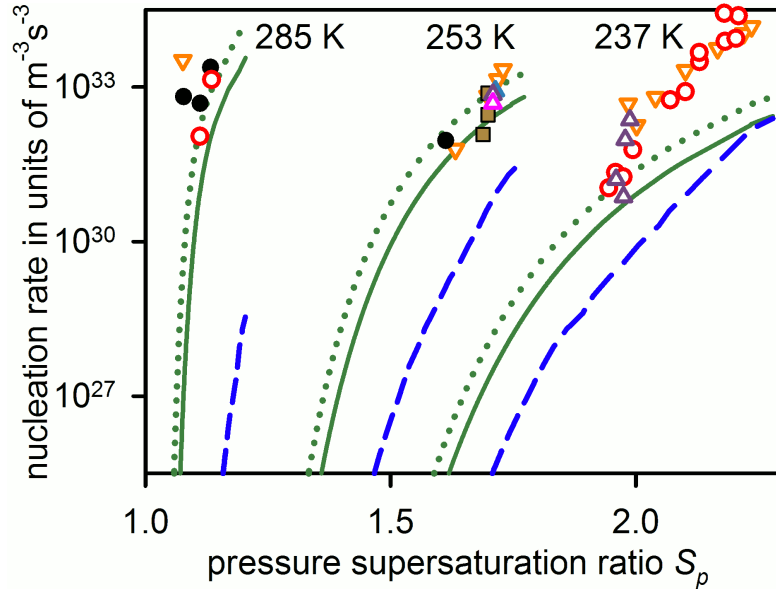


Figure 3.3: Droplet formation rate over pressure supersaturation ratio S_p for carbon dioxide from the present direct simulations for threshold values ℓ of (∇) 25, (\bullet) 50, (\circ) 75, (\blacksquare) 100, as well as (\triangle) $\ell \geq 200$ molecules, and nucleation rate following CNT (solid lines), CNT without the pressure effect (dotted lines) as well as LFK theory (dashed lines). The supersaturation is given in terms of the pressure supersaturation ratio S_p .

under the assumption that the reaction coordinate of the nucleation process can be approximated by the order parameter ν .

Series of MD simulations of nucleating vapors were conducted using a version of the program *ls1 moldy*, the precursor [232] of *ls1 mardyn*. The simulations were carried out in the canonical ensemble with a time step between 2.5 and 7 fs, depending on the density and the system temperature. In all simulations of the investigated full LJ and 2CLJQ fluid models for methane, ethane, and carbon dioxide, the cutoff radius r_c was larger than 4.5σ . The LJ-TS fluid was, of course, considered with $r_c = 2.5 \sigma$.

Fluid argon can be represented accurately by a LJ-TS molecular model. The corresponding potential parameters are $\sigma = 3.3916 \text{ \AA}$ and $\varepsilon = 137.90 \text{ K}$ [85], cf. Tab. 1.1. Experimental nucleation data for pure argon are available, however, at very low temperatures below the triple point predominantly.² The onset pressure p_ω , defined as the pressure where the nucleation rate exceeds a certain minimal value J_ω , was determined for homogeneous nucleation of argon by *Pierce et al.* [243], *Zahoransky et al.* [332, 333], and *Iland et al.* [334]. The onset nucleation rate J_ω depends on the experimental setup and was provided (or estimated) by the authors of the respective studies, with the exception of the measurements of *Pierce et al.* [243], for which $J_\omega = 10^{19} \text{ m}^{-3}\text{s}^{-1}$, as given by *Iland* [320], was assumed here.

Note that direct MD simulation of nucleation, where droplet formation is observed in a near-spinodal supersaturated vapor, has its limits: if nucleation occurs too fast, it affects the properties of the vapor to a significant extent [335], so that the droplet formation rate, and

²In recent supersonic expansion experiments [330], the «stagnation» temperature reached at the end of the expansion can even be lower than 0.1 K. Understanding such processes, however, requires a profound adaptation of the theoretical approach [331] and the simulation methodology [326] to the instationary experimental conditions.

Table 3.1: Nucleation onset pressure p_ω (in units of kPa) for argon at low temperatures (in units of K) from experimental data in comparison with the pressure where the assumed onset nucleation rate J_ω (in units of $\text{m}^{-3}\text{s}^{-1}$) is reached according to CNT without the pressure effect; the data of *Pierce et al.* [243] were published in graphical form only.

ref.	T	J_ω	$p_\omega(\text{exp})$	$p_\omega(\text{CNT}^{\Delta\mu})$
[332]	48.2	10^3	0.31	1.2
[334]	48.2	10^{10}	1.3	2.1
[243]	55	10^{19}	19	16
[332]	55.8	10^3	0.99	4.8
[333]	55.9	10^9	5.28	6.7
[334]	55.9	10^{10}	6.2	7.1
[333]	60.2	10^9	11.1	12
[332]	60.3	10^3	2.27	9.5
[333]	62.7	10^9	12.7	17
[243]	63	10^{19}	52	34
[333]	69.9	10^9	23.9	42
[332]	85.1	10^3	114	180
[243]	98	10^{19}	690	570

hence the nucleation rate determined by the YM method varies over simulation time [336]. On the other hand, equilibrium simulations fail to reproduce kinetic properties of nucleation processes such as the overheating of growing droplets due to latent heat. Although it is more rigorous to calculate J from a MFPT analysis, *Chkonja et al.* [336] point out that «the computational costs of making the necessary repetitions to evaluate the MFPT can be very high,» while «YM requires many clusters forming and it therefore becomes more sensible to deviations coming from vapor depletion or coalescence of clusters.»

It is therefore more adequate to investigate homogeneous nucleation as a steady-state non-equilibrium process, which can be achieved by combining grand canonical MD (GCMD) and *McDonald's* demon [250], an «intelligent being» that eliminates large droplets from the system. The novel simulation approach introduced here for this purpose thus facilitates sampling over an arbitrary time span, as opposed to the YM method which is limited to the relatively short interval where nucleation, instead of relaxation or droplet growth, dominates the dynamics. On the other hand, it retains the advantages of the YM method, so that a single direct MD simulation run is sufficient and the nucleation rate is straightforwardly determined from the number of relatively large droplets formed over time.

Whenever a droplet exceeds the specified threshold size, an intervention of *McDonald's* demon [250], which is also erroneously called *Szilárd's* demon³ by *Schmelzer et al.* [340], removes

³*Szilárd* [337] actually discussed a variant of *Maxwell's* demon that is usually – and correctly – called *Szilárd's* engine or demon [338]. However, that demon deals with much simpler systems, ideally containing only a single particle, and is hardly related to the work of *McDonald*. In the present case, the connection to *Szilárd* can actually be traced back to *McDonald* himself who introduced his demon «by invoking a notion due, according to Dunning, to Szilard» [250]. Via a related article [339], he indirectly referred to the work of *Farkas* [172] which contains an idea akin to *McDonald's* approach: «nach oben hingegen muss für sehr grosse n die Konzentration der Tröpfchen verschwinden». *Farkas* acknowledged *Szilárd* for this: «Die Idee die der strengen Betrachtung zugrunde liegt, stammt von L. Szilard» [172]. It should be noted, however, that none of the previous considerations included the intervention of a demon, i.e. an intelligent being.

it from the system and replaces it by a representative configuration of the metastable phase. If a dense phase is simulated, this can for instance be achieved by inserting an equilibrated homogeneous configuration in the center of the free volume, followed by preferential test insertions and deletions in the affected region. In a supersaturated vapor, however, the density is usually so low that it is sufficient to leave a vacuum behind.

The chemical potential of the vapor can be regulated by GCMD, cf. Section 1.4. Thereby, the number of MC test actions, i.e. probabilistic insertions and deletions, must be sufficiently high to compensate for the interventions of *McDonald's* demon. For the present series of simulations, the number of test actions per simulation time step was chosen between 10^{-5} and $10^{-3} N$, a value which was occasionally further decreased after equilibration if very low intervention rates were observed.

The new method was applied to homogeneous nucleation of the LJ-TS fluid here as well. For the present series of simulations, the *Stillinger* [341] criterion was used to define the liquid phase, and droplets were determined as biconnected components. After a temporal delay, depending on the threshold size, the intervention rate thereby reached a perfectly stationary value, cf. Fig. 3.4.

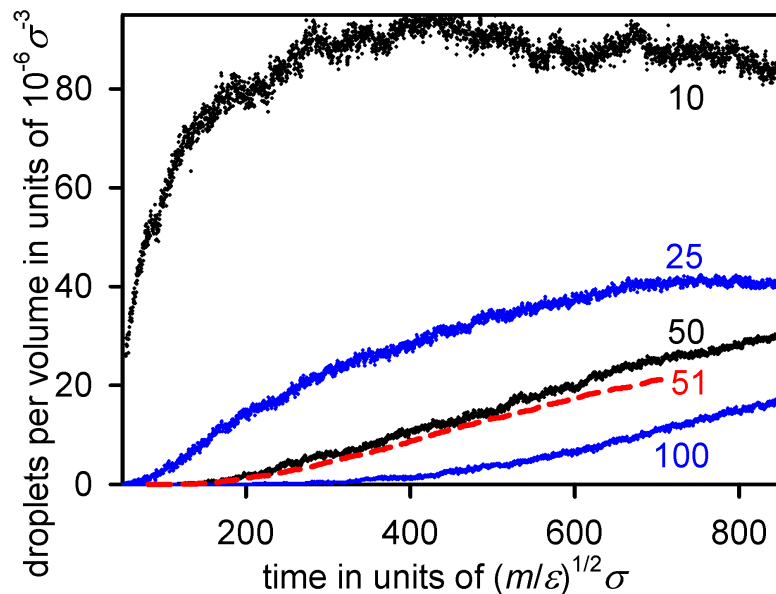


Figure 3.4: Number of droplets per volume over simulation time for droplets containing $i > 10, 25, 50,$ and 100 particles in a canonical ensemble MD simulation of the LJ-TS fluid at $T = 0.7 \varepsilon$ and $\rho = 0.03421 \sigma^{-3}$ in comparison with the aggregated number of demon interventions per volume in a GCMD simulation with $T = 0.7 \varepsilon$, $S_\mu = 2.8658$, and $\ell = 51$.

Figure 3.4 shows the aggregated number of demon interventions in one of the present GCMD simulations and, for comparison, the number of droplets in a MD simulation of the canonical ensemble under similar conditions. The constant supersaturation ratio of the GCMD simulation was the same as the time-dependent supersaturation in the canonical simulation about $t = 580 (m/\varepsilon)^{1/2} \sigma$ after simulation onset, where it can be seen that the YM droplet formation rate for $\ell = 50$ roughly agrees with the intervention rate of *McDonald's* demon for $\ell = 51$.

With a threshold far below the critical droplet size, the intervention rate of *McDonald's* demon is many orders of magnitude higher than the steady-state nucleation rate. In agreement

Table 3.2: Logarithm of the demon intervention rate J_ℓ (in units of $(\varepsilon/m)^{1/2}\sigma^{-4}$) from GCMD simulation of the LJ-TS fluid and the committor function \mathcal{Q} estimated as J_ℓ/J_ℓ^{\min} from comparison of simulation results for different values of the threshold size ℓ , where J_ℓ^{\min} is the intervention rate obtained for the maximal applied value of ℓ , cf. Eq. (3.11), as well as according to CNT without the pressure effect.

T	S_μ	ℓ	$\ln J_\ell$	$\ln (J_\ell/J_\ell^{\min})$	$\ln \mathcal{Q}(\text{CNT}^{\Delta\mu})$	
0.7	2.496	10	-13.6	-8.5	-14.7	
		15	-15.7	-6.4	-9.98	
		20	-17.0	-5.1	-6.68	
		25	-17.6	-4.5	-4.35	
		30	-19.2	-2.9	-2.70	
		35	-19.9	-2.2	-1.59	
		48	-21.7	-0.4	-0.255	
		56	-21.2	-0.9	-0.0528	
		65	-21.9	-0.2	-0.0053	
		74	-22.1	0	-0.0003	
0.9	1.24	89	-18.9	-2.4	-3.28	
		149	-19.8	-1.5	-0.474	
		209	-21.3	0	-0.0205	
		1.26	70	-16.6	-1.6	-3.21
			116	-17.8	-0.4	-0.594
	1.28	162	-18.2	0	-0.0463	
		55	-15.7	-1.3	-3.28	
		91	-16.1	-0.9	-0.748	
		127	-17.0	0	-0.0915	

with Eq. (3.10), J_ℓ reaches a plateau for $\ell > \ell^*$, cf. Tab. 3.2. In particular, the approximation $J \approx J_\ell$ is valid for all values shown in Fig. 3.5.

In Fig. 3.6, it can be seen how the decreasing supersaturation in a canonical ensemble MD simulation affects the droplet size distribution. The droplet size distribution from GCMD with *McDonald's* demon, however, is constant after equilibration and can therefore straightforwardly be compared with theoretical predictions, following the approach⁴ of *Toxværd* [342]. In case of the simulation run shown in Fig. 3.6, the distribution of small droplets present per volume at about $t = 400 (m/\varepsilon)^{1/2}\sigma$ after simulation onset was similar for both approaches, due to similar values of the supersaturation ratio.

Near and above the critical size, i.e. 27 particles according to $\text{CNT}^{\Delta\mu}$, deviations arise because of the use of different boundary conditions. A comparison with the theoretical prediction corroborates the statement of *Talanquer* [343] that CNT overestimates the free energy of droplet formation and therefore underpredicts the number of droplets present in the metastable state.

⁴«Instead of a direct comparison of nucleation times one can, however, compare the different quasi-equilibrium states in which the nucleation events appear. The (partial) pressures, temperatures and distributions of clusters in these states can be determined very accurately from ensembles of many millions of timesteps» [342].

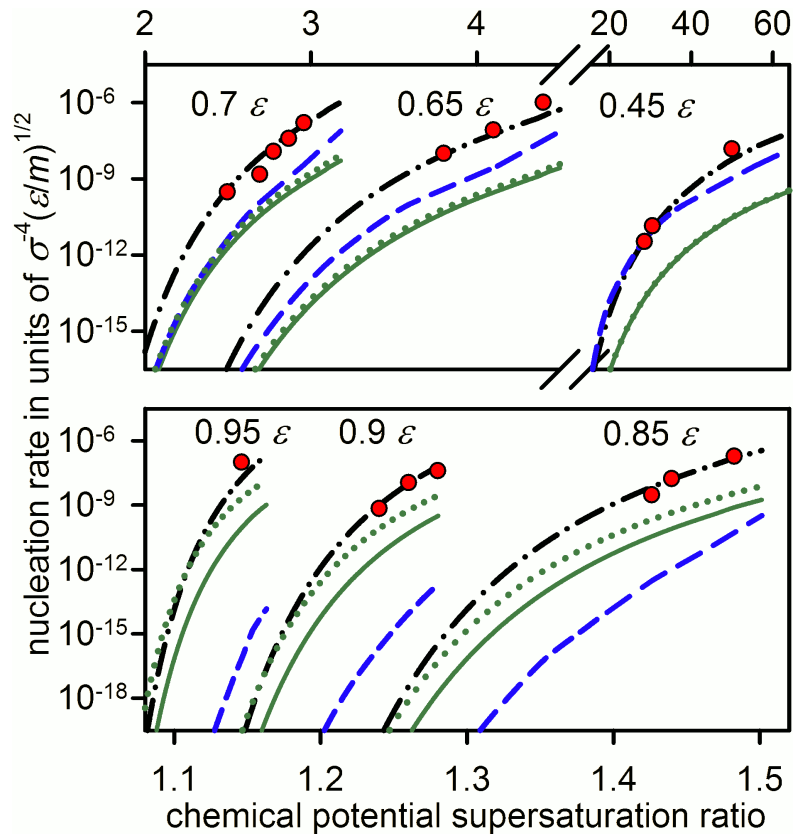


Figure 3.5: Nucleation rate of the LJ-TS fluid over supersaturation from the present GCMC simulations with *McDonald's* demon (\bullet) as well as according to CNT (solid lines), CNT without the pressure effect (dotted lines), CNT with $C = 200$ (dashes and dots) and LFK theory (dashed lines) at temperatures of 0.45ϵ , 0.65ϵ , 0.7ϵ , 0.85ϵ , 0.9ϵ , and 0.95ϵ . The supersaturation is given in terms of the chemical potential supersaturation ratio S_μ .

3.2 Carrier gas pressure effect

Although a systematic discussion of CO_2 nucleation was, surprisingly enough, published for the ambient conditions prevailing on Mars [344], to the author's knowledge no analogous study is available for the ecologically and technically more relevant atmosphere composition of our own planet. That gap is closed by the present series of simulations⁵ which characterizes the air pressure effect on the condensation process in a vapor containing more CO_2 than at saturation. The employed molecular models, cf. Tab. 1.1, are known to reproduce VLE properties with a good accuracy [121, 345, 346]. The emphasis is laid on the intermediate regime, which is where the YM method can best be applied, and the simulation results are compared with theoretical predictions on the basis of CNT as well as $\text{CNT}^{\Delta\mu}$.

For the following considerations, p_s refers to the pure substance vapor pressure of the nucleating component, whereas p is the total pressure including the pressure contribution of an inert carrier gas. According to internally consistent CNT [258], cf. Eq. (2.23),

⁵The help of *Lin Zengyong* (蔭增勇), who carried out the simulation work presented in this section, is gratefully acknowledged.

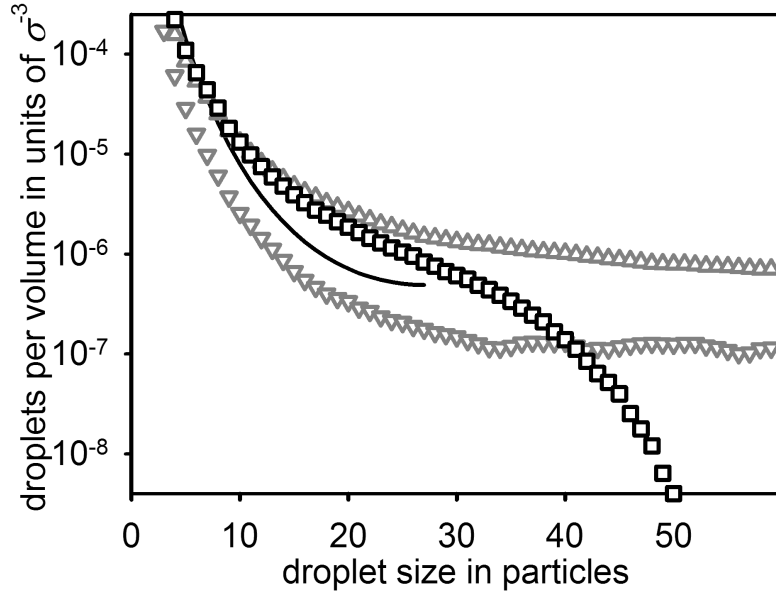


Figure 3.6: Number of droplets per vapor volume over droplet size from canonical ensemble MD simulation of the LJ-TS fluid at $T = 0.7 \varepsilon$ and $\rho = 0.04044 \sigma^{-3}$, averaged over sampling intervals of $320 < t < 480$ (\triangle) and $970 < t < 1130$ (m/ε) $^{1/2}\sigma$ (∇) after simulation onset, and from GCMD simulation with $T = 0.7 \varepsilon$, $S_\mu = 2.8658$, and $\ell = 51$ (\square) in comparison with a prediction for the same conditions based on CNT without the pressure effect (solid line).

the free energy barrier of the nucleation process⁶

$$\Delta A^* = \frac{16\pi\gamma_\infty^3}{3(\rho'\Delta\mu_e)^2} + \Delta\mu_e - \pi^{1/3} \left(\frac{6}{\rho'}\right)^{2/3} \gamma_\infty, \quad (3.12)$$

is reached for the critical droplet size, wherein the effective chemical potential difference $\Delta\mu_e$ is defined by Eq. (2.22).

Considering that the kinetic prefactor

$$zF^* = \frac{2}{\rho'} \left(\frac{\gamma_\infty}{T}\right)^{1/2}, \quad (3.13)$$

which consists of the *Zel'dovič* factor z , cf. Eq. (2.27), and the surface area of the critical droplet F^* , cf. Eqs. (2.14) and (2.21), does not depend on $\Delta\mu_e$ according to CNT, only two contributions to J have to be considered for the carrier gas effect as long as the pressure contribution P of the nucleating component remains constant [254]. On the one hand, a higher carrier gas density decreases $\Delta\mu_e$, leading to a higher value of the free energy barrier, cf. Fig. 3.7. On the other hand, its presence facilitates the thermalization of the emerging droplets, such that the non-isothermal factor \mathcal{N} , cf. Eq. (2.30), also increases, which can be expressed as

$$\frac{B^2}{T^2[c_V(0) + 0.5]} = \sum_{\mathcal{A}=0}^k \frac{y_{\mathcal{A}}m_0^{1/2}[c_V(\mathcal{A}) + 0.5]}{y_0m_{\mathcal{A}}^{1/2}[c_V(0) + 0.5]}, \quad (3.14)$$

⁶Since in CNT $^{\Delta\mu}$, the pressure effect is not taken into account, the chemical potential difference $\Delta\mu$ is used instead of $\Delta\mu_e$.

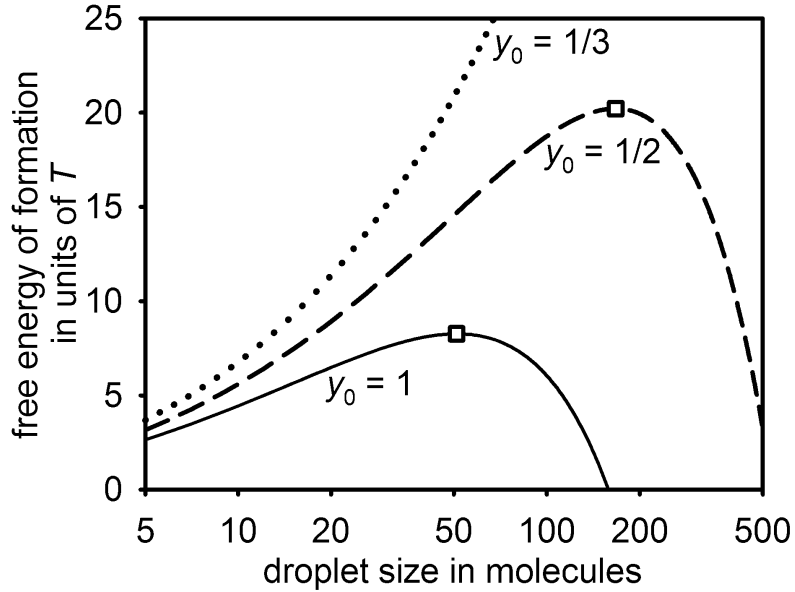


Figure 3.7: Free energy of formation according to CNT for CO₂ droplets in supersaturated vapors at $T = 250.2$ K with $S_\rho = 2.72$ and CO₂ mole fractions of $y_0 = 1$ (solid line), $1/2$ (dashed line), and $1/3$ (dotted line), reaching a maximum for the critical size (□). Note that in the thermodynamic limit, i.e. in a macroscopic system, the *Gibbs*, *Helmholtz*, and *Landau* free energies of formation are equal.

according to *Feder et al.* [261]. In this expression, \mathcal{A} enumerates the components and k is the number of components pertaining to the carrier gas, while $\mathcal{A} = 0$ corresponds to the nucleating component, e.g. m_1 is the molecular mass for the first component of the carrier gas and $c_V(0)$ is the isochoric heat capacity of the pure nucleating component. The mole fraction of component \mathcal{A} in the supersaturated vapor is indicated by $y_{\mathcal{A}}$. If these two main aspects of the pressure effect, discussed by *Wedekind et al.* [254], are combined for systems with an inert carrier gas, one obtains the factor

$$\mathcal{W} = \frac{J_{\text{CNT}}}{J_{\text{CNT}(\text{pure})}} = \frac{\mathcal{N}}{\mathcal{N}(\text{pure})} \exp\left(\frac{\Delta A^*(\text{pure}) - \Delta A^*}{T}\right). \quad (3.15)$$

Note that the heat Q transferred to a droplet by the absorption of a monomer and the number N' of monomers in the system are affected by the density of the carrier gas as well, because it influences the size and hence the surface area of the critical droplet. Whenever CNT is evaluated here, these contributions are also considered. However, it should be kept in mind that their influence on the nucleation rate is much smaller than the effects caused by the change of the free energy barrier ΔA^* and the kinetic energy variance of vapor molecules B^2 . For the *Wedekind* factor \mathcal{W} , the total influence of the carrier gas on thermal non-accommodation is taken into account, while the variation of the monomer density is neglected, following the approach of *Wedekind et al.* [254].

Under certain conditions, the pressure effect does not exceed the experimental uncertainty and can thus be neglected [347]. In other cases, however, the influence can be experimentally detected, with apparently contradictory results: sometimes J increases with the amount of carrier gas, in other cases the opposite tendency is observed [348, 349]. The \mathcal{W} factor explains this in principle, since it combines the thermal non-accommodation factor, which increases

with $y_o \rightarrow 0$, and the free energy effect that leads to an effective chemical potential difference $\Delta\mu_e < \Delta\mu$. Depending on the thermodynamic conditions, each of these contributions can be predominant [254].

To complement the present results regarding supersaturated vapors, the saturated state was also investigated by applying the Grand Equilibrium method [217], as implemented in the code provided by the *ms2* project [234], to the VLE of the quaternary system under consideration. The employed molecular models were extensively validated with respect to the VLE behavior for all six binary [121] and two out of four ternary subsystems [345], i.e. $\text{N}_2 + \text{O}_2 + \text{Ar}$ as well as $\text{CO}_2 + \text{N}_2 + \text{O}_2$. The present Grand Equilibrium simulations cover a broad temperature range with CO_2 bubble line mole fractions $x(\text{CO}_2)$ of 0.910, 0.941, and 0.969 mol/mol.

Except for the highest temperature, which corresponds to 93 % of the critical temperature for pure carbon dioxide, the mole fractions $y(\text{N}_2)$, $y(\text{O}_2)$, and $y(\text{Ar})$ on the dew line are one order of magnitude higher than the corresponding bubble line mole fractions, cf. Tab. 3.3. This confirms that for temperatures sufficiently below $T_c(\text{CO}_2)$, the air components only accumulate to a limited extent in the liquid carbon dioxide phase. As a first approximation, the air can therefore be treated as a carrier gas for CO_2 nucleation so that CNT can be applied as presented above, i.e. with a single nucleating component. For mixtures with a more complex behavior, such as ethanol + hexanol [350], water-alcohol mixtures [351, 352], or water + nonane + butanol [353], multi-component nucleation occurs. In these cases, a different theoretical approach has to be applied, e.g. CNT for binary systems as discussed by *Reiss* in 1950 [192].

T [K]	$x(\text{CO}_2)$	p_s [MPa]	$y/x(\text{N}_2)$	$y/x(\text{O}_2)$	$y/x(\text{Ar})$	ρ' [mol/l]	ρ'' [mol/l]
182.7	0.969	2.53(8)	40(2)	24.5(9)	24.7(9)	29.24(1)	1.85(6)
	0.941	3.9(1)	21.5(8)	13.9(5)	13.7(5)	29.13(1)	3.03(8)
	0.910	6.0(2)	13.7(4)	9.1(3)	9.0(3)	29.01(2)	5.3(2)
232.9	0.941	4.38(5)	14.0(2)	10.8(1)	10.3(1)	24.94(3)	2.66(3)
	0.910	5.30(4)	9.7(1)	7.72(8)	7.34(8)	24.47(2)	3.25(2)
263.5	0.969	5.97(4)	5.6(1)	4.88(8)	4.72(7)	19.3(2)	3.90(3)
	0.941	6.98(3)	4.31(5)	3.82(5)	3.67(4)	18.55(9)	4.63(2)

Table 3.3: VLE data for the quaternary system $\text{CO}_2 + \text{N}_2 + \text{O}_2 + \text{Ar}$. The liquid composition is equimolar in nitrogen, oxygen, and argon, i.e. $x(\text{N}_2) = x(\text{O}_2) = x(\text{Ar}) = [1 - x(\text{CO}_2)] / 3$. The values in parentheses indicate the uncertainty in the last digit.

For the present homogeneous nucleation simulations, the YM method was applied to systems with $N(\text{CO}_2) = 300\,000$. The total number of molecules was up to $N = 900\,000$ such that the carrier gas with $N(\text{N}_2) : N(\text{O}_2) : N(\text{Ar}) = 7812 : 2095 : 93$ corresponded to the earth's atmosphere composition. Liquid and vapor were distinguished according to a *Stillinger* criterion [341], i.e. molecules separated by distances of their centers of mass below $R_\ell = 5.08 \text{ \AA}$ were considered as part of the liquid, and droplets were determined as biconnected components.

The evaluation of the theoretical predictions relies on knowledge about the chemical potential difference between the saturated and the supersaturated state. This was obtained for pure carbon dioxide by *Gibbs-Duhem* integration over the metastable extension of the isotherms in the p - ρ diagram, while the carrier gas influence was evaluated by assuming ideal gas properties

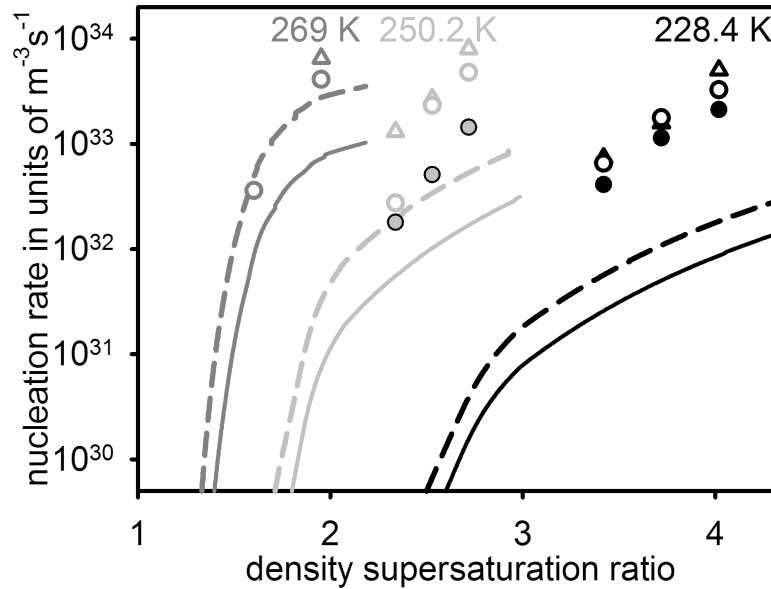


Figure 3.8: Pure CO₂ nucleation rate J according to CNT (solid lines) and CNT ^{$\Delta\mu$} (dashed lines) in comparison to the YM droplet formation rate for threshold sizes of $\ell = (\triangle)$ 50, (\circ) 75, and 250 (\bullet) molecules from canonical ensemble MD simulation over the supersaturation ratio with respect to density $S_\rho = \rho/\rho''(T)$ at temperatures of $T = 228.4$, 250.2, and 269 K. For the simulations at 269 K, the *Kible* [354] cluster criterion was used.

for air as well as ideal mixing behavior, i.e.

$$p = (1 - y_o)\rho T + P, \quad (3.16)$$

where P is the pressure of the pure nucleating component at the same partial density. The data underlying to *Gibbs-Duhem* integration were determined by canonical ensemble MD simulation of small systems ($N \approx 10\,000$) and the results were interpolated by local fits to cubic polynomials. From these simulations, the spinodal value $S_\rho^\#$ of the supersaturation with respect to density was determined to be in the range $4.3 \leq S_\rho^\# \leq 5.1$ at 228.4 K, $3.6 \leq S_\rho^\# \leq 4.3$ at 238.4 K, and $3.0 \leq S_\rho^\# \leq 3.6$ at 250.2 K for pure carbon dioxide.

At these temperatures (and also at $T = 269$ K), canonical ensemble MD simulations for CO₂ nucleation were conducted with CO₂ mole fractions of $y_o = 1/3$, $1/2$, and 1 at supersaturation ratios below the spinodal value $S_\rho^\#$, but still high enough to obtain statistically reliable droplet formation rates in a nanoscopic volume on the timescale of a few nanoseconds. Droplet formation rates J_ℓ for pure carbon dioxide are shown in Fig. 3.8. They reproduce the typical tendencies that were already observed by *Yasuoka* and *Matsumoto* [255, 321] and discussed above, namely elevated formation rates for small droplet sizes and depletion effects influencing the formation of the largest droplets, cf. Fig. 3.9. It can be observed that while both variants of CNT predict the value of J in the spinodal limit to increase with temperature, mainly because T occurs in the denominator of the exponential in the *Arrhenius* term of Eq. (2.31), the simulation results do not exhibit any significant temperature dependence for the attainable value of J . In the spinodal limit, the nucleation rate appears to be about $J(S_\rho^\#, T) \approx 10^{33} \text{ m}^{-3}\text{s}^{-1}$ over the whole temperature range.

Table 3.4 and Fig. 3.10 indicate the theoretical predictions and the simulation results for the carrier gas effect on CO₂ nucleation. The pressure effect according to CNT is most significant

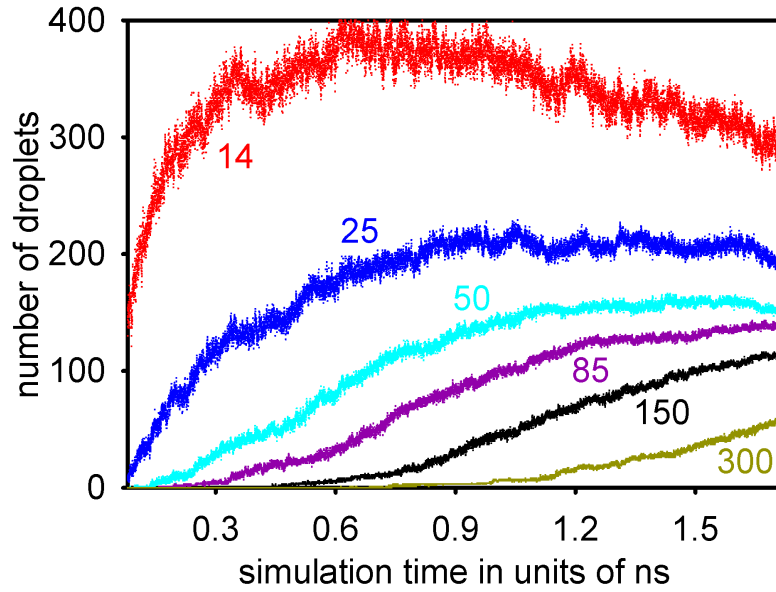


Figure 3.9: Number of droplets containing more than $\ell = 14, 25, 50, 85, 150,$ and 300 molecules over time from canonical ensemble MD simulation of pure CO_2 at $T = 228.4$ K with $S_p = 3.42$ for a system containing 300 000 molecules.

at high temperatures, because this corresponds to a lower density of the liquid and also because $\Delta\mu$ is smaller, so that the relative deviation between $\Delta\mu_e$ and $\Delta\mu$ is increased.

As usual, J_ℓ decreases when larger values of the threshold size ℓ are regarded, but it was also found that this effect is clearly stronger when more air is present in the system. This may be a consequence of the larger value of v^* which is in turn caused by the smaller value of the effective chemical potential difference as y_o is decreased. Thus, for relatively small threshold sizes, the committor function $Q(\ell)$ is significantly smaller, cf. Eq. (3.10), which increases the droplet formation rate according to Eq. (3.11).

The overall carrier gas effect determined from MD simulation qualitatively confirms the theory outlined by *Wedekind et al.* [254]. A tendency of J to decrease when more air is introduced can be detected in all cases for $\ell \rightarrow \infty$. However, the extent of this effect is significantly more limited than predicted by CNT, particularly at high temperatures. This is partly due to the fact that at high densities, air cannot be reliably described by the ideal gas equation. The non-ideality leads to a lower total pressure and thereby reduces the magnitude of the pressure effect to a certain extent, cf. Fig. 3.11, in case of high supersaturation ratios. But predominantly, the deviation has to be attributed to a quantitative inaccuracy of the classical approach with respect to the present system.

T	ρ/ρ''	y_o	ℓ	J_ℓ	i^*	\mathcal{W}	J/Q_{CNT}	
238.4	2.80	1/2	50	$1.5 \cdot 10^{33}$	66	0.03	$2.6 \cdot 10^{31}$	
			85	$1.6 \cdot 10^{32}$			$3.3 \cdot 10^{30}$	
		1		50	$5.6 \cdot 10^{32}$	41	1	$9.9 \cdot 10^{31}$
				85	$2.1 \cdot 10^{32}$			$7.6 \cdot 10^{31}$
	3.08	1/2		50	$5.5 \cdot 10^{33}$	65	0.02	$3.1 \cdot 10^{31}$
				150	$3.1 \cdot 10^{32}$			$3.9 \cdot 10^{30}$
		1		50	$6.3 \cdot 10^{33}$	39	1	$1.6 \cdot 10^{32}$
				150	$2.9 \cdot 10^{32}$			$1.3 \cdot 10^{32}$
	3.36	1/3	—	—	$\ll 10^{31}$	127	$4.2 \cdot 10^{-6}$	$1.1 \cdot 10^{27}$
				1/2	50			$1.1 \cdot 10^{34}$
		1		300	$3.2 \cdot 10^{32}$	37	1	$4.2 \cdot 10^{30}$
				50	$6.7 \cdot 10^{33}$			$2.1 \cdot 10^{32}$
			300	$1.4 \cdot 10^{33}$			$1.8 \cdot 10^{32}$	
250.2	2.34	1/2	50	$1.1 \cdot 10^{34}$	140	$1.9 \cdot 10^{-4}$	$1.8 \cdot 10^{33}$	
			100	$1.1 \cdot 10^{33}$			$7.8 \cdot 10^{29}$	
		1		50	$1.3 \cdot 10^{33}$	54	1	$3.9 \cdot 10^{32}$
				100	$3.4 \cdot 10^{32}$			$1.4 \cdot 10^{32}$
	2.53	1/2		85	$7.4 \cdot 10^{33}$	143	$1.0 \cdot 10^{-4}$	$3.9 \cdot 10^{30}$
				200	$7.4 \cdot 10^{32}$			$3.1 \cdot 10^{28}$
		1		85	$2.2 \cdot 10^{33}$	52	1	$1.9 \cdot 10^{32}$
				200	$7.7 \cdot 10^{32}$			$1.9 \cdot 10^{32}$
	2.72	1/3	—	—	$\ll 10^{31}$	879	$4.3 \cdot 10^{-25}$	$2.3 \cdot 10^8$
				1/2	75			$1.3 \cdot 10^{34}$
		1		250	$1.6 \cdot 10^{33}$	50	1	$1.7 \cdot 10^{28}$
				75	$4.8 \cdot 10^{33}$			$2.6 \cdot 10^{32}$
			250	$1.4 \cdot 10^{33}$			$2.5 \cdot 10^{32}$	

Table 3.4: Droplet formation rate from YM canonical ensemble MD simulation as well as critical droplet size (in molecules), *Wedekind* factor \mathcal{W} , and the CNT prediction for the droplet formation rate $J_\ell/Q(\ell)$, in dependence of temperature (in units of K), supersaturation and mole fraction of CO_2 in the vapor as well as the YM threshold size ℓ (in molecules). The rates are given in units of $\text{m}^{-3}\text{s}^{-1}$. Where no nucleation was observed during simulation, no value of ℓ is listed and J according to CNT is shown instead of J/Q .

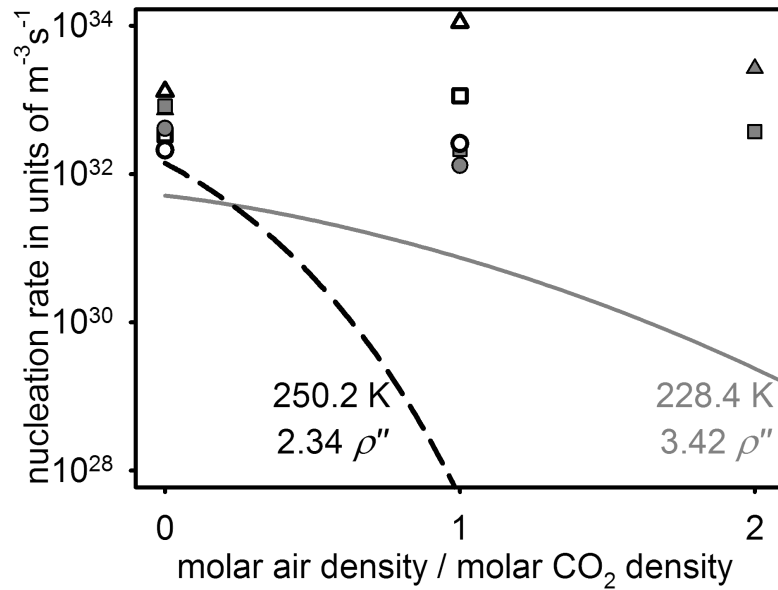


Figure 3.10: Nucleation rate J_{CNT} according to CNT with the pressure effect at $T = 228.4$ K and $\rho(\text{CO}_2)/\rho''(\text{CO}_2) = 3.42$ (solid line) as well as $T = 250.2$ K and $\rho(\text{CO}_2)/\rho''(\text{CO}_2) = 2.34$ (dashed line), in comparison with the droplet formation rate J_ℓ from MD simulation for $\ell = 50$ (Δ), 100 (\square), and 150 (\circ), whereby full symbols correspond to $T = 228.4$ K and empty symbols to 250.2 K, plotted over the ratio between air and CO_2 molecules in the system, i.e. over $y_0^{-1} - 1$. It should be noted that at $T = 250.2$ K (and at 228.4 K regarding droplets with more than 150 molecules) no formation rate could be determined for $y_0^{-1} - 1 = 2$, implying that the value must be smaller than $10^{29} \text{ m}^{-3}\text{s}^{-1}$.

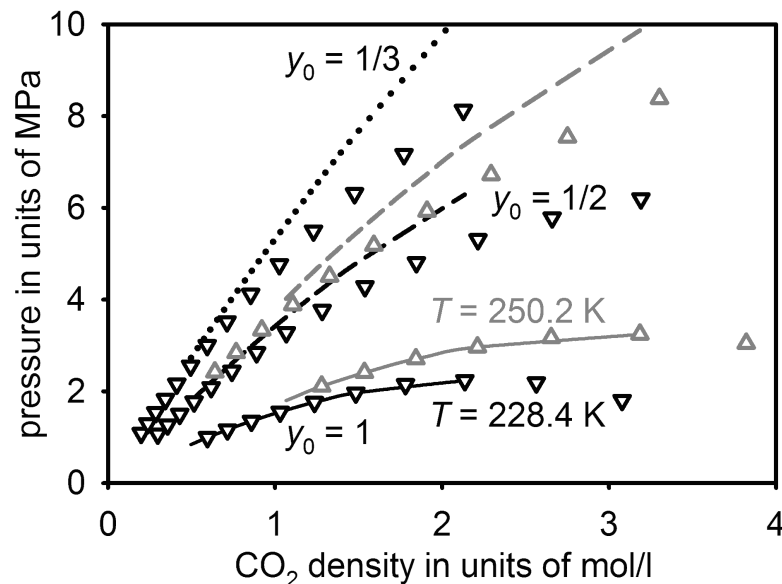


Figure 3.11: Pressure over CO_2 density from canonical ensemble MD simulation of small homogeneous systems at $T = 228.4$ (∇) and 250.2 K (Δ) in comparison with the metastable section of the vapor pressure isotherm for pure CO_2 (solid lines) – correlated to the simulation results – increased by an ideal carrier gas contribution, cf. Eq. (3.16), for CO_2 molar fractions $y_0 = 1/2$ (dashed lines) and $1/3$ (dotted line).

4 Conclusion

From the preceding analysis of homogeneous nucleation and vapor-liquid interfaces it can be concluded that CNT is able to capture both the nucleation rate and the critical droplet size of non-polar fluids, represented by the LJ-TS model. This requires a *Farkas* [172] prefactor of $\mathcal{C} = 200$, cf. Eq. (2.24), as well as taking the *Zel'dovič* [264] factor, the thermal non-accommodation correction of *Feder et al.* [261], and the pressure effect on the free energy of droplet formation into account, cf. Eq. (2.31).

The main criticism usually made of CNT is that it applies the capillarity approximation to small droplets where significant curvature effects can be expected and have for certain systems even been proven by molecular simulation [85, 87, 355–358]. While CNT is based on the assumption $\gamma = \gamma_\infty$, the deviation from capillarity is still considered for J by the prefactor $\mathcal{C} > 1$ which empirically accounts for the overall perturbation effect. This corresponds to stating that the capillarity approximation overestimates the free energy barrier ΔA^* by an amount of $T \ln \mathcal{C}$.

According to the CNT expression for $\partial A / \partial v$ given by Eq. (2.49), the critical droplet is characterized by the condition

$$\frac{2\gamma^*}{R_\gamma^* \rho_i^*} - (\mu - \mu^*) - \frac{2\gamma^*}{R_{\mathcal{L}}^* \rho_i^*} = 0. \quad (4.1)$$

Since the surface of tension radius R_γ and the *Laplace* radius $R_{\mathcal{L}}$ are equal, cf. Eq. (2.51), only the immediate equilibrium condition remains, i.e.

$$\mu = \mu^*. \quad (4.2)$$

No particular assumptions are made for the chemical potential of the supersaturated vapor μ which can be related to its other thermophysical properties according to an EOS or by molecular simulation. However, the chemical potential μ^* inside the critical droplet is given by Eq. (2.18) which relies on the pressure difference from the *Laplace* equation using the surface tension of the planar interface.

As demonstrated by canonical ensemble MD simulation of single droplets, the *Tolman* length is positive over the whole range of vapor-droplet equilibrium configurations and becomes larger for smaller droplets. This implies that the adsorption radius R_ρ of a droplet in equilibrium does not approach zero, since R_ρ is always greater than δ . Hence, only droplets exceeding a certain minimal size can be described by the approach based on formal effective dividing surfaces as introduced by *Gibbs* and applied by *Tolman* [174, 187].

The limit $R_\gamma \rightarrow 0$ is also problematic, because the *Laplace* equation requires that the pressure inside the droplet goes to infinity. The chemical potential increases as well until it exceeds the chemical potential $\mu^\#$ of the vapor at the spinodal line. At this point, the entire approach behind that description breaks down, because a vapor beyond the spinodal, which could be in equilibrium with such a droplet, does not exist. For these extremely small droplets, no equilibrium radial profiles can be obtained for the density and for the normal or tangential

pressure, because they can never be in a stable or unstable equilibrium with a vapor phase. For the same reason, the *Laplace* equation, which is based on the mechanical equilibrium condition, does not apply either.

Since δ increases with droplet curvature, the *Tolman* length becomes the dominant contribution to the adsorption radius $R_\rho = R_\gamma + \delta$ of extremely small droplets, which goes through a minimum and diverges for $R_\gamma \rightarrow 0$, cf. Fig. 4.1. If this is extrapolated to extremely small radii according to the first-order curvature expansion given by Eq. (2.72), a droplet stability limit is obtained for the *Tolman* model, i.e.

$$R_\gamma^\#(T) = 0.3317 \left(1 - \frac{T}{T_c}\right)^{-1.05} \sigma, \quad (4.3)$$

$$R_\rho^\#(T) = 2R_\gamma^\#(T) + \delta_\infty(T). \quad (4.4)$$

in case of the LJ-TS fluid, which is probably related to the critical droplet size at the spinodal supersaturation $S_\mu^\#$.

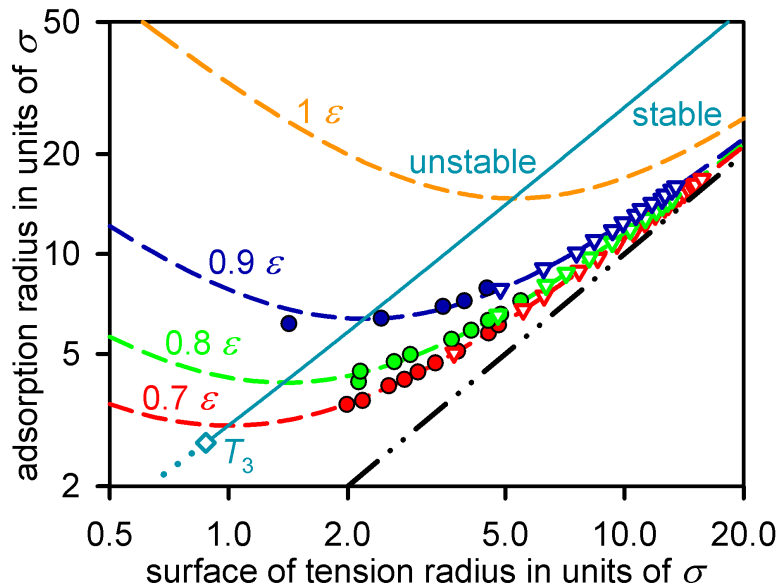


Figure 4.1: Adsorption radius R_ρ over surface of tension radius R_γ for droplets of the LJ-TS fluid at temperatures of 0.7, 0.8, 0.9, and 1 ε according to the first-order curvature expansion of the *Tolman* length (dashed lines), cf. Eq. (2.72), and determined by canonical ensemble equilibrium MD simulation, (\bullet) from the present work and (∇) from an earlier study [85]. The droplet stability limit (solid line) is based on the first-order curvature expansion, cf. Eq. (4.4), and is shown together with its extension (dotted line) below the triple point temperature $T_3 \approx 0.65 \varepsilon$. The dashed-dotted line corresponds to $\delta = 0$, i.e. equal surface of tension and adsorption radii.

Both limits describe the transition to instability, and the smallest droplet which can be stabilized has to be in equilibrium with the most dense metastable vapor state, i.e. the supersaturated vapor on the spinodal line. Furthermore, the droplet stability limit for the *Tolman* model and the CNT value for the critical droplet size on the spinodal line are of the same order of magnitude and exhibit the same tendency with respect to temperature variations.

Many problems and inherent contradictions demonstrate that CNT and, generally, all theories that rely on a stationary and spherical effective dividing surface, as discussed by *Gibbs*,

are not entirely satisfactory on the molecular level. Even for simple fluids where nucleation can be reproduced and observed in all its details by molecular simulation, fundamental issues thus remain to be solved, e.g.

- how to characterize droplets on the length scale where the *Gibbs* approach becomes inapplicable, and
- based on a thermodynamic understanding of droplets on the molecular length scale, how to formulate a consistent treatment of nucleation kinetics.

The present work does not pretend to settle these questions. Instead, the following questions are raised as a point of departure for future projects:

- A) What is the rate of evaporation \mathcal{E} for a nanoscopic droplet?
- B) Is it sufficiently accurate to use expressions based on the droplet size r as an approximation for the reaction coordinate Q of vapor to liquid nucleation? If that is not the case, what would be a more suitable order parameter?
- C) Can an aggregated kinetic model, relying on a relatively small set of adequately chosen order parameters, reproduce the details of nucleation processes as determined by direct MD simulation?

List of previous publications

Previous to the dissertation work:

- C. Makala and M. Horsch: 2003, 'GIS und modellgestütztes Lernen am Beispiel von Bewertungsaufgaben im Rahmen der Flächennutzungs- und Landschaftsplanung'. In: *Beiträge zum AGIT-Symposium 2003 in Salzburg – Angewandte Geographische Informationsverarbeitung XV*. Heidelberg: Wichmann, pp. 274–279.
- M. Horsch: 2005, 'Test case generation for rule-based translators'. Technical report nr. 1984 (Studienarbeit), Universität Stuttgart, Fakultät Informatik, Elektrotechnik und Informationstechnik.
- M. Horsch: 2006, 'Spiele und temporallogische Fragmente über Spuren'. Technical report nr. 2391 (Diplomarbeit), Universität Stuttgart, Fakultät Informatik, Elektrotechnik und Informationstechnik.
- V. Diekert, M. Horsch, and M. Kufleitner: 2007, 'On first-order fragments for Mazurkiewicz traces'. *Fundamenta Informaticæ* **80**(1–3): 1–29.

Publications related to the thesis (appeared until November 11, 2010):

- M. Horsch, J. Vrabec, M. Bernreuther, S. Grottel, G. Reina, A. Wix, K. Schaber, and H. Hasse: 2008, 'Homogeneous nucleation in supersaturated vapors of methane, ethane, and carbon dioxide predicted by brute force molecular dynamics'. *The Journal of Chemical Physics* **128**: 164510.
- M. Horsch, J. Vrabec, and H. Hasse: 2008, 'Molecular dynamics based analysis of nucleation and surface energy of droplets in supersaturated vapors of methane and ethane'. In: *2008 Proceedings of the ASME Micro/Nanoscale Heat Transfer International Conference*. Biggleswade: Eurospan, pp. 185–186.
- M. Horsch, J. Vrabec, and H. Hasse: 2008, 'Modification of the classical nucleation theory based on molecular simulation data for surface tension, critical nucleus size, and nucleation rate'. *Physical Review E* **78**: 011603.
- J. Vrabec, M. Horsch, and H. Hasse: 2009, 'Molecular dynamics based analysis of nucleation and surface energy of droplets in supersaturated vapors of methane and ethane'. *Journal of Heat Transfer* **131**: 043202.
- B. Eckl, M. Horsch, J. Vrabec, and H. Hasse: 2009, 'Molecular modeling and simulation of thermophysical properties: Application to pure substances and mixtures'. In: *High Performance Computing in Science and Engineering '08 – Transactions of the High Performance Computing Center Stuttgart (HLRS)*. Heidelberg: Springer, pp. 119–133.

-
- M. Horsch and J. Vrabec: 2009, 'Steady-state simulation of homogeneous vapor-liquid nucleation «by the intervention of intelligent beings»'. In: *Nucleation and Atmospheric Aerosols*. Prague: Czech Aerosol Society, pp. 585-588.
 - M. Bernreuther, C. Niethammer, M. Horsch, J. Vrabec, S. Deublein, H. Hasse, and M. Buchholz: 2009, 'Innovative HPC methods and application to highly scalable molecular simulation'. *Innovatives Supercomputing in Deutschland* **7**(1): 50–53.
 - M. Horsch, J. Vrabec, M. Bernreuther, and H. Hasse: 2009, 'Poiseuille flow of liquid methane in nanoscopic graphite channels by molecular dynamics simulation'. In: *Proceedings of the International Symposium Turbulence, Heat and Mass Transfer 6*. New York: Begell House, pp. 89–92.
 - M. Horsch and J. Vrabec: 2009, 'Grand canonical steady-state simulation of nucleation'. *The Journal of Chemical Physics* **131**: 184104.
 - M. Horsch, S. Miroshnichenko, and J. Vrabec: 2009, 'Steady-state molecular dynamics simulation of vapour to liquid nucleation with McDonald's daemon'. *Žurnal Fizičnih Dosliden' (Журнал Фізичних Досліджень)* **13**: 4004.
 - M. Horsch, M. Heitzig, T. Merker, T. Schnabel, Y.-L. Huang, H. Hasse, and J. Vrabec: 2010, 'Molecular modeling of hydrogen bonding fluids: Vapor-liquid coexistence and interfacial properties'. In: *High Performance Computing in Science and Engineering '09 – Transactions of the High Performance Computing Center Stuttgart (HLRS)*. Heidelberg: Springer, pp. 471–483.
 - J. Vrabec, E. Baumhögger, A. Elsner, M. Horsch, Z. Liu, S. Miroshnichenko, A. Nazdrajić, and T. Windmann: 2010, 'Molecular simulation of fluid dynamics on the nanoscale'. In: *Sixth International Conference on Computational Fluid Dynamics*. St. Petersburg: VVM Publishing Co., pp. 106–107.
 - G. C. Lehmann, F. Dubberke, M. Horsch, Y.-L. Huang, S. Miroshnichenko, R. Pflock, G. Sonnenrein, and J. Vrabec: 2010, 'Research on the behavior of liquid fluids atop superhydrophobic gas-bubbled surfaces'. In: *Sixth International Conference on Computational Fluid Dynamics*. St. Petersburg: VVM Publishing Co., pp. 108–109.
 - M. Horsch, M. Heitzig, C. Dan, J. Harting, H. Hasse, and J. Vrabec: 2010, 'Contact angle dependence on the fluid-wall dispersive energy'. *Langmuir* **26**(13): 10913–10917.

Scheduled articles (accepted for publication as of November 11, 2010):

- J. Walter, T. Merker, M. Horsch, J. Vrabec, and H. Hasse: 2010, 'Development of models and methods for the molecular simulation of large systems and molecules'. Technical report arXiv:1005.4202v1 [physics.comp-ph], to appear in *High Performance Computing in Science and Engineering '10 – Transactions of the High Performance Computing Center Stuttgart (HLRS)*.
- M. Horsch, Z. Lin, T. Windmann, H. Hasse, and J. Vrabec: 2010, 'The air pressure effect on the homogeneous nucleation of carbon dioxide by molecular simulation'. Technical report arXiv:1001.1857v1 [physics.ao-ph], to appear in *Atmospheric Research*.

Bibliography

- [1] *J. Walter*: 2006, 'Molekulare Simulation und Visualisierung der Keimbildung in Mischungen'. Studienarbeit, Institut für Technische Thermodynamik und Thermische Verfahrenstechnik, Universität Stuttgart. ITT report number 06/06.
- [2] *J. J. O'Connor* and *E. F. Robertson*: 2010, 'The MacTutor history of mathematics archive'. <http://www-groups.dcs.st-and.ac.uk/~history/>.
- [3] *L. Boltzmann*: 1898, *Vorlesungen über Gastheorie, Band II*. Leipzig: Johann Ambrosius Barth.
- [4] *G. Gallavotti*, *F. Bonetto*, and *G. Gentile*: 2004, *Aspects of ergodic, qualitative, and statistical theory of motion*, Texts and Monographs in Physics. Berlin – Heidelberg – New York: Springer. ISBN 3-540-40879-7.
- [5] *L. Boltzmann*: 1868, 'Studien über das Gleichgewicht der lebendigen Kraft zwischen bewegten und materiellen Punkten'. *Sitzungsberichte der Kaiserlichen Akademie der Wissenschaften (Wien)* **58**, 517–560.
- [6] *L. Boltzmann*: 1871, 'Einige allgemeine Sätze über Wärmegleichgewicht'. *Sitzungsberichte der Kaiserlichen Akademie der Wissenschaften (Wien)* **63**, 679–711.
- [7] *J. Uffink*: 2008, 'Boltzmann's work in statistical physics'. In: *E. N. Zalta* (ed.): *The Stanford encyclopedia of philosophy*. Winter 2008 edition. <http://plato.stanford.edu/archives/win2008/entries/statphys-boltzmann/>.
- [8] *L. Boltzmann*: 1872, 'Weitere Studien über das Wärmegleichgewicht unter Gasmolekülen'. *Sitzungsberichte der Kaiserlichen Akademie der Wissenschaften (Wien)* **66**, 275–370.
- [9] *L. Boltzmann*: 1877, 'Über die Beziehung zwischen dem zweiten Hauptsatz der mechanischen Wärmetheorie und der Wahrscheinlichkeitsrechnung resp. den Sätzen über das Wärmegleichgewicht'. *Sitzungsberichte der Kaiserlichen Akademie der Wissenschaften (Wien)* **76**, 373–435.
- [10] *G. Jaffé*: 1930, 'Zur Methodik der kinetischen Gastheorie'. *Annalen der Physik* **398**(2), 195–252.
- [11] *P. H. Thiry d'Holbach*: 1781, *Systeme de la nature – des lois du monde physique et du monde moral*. Published in London under the name of *J.-B. de Mirabaud*.
- [12] *V. I. Lenin*: 1909, *Materializm" i èmpiriokriticizm"* (Материализмъ и эмпириокритицизмъ). Moscow: Zveno (Звено).
- [13] *U. von Hehl* and *U. Morgenstern*: 2010. *Catalogus Professorum Lipsiensis*. <http://www.uni-leipzig.de/unigeschichte/professorenkatalog/>.

-
- [14] *L. Boltzmann*: 1866, 'Über die mechanische Bedeutung des zweiten Hauptsatzes der mechanischen Wärmetheorie'. *Sitzungsberichte der Kaiserlichen Akademie der Wissenschaften (Wien)* **53**(2), 195–200.
- [15] *P. L. Duren*, *R. Askey*, and *U. C. Merzbach*: 1989, *A century of mathematics in America, part II*, No. 2 in *History of Mathematics*. Providence, Rhode Island: American Mathematical Society. ISBN 0-8218-0130-9.
- [16] *J. W. Gibbs*: 1902, *Elementary Principles in Statistical Mechanics – developed with especial reference to the rational foundation of thermodynamics*. New York: Charles Scribner's Sons.
- [17] *J. W. Gibbs*: 1928, *Collected Works*. New York: Longmans Green.
- [18] *J. W. Gibbs*: 1878, 'On the equilibrium of heterogeneous substances'. *Transactions of the Connecticut Academy of Arts and Sciences* **3**, 108–248 (1876), 343–524 (1878).
- [19] *J. W. Gibbs*: 1878, 'Abstract of the «Equilibrium of heterogeneous substances»'. *American Journal of Science, series 3* **16**, 441–458.
- [20] *Nobel Foundation*: 2010, 'The Nobel Prize website'. <http://nobelprize.org/>.
- [21] *J. W. Gibbs*: 1947, 'On the form of the teeth of wheels in spur gearing'. In: *L. P. Wheeler*, *E. O. Waters*, and *S. W. Dudley* (eds.): *The early work of Willard Gibbs in applied mechanics*. New York: H. Schuman, pp. 7–39. ISBN 1881987175.
- [22] *J. D. van der Waals*: 1873, 'Over de continuïteit van den gas- en vloeistooftoestand'. Ph.D. thesis, Universiteit Leiden.
- [23] *J. Clerk-Maxwell*: 1874, 'Van der Waals on the continuity of the gaseous and liquid states'. *Nature* **10**(259), 477–480.
- [24] *J. O. Hirschfelder*: 1960, 'Classical and quantum mechanical hypervirial theorems'. *The Journal of Chemical Physics* **33**(5), 1462–1466.
- [25] *R. Clausius*: 1870, 'Ueber einen auf die Wärme anwendbaren mechanischen Satz'. *Annalen der Physik* **217**(9), 124–130.
- [26] *J. D. van der Waals*: 1899, 'On the deduction of the characteristic equation'. *Proceedings of the Koninklijke Nederlandse Akademie van Wetenschappen* **1**, 468–473.
- [27] *A. A. Abrikosov*, *L. P. Gorkov*, and *I. E. Dzyaloshinski*: 1975, *Methods of quantum field theory in statistical physics*. Dover. ISBN 0-486-63228-8.
- [28] *J. D. van der Waals*: 1911, 'On the value of the critical quantities'. *Proceedings of the Koninklijke Nederlandse Akademie van Wetenschappen* **13**(2), 1211–1231.
- [29] *A. Müller*, *J. Winkelmann*, and *J. Fischer*: 1996, 'The BACKONE family of equations of state: 1. Nonpolar and polar pure fluids'. *AIChE Journal* **42**(4), 1116–1126.
- [30] *J. Gross* and *G. Sadowski*: 2001, 'Perturbed-Chain SAFT: An equation of state based on a perturbation theory for chain molecules'. *Industrial & Engineering Chemistry Research* **40**(4), 1244–1260.

- [31] S. Korden, V. N. Nguyen, J. Vrabec, J. Gross, and K. Leonhard: 2010, 'On the treatment of electrostatic interactions of non-spherical molecules in equation of state models'. To appear in *Soft Materials*.
- [32] E. M. Blokhuis and D. Bedeaux: 1993, 'Van der Waals theory of curved surfaces'. *Molecular Physics* **80**(4), 705–720.
- [33] K. Katsov and J. D. Weeks: 2002, 'Incorporating molecular scale structure into the van der Waals Theory of the liquid-vapor interface'. *Journal of Physical Chemistry B* **106**(33), 8429–8436.
- [34] T. Kraska, F. Römer, and A. Imre: 2009, 'The relation of interface properties and bulk phase stability'. *Journal of Physical Chemistry B* **113**(14), 4688–4697.
- [35] *Smithsonian Institution Libraries*: 2010, 'Dibner library of the history of science and technology'. <http://www.sil.si.edu/digitalcollections/hst/scientific-identity/>.
- [36] W. Ostwald: 1900, 'Über die vermeintliche Isomerie des roten und gelben Quecksilberoxyds und die Oberflächenspannung fester Körper'. *Zeitschrift für physikalische Chemie (Leipzig)* **34**, 495.
- [37] W. Ostwald: 1906, *Die internationale Hilfssprache und das Esperanto*. Berlin: Esperanto Verlag Möller & Borel.
- [38] W. Ostwald: 1912, *Monismus als Kulturziel*. Wien – Leipzig: Suschitzky.
- [39] W. Ostwald: 1919, *Grundsätzliches zur Erziehungsreform*. Berlin: Verlag Gesellschaft und Erziehung.
- [40] H. Abert: 1931, *Das Geldkapital als Perpetuum mobile: Über die unendliche Zinspflicht*. Darmstadt – Leipzig: Ernst Hofmann & Co. Preface by W. Ostwald.
- [41] J.-P. Domschke and P. Lewandowski: 1982, *Wilhelm Ostwald: Chemiker, Wissenschaftstheoretiker, Organisator*. Leipzig – Jena – Berlin: Urania.
- [42] W. Ostwald: 1912, *Der energetische Imperativ*. Leipzig: Akademische Verlagsgesellschaft.
- [43] W. Ostwald: 1902, *Vorlesungen über Naturphilosophie*. Leipzig: Veit. ASIN B001VCL4C4.
- [44] W. Ostwald: 1895, 'Die Überwindung des wissenschaftlichen Materialismus'. In: *Verhandlungen der Gesellschaft deutscher Naturforscher und Ärzte 1895. 67. Versammlung*.
- [45] W. Ostwald: 1910, *Die Forderung des Tages*. Leipzig: Akademische Verlagsgesellschaft. ASIN B002C1Q0MM.
- [46] W. Ostwald: 1919, *Einführung in die Farbenlehre*. Leipzig: Reclam.
- [47] *Public domain. Problemy (monthly journal)* December 1967: 726, retrieved via Wikipedia.
- [48] W. Ostwald: 1878, 'Volumchemische und optisch-chemische Studien'. Ph.D. thesis, Kaiserliche Universität in Dorpat, physiko-mathematische Fakultät, Dorpat.

- [49] *W. Ostwald*: 1885, 'Elektrochemische Studien. Zweite Abhandlung: Das Verdünnungsgesetz'. *Journal für Praktische Chemie* **31**, 433–462.
- [50] *M. von Smoluchowski*: 1908, 'Molekular-kinetische Theorie der Opaleszenz von Gasen im kritischen Zustande, sowie einiger verwandter Erscheinungen'. *Annalen der Physik* **330**(2), 205–226.
- [51] *A. Einstein*: 1910, 'Theorie der Opaleszenz von homogenen Flüssigkeiten und Flüssigkeitsgemischen in der Nähe des kritischen Zustandes'. *Annalen der Physik* **338**(16), 1275–1297.
- [52] *M. von Smoluchowski*: 1915, 'Molekulartheoretische Studien über Umkehr thermodynamisch irreversibler Vorgänge und über Wiederkehr abnormaler Zustände'. *Sitzungsberichte der Kaiserlichen Akademie der Wissenschaften (Wien)* **5**, 339–368.
- [53] *M. von Smoluchowski*: 1915, 'Über gewisse Mängel in der Begründung des Entropiesatzes sowie der Boltzmann'schen Grundgleichung in der kinetischen Gastheorie'. *Bulletin International de l'Académie des Sciences de Cracovie, classe des sciences mathématiques et naturelles, série A* **1**, 164–178.
- [54] *M. von Smoluchowski*: 1906, 'Zur kinetischen Theorie der Brownschen Molekularbewegung und der Suspensionen'. *Annalen der Physik* **326**(14), 756–780.
- [55] *M. von Smoluchowski*: 1912, 'Experimentell nachweisbare, der üblichen Thermodynamik widersprechende Molekularphänomene'. *Physikalische Zeitschrift* **13**, 1069–1080.
- [56] *M. von Smoluchowski*: 1914, 'Gültigkeitsgrenzen des zweiten Hauptsatzes der Wärmetheorie'. In: *Vorträge über die Kinetische Theorie der Materie und der Elektrizität*. Berlin–Leipzig: *Teubner*, pp. 89–121.
- [57] *O. Preining*: 2009, 'Smoluchowski von Smolan'. In: *E. Bruckmüller et al. (eds.): Österreichisches Biographisches Lexikon 1815–1950*, Vol. 12. Wien: Verlag der Österreichischen Akademie der Wissenschaften, pp. 380–381. ISBN 3-7001-3213-4, <http://www.biographien.ac.at/oeb1/>.
- [58] *M. von Smoluchowski*: 1894, *Akustische Untersuchungen über die Elasticität weicher Körper*. Wien: *Gerold*.
- [59] *M. P. Allen and D. J. Tildesley*: 1987, *Computer simulation of liquids*. Oxford: *Clarendon*.
- [60] *D. Frenkel and B. Smit*: 2002, *Understanding molecular simulation*. San Diego – San Francisco – New York: *Academic Press*. Second edition. ISBN 0-12-267351-4.
- [61] *M. Griebel, S. Knapek, G. Zumbusch, and A. Caglar*: 2004, *Numerische Simulation in der Moleküldynamik*. Berlin – Heidelberg – New York: *Springer*. ISBN 3-540-41856-3.
- [62] *L. D. Landau and E. M. Lifšic*: 1951, *Statističeskaâ fizika (Статистическая физика)*. GIITL (ГИИТЛ). Volume 5, part 1 of *Kurs teoretičeskoj fiziki (Курс теоретической физики)*. ISBN 5-02-014421-5.

- [63] C. A. de Coulomb: 1785, 'Premier mémoire sur l'électricité et le magnétisme: Construction et usage d'une balance électrique, fondée sur la propriété qu'ont les fils de métal, d'avoir une force de réaction de torsion proportionnelle à l'angle de torsion'. *Mémoires de l'Académie Royale des Sciences* **88**, 569–577.
- [64] C. A. de Coulomb: 1785, 'Second mémoire sur l'électricité et le magnétisme, où l'on détermine, suivant quelles lois le fluide magnétique, ainsi que le fluide électrique, agissent, soit par répulsion, soit par attraction, avec 1 planche'. *Mémoires de l'Académie Royale des Sciences* **88**, 578–611.
- [65] J. Vrabec and J. Groß: 2008, 'Vapor-liquid equilibria simulation and an equation of state contribution for dipole-quadrupole interactions'. *Journal of Physical Chemistry B* **112**(1), 51–60.
- [66] J. Vrabec: 2009, 'Molekulare Thermodynamik'. Lecture notes, Universität Paderborn, Institut für Verfahrenstechnik. Winter semester 2009/10.
- [67] B. Eckl, J. Vrabec, and H. Hasse: 2008, 'On the application of force fields for predicting a wide variety of properties: Ethylene oxide as an example'. *Fluid Phase Equilibria* **274**(1–2), 16–26.
- [68] B. Eckl, J. Vrabec, and H. Hasse: 2008, 'Set of molecular models based on quantum mechanical ab initio calculations and thermodynamic data'. *Journal of Physical Chemistry B* **112**(40), 12710–12721.
- [69] R. W. Zwanzig: 1954, 'High-temperature equation of state by a perturbation method. I. Nonpolar gases'. *The Journal of Chemical Physics* **22**(8), 1420–1426.
- [70] J. Fischer: 2010, 'Ausgewählte Kapitel der Molekularen Thermodynamik'. Lecture notes, Universität Paderborn, Institut für Verfahrenstechnik. Winter semester 2009/10.
- [71] J. R. Henderson and P. Schofield: 1982, 'Statistical mechanics of a fluid drop'. *Proceedings of the Royal Society of London A* **380**, 211–227.
- [72] H. C. Longuet-Higgins and B. Widom: 1965, 'A rigid sphere model for the melting of argon'. *Molecular Physics* **8**(6), 549–556.
- [73] W. Sutherland: 1893, 'The viscosity of gases and molecular force'. *Philosophical Magazine, series 5* **36**(223), 507–531.
- [74] N. F. Carnahan and K. E. Starling: 1969, 'Equation of state for nonattracting rigid spheres'. *The Journal of Chemical Physics* **51**(2), 635–636.
- [75] N. F. Carnahan and K. E. Starling: 1970, 'Analytical equation for rigid spheres: Application to the model of Longuet-Higgins and Widom for the melting of argon'. *Physical Review A* **1**(6), 1672–1673.
- [76] F. London: 1930, 'Über einige Eigenschaften und Anwendungen der Molekularkräfte'. *Zeitschrift für physikalische Chemie (Leipzig)* **11**, 222–251.
- [77] F. London: 1937, 'The general theory of molecular forces'. *Transactions of the Faraday Society* **33**, 8–26.

- [78] R. A. Buckingham: 1938, 'The classical equation of state of gaseous helium, neon and argon'. *Proceedings of the Royal Society of London A* **168**(933), 264–283.
- [79] J. E. Jones: 1924, 'On the determination of molecular fields'. *Proceedings of the Royal Society of London A* **106**(738), 441–477.
- [80] P. Adams and J. R. Henderson: 1991, 'Molecular dynamics simulations of wetting and drying in LJ models of solid-fluid interfaces in the presence of liquid-vapour coexistence'. *Molecular Physics* **73**(6), 1383–1399.
- [81] B. Smit: 1992, 'Phase diagrams of Lennard-Jones fluids'. *The Journal of Chemical Physics* **96**(11), 8639–8640.
- [82] C. D. Holcomb, P. Clancy, and J. A. Zollweg: 1993, 'A critical study of the simulation of the liquid-vapour interface of a Lennard-Jones fluid'. *Molecular Physics* **78**(2), 437–459.
- [83] A. Trokhymchuk and J. Alejandre: 1999, 'Computer simulations of liquid/vapor interface in Lennard-Jones fluids: Some questions and answers'. *The Journal of Chemical Physics* **111**(18), 8510–8523.
- [84] D. O. Dunikov, S. P. Malysenko, and V. V. Zhakhovskii: 2001, 'Corresponding states law and molecular dynamics simulations of the Lennard-Jones fluid'. *The Journal of Chemical Physics* **115**(14), 6623–6631.
- [85] J. Vrabec, G. K. Kedia, G. Fuchs, and H. Hasse: 2006, 'Comprehensive study on vapour-liquid coexistence of the truncated and shifted Lennard-Jones fluid including planar and spherical interface properties'. *Molecular Physics* **104**(9), 1509–1527.
- [86] C. Valeriani, Z.-J. Wang, and D. Frenkel: 2007, 'Comparison of simple perturbation-theory estimates for the liquid-solid and liquid-vapor interfacial free energies of Lennard-Jones systems'. *Molecular Simulation* **33**(13), 1023–1028. Corrigendum: 2009, *Molecular Simulation* **35**(5), 429–430.
- [87] M. Schrader, P. Virnau, and K. Binder: 2009, 'Simulation of vapor-liquid coexistence in finite volumes: A method to compute the surface free energy of droplets'. *Physical Review E* **79**, 061104.
- [88] M. Schrader, P. Virnau, D. Winter, T. Zykova-Timan, and K. Binder: 2009, 'Methods to extract interfacial free energies of flat and curved interfaces from computer simulations'. *European Physical Journal Special Topics* **177**(1), 103–127.
- [89] J. D. Weeks, D. Chandler, and H. C. Andersen: 1971, 'Role of repulsive forces in determining the equilibrium structure of simple liquids'. *The Journal of Chemical Physics* **54**(12), 5237–5247.
- [90] D. Chandler, J. D. Weeks, and H. C. Andersen: 1983, 'Van der Waals picture of liquids, solids, and phase transformations'. *Science* **220**(4599), 787–794.
- [91] Z. S. Ziarani and A. A. Mohamad: 2005, 'A molecular dynamics study of perturbed Poiseuille flow in a nanochannel'. *Microfluidics and Nanofluidics* **2**, 12–20.

- [92] D. M. Heyes and H. Okumura: 2006, 'Some physical properties of the Weeks-Chandler-Andersen fluid'. *Molecular Simulation* **32**(1), 45–50.
- [93] J. Horbach and S. Succi: 2006, 'Lattice Boltzmann versus molecular dynamics simulation of nanoscale hydrodynamic flows'. *Physical Review Letters* **96**, 224503.
- [94] R. A. Aziz and H. H. Chen: 1977, 'An accurate intermolecular potential for argon'. *The Journal of Chemical Physics* **67**(12), 5719–5726.
- [95] A. Janzen and R. A. Aziz: 1995, 'Transport properties and second virial coefficients for xenon'. *Chemical Engineering Communications* **135**(1), 161–173.
- [96] J. Vrabec, J. Stoll, and H. Hasse: 2001, 'A set of molecular models for symmetric quadrupolar fluids'. *Journal of Physical Chemistry B* **105**(48), 12126–12133.
- [97] A. Lotfi, J. Vrabec, and J. Fischer: 1992, 'Vapour liquid equilibria of the Lennard-Jones fluid from the NpT plus test particle method'. *Molecular Physics* **76**(6), 1319–1333.
- [98] J. J. Potoff and A. Z. Panagiotopoulos: 1998, 'Critical point and phase behavior of the pure fluid and a Lennard-Jones mixture'. *The Journal of Chemical Physics* **109**(24), 10914–10920.
- [99] J. Stoll, J. Vrabec, H. Hasse, and J. Fischer, 'Comprehensive study of the vapour-liquid equilibria of the two-centre Lennard-Jones plus pointquadrupole fluid'. *Fluid Phase Equilibria* **179**(1–2), 339–362.
- [100] C. Kriebel, M. Mecke, J. Winkelmann, J. Vrabec, and J. Fischer: 1998, 'An equation of state for dipolar two-center Lennard-Jones molecules and its application to refrigerants'. *Fluid Phase Equilibria* **142**(1–2), 15–32.
- [101] J. Stoll, J. Vrabec, and H. Hasse: 2003, 'A set of molecular models for carbon monoxide and halogenated hydrocarbons'. *The Journal of Chemical Physics* **119**(21), 11396–11407.
- [102] J. Stoll, J. Vrabec, and H. Hasse: 2003, 'Comprehensive study of the vapour-liquid equilibria of the two-centre Lennard-Jones plus pointdipole fluid'. *Fluid Phase Equilibria* **209**(1), 29–53.
- [103] J. Gross and J. Vrabec: 2006, 'An equation-of-state contribution for polar components: Dipolar molecules'. *AIChE Journal* **52**(3), 1194–1204.
- [104] H. Marchman, H. W. Prengle, and R. L. Motard: 1949, 'Compressibility and critical constants of propylene vapor'. *Industrial & Engineering Chemistry* **41**, 2658.
- [105] W. D. McCain jr. and W. T. Ziegler: 1967, 'The critical temperature, critical pressure, and vapor pressure of argon'. *Journal of Chemical & Engineering Data* **12**(2), 199–202.
- [106] L. A. Makarevich, E. S. Sokolova, and G. A. Sorina: 1968, 'Critical parameters of sulfur hexafluoride'. *Russian Journal of Physical Chemistry* **42**(1), 10.
- [107] F. Theeuwes and R. J. Bearman: 1970, 'The p,V,T behaviour of dense fluids. III. The vapor pressure and orthobaric densities of krypton'. *The Journal of Chemical Thermodynamics* **2**(2), 179–185.

- [108] F. Theeuwes and R. J. Bearman: 1970, 'The p,V,T behaviour of dense fluids. V. The vapor pressure and saturated liquid density of xenon'. *The Journal of Chemical Thermodynamics* **2**(4), 507–512.
- [109] N. E. Khazanova and E. E. Sominskaya: 1971, 'Changes in the volume of ethane near its critical point'. *Russian Journal of Physical Chemistry* **45**, 88–89.
- [110] W. Wagner, J. Ewers, and W. Pentermann: 1976, 'A new vapor-pressure measurement and a new rational vapor-pressure equation for oxygen'. *The Journal of Chemical Thermodynamics* **8**(11), 1049–1060.
- [111] J. Kijima, K. Saikawa, K. Watanabe, K. Oguchi, and I. Tanishita: 1977, 'Experimental study of thermodyn. prop. of hexafluoroethane (R116)'. In: A. Cezairliyan (ed.): *Proceedings of the 7th Symposium on Thermophysical Properties*. New York: ASME, p. 480.
- [112] J. R. Hastings, J. M. H. Levelt Sengers, and F. W. Balfour: 1980, 'The critical-region equation of state of ethene and the effect of small impurities'. *The Journal of Chemical Thermodynamics* **12**(11), 1009–1045.
- [113] R. T. Jacobsen, R. B. Stewart, and M. Jahangiri: 1986, 'Thermodynamic properties of nitrogen from the freezing line to 2000 K at pressures to 1000 MPa'. *Journal of Physical and Chemical Reference Data* **15**(2), 735–909.
- [114] D. Ambrose and C. Tsonopoulos: 1995, 'Vapor-liquid critical properties of elements and compounds. 2. Normal alkenes'. *Journal of Chemical & Engineering Data* **40**(3), 531–546.
- [115] Y. Suehiro, M. Nakajima, K. Yamada, and M. Uematsu: 1996, 'Critical parameters of x CO₂ + (1 - x) CHF₃ for $x = 1.0000, 0.7496, 0.5013, \text{ and } 0.2522$ '. *The Journal of Chemical Thermodynamics* **28**(10), 1153–1164.
- [116] T. Schnabel, J. Vrabec, and H. Hasse: 2007, 'Unlike Lennard-Jones parameters for vapor-liquid equilibria'. *Journal of Molecular Liquids* **135**(1–3), 170–178.
- [117] H. A. Lorentz: 1881, 'Ueber die Anwendung des Satzes vom Virial in der kinetischen Theorie der Gase'. *Annalen der Physik (Leipzig)* **12**(1), 127–136. Addendum: 1881, *Annalen der Physik (Leipzig)* **12**(4): 660–661.
- [118] D. Berthelot: 1898, 'Sur le mélange des gaz'. *Comptes rendus hebdomadaires des séances de l'Académie des Sciences* **126**, 1703–1706, 1857–1858.
- [119] J. Stoll, J. Vrabec, and H. Hasse: 2003, 'Vapor-liquid equilibria of mixtures containing nitrogen, oxygen, carbon dioxide, and ethane'. *AIChE Journal* **49**(8), 2187–2198.
- [120] J. Vrabec, J. Stoll, and H. Hasse: 2005, 'Molecular models of unlike interactions in fluid mixtures'. *Molecular Simulation* **31**(4), 215–221.
- [121] J. Vrabec, Y.-L. Huang, and H. Hasse: 2009, 'Molecular models for 267 binary mixtures validated by vapor-liquid equilibria: A systematic approach'. *Fluid Phase Equilibria* **279**(2), 120–135.
- [122] S. Angus, B. Armstrong, and K. M. de Reuck: 1976, *International thermodynamic tables of the fluid state. 3. Carbon dioxide*. New York: Pergamon.

- [123] K. Marsh: 1987, *Recommended reference materials for the realization of physicochemical properties*. Oxford: Blackwell.
- [124] J. Stoll: 2005, *Molecular Models for the Prediction of Thermophysical Properties of Pure Fluids and Mixtures*, No. 836 in VDI Fortschritt-Berichte, Reihe 3. Düsseldorf: VDI. Ph.D. thesis, Universität Stuttgart, Institut für Technische Thermodynamik und Thermische Verfahrenstechnik.
- [125] W. A. Steele: 1974, *The Interaction of Gases with Solid Surfaces*. Oxford: Pergamon.
- [126] Y.-L. Huang, S. Miroshnichenko, H. Hasse, and J. Vrabec: 2009, 'Henry's law constant from molecular simulation: A systematic study of 95 systems'. *International Journal of Thermophysics* **30**(6), 1791–1810.
- [127] T. Merker, C. Engin, J. Vrabec, and H. Hasse: 2010, 'Molecular model for carbon dioxide optimized to vapor-liquid equilibria'. *The Journal of Chemical Physics*. In press.
- [128] F. de Brito Mota, J. F. Justo, and A. Fazzio: 1998, 'Structural properties of amorphous silicon nitride'. *Physical Review B* **58**(13), 8323–8328.
- [129] J. Tersoff: 1989, 'Modeling solid-state chemistry: Interatomic potentials for multicomponent systems'. *Physical Review B* **39**(8), 5566–5568.
- [130] J. Tersoff: 1988, 'Empiric interatomic potential for carbon, with applications to amorphous carbon'. *Physical Review Letters* **61**(25), 2879–2882.
- [131] J.-P. Ryckaert, G. Ciccotti, and H. J. C. Berendsen: 1977, 'Numerical integration of the cartesian equations of motion of a system with constraints: Molecular dynamics of *n*-alkanes'. *Journal of Computational Physics* **23**(3), 327–341.
- [132] C. Engin, L. Sandoval, and H. M. Urbassek: 2008, 'Characterization of Fe potentials with respect to the stability of the bcc and fcc phase'. *Modelling and Simulation in Materials Science and Engineering* **16**, 35005.
- [133] L. M. Ghiringhelli, C. Valeriani, J. H. Los, E. J. Meijer, A. Fasolino, and D. Frenkel: 2008, 'State-of-the-art models for the phase diagram of carbon and diamond nucleation'. *Molecular Physics* **106**(16–18), 2011–2038.
- [134] N. Resta: 2005, 'Molecular dynamics simulations of precursor-derived Si–C–N ceramics'. Ph.d. thesis, Institut für Theoretische und Angewandte Physik, Universität Stuttgart.
- [135] D. W. Brenner: 1990, 'Empirical potential for hydrocarbons for use in simulating the chemical vapor deposition of diamond films'. *Physical Review B* **42**(15), 9458–9471.
- [136] L. M. Ghiringhelli, C. Valeriani, E. J. Meijer, and D. Frenkel: 2007, 'Local structure of liquid carbon controls diamond nucleation'. *Molecular Physics* **99**(055702).
- [137] P. C. Kelires: 1993, 'Structural properties and energetics of amorphous forms of carbon'. *Physical Review B* **47**(4), 1829–1839.
- [138] N. Wiberg: 2001, *Holleman-Wiberg Inorganic Chemistry*. San Diego: Academic Press.

-
- [139] Y. Wang, K. Scheerschmidt, and U. Gösele: 2000, 'Theoretical investigations of bond properties in graphite and graphitic silicon'. *Physical Review B* **61**(19), 12864–12869.
- [140] R. C. Thompson-Flagg, M. J. B. Moura, and M. Marder: 2009, 'Rippling of graphene'. *EPL* **85**, 46002.
- [141] R. Rojas, F. Darius, and C. Göktekin: 2010, 'Konrad Zuse Internet Archive'. <http://www.zib.de/zuse/>.
- [142] J. Ottaviani, J. Johnston, S. Lieber, V. Locke, B. Mireault, and J. Parker: 2001, *fallout: J. Robert Oppenheimer, Leo Szilard, and the Political Science of the Atomic Bomb*. Ann Arbor (Michigan): G.T. Labs. ISBN 0-9660106-3-9.
- [143] K. Bird and M. J. Sherwin: 2005, *American Prometheus: The triumph and tragedy of J. Robert Oppenheimer*. New York: Alfred A. Knopf.
- [144] J. Conant: 2005, *109 East Palace: Robert Oppenheimer and the Secret City of Los Alamos*. New York: Simon & Schuster. ISBN 0-7432-5008-7.
- [145] J. Bernstein: 1980, *Hans Bethe: Prophet of energy*. New York: Basic Books. ISBN 978-0465029037.
- [146] A. K. Esterer and L. A. Esterer: 1972, *Prophet of the atomic age: Leo Szilard*. New York: Julian Messner. ISBN 067132523X.
- [147] S. A. Blumberg and L. G. Panos: 1990, *Edward Teller: Giant of the Golden Age of physics*. HarperCollins. ISBN 0684190427.
- [148] U. Hashagen: 2006, 'Johann Ludwig Neumann von Margitta (1903-1957). Teil 1: Lehrjahre eines jüdischen Mathematikers während der Zeit der Weimarer Republik'. *Informatik-Spektrum* **29**(2), 133–141.
- [149] U. Hashagen: 2006, 'Johann Ludwig Neumann von Margitta (1903-1957). Teil 2: Ein Privatdozent auf dem Weg von Berlin nach Princeton'. *Informatik-Spektrum* **29**(2), 133–141.
- [150] K. Zuse: 1948, 'Über Theorie und Anwendungen logistischer Rechengерäte'. Technical report, Zuse-Ingenieurbüro.
- [151] K. Zuse: 1948, 'Über den Allgemeinen Plankalkül als Mittel zur Formulierung schematisch-kombinativer Aufgaben'. Technical report ZIA 0242, ZuP 015/001, *Konrad Zuse Internet Archive*. <http://www.zib.de/zuse/>.
- [152] K. Zuse: 1950, 'Bürokratismus und Rechenmaschinen'. Technical report, Dipl.-Ing. K. Zuse Ingenieurbüro und Apparatebau, Berlin.
- [153] K. Zuse: 1958, 'Die Feldrechenmaschine'. Technical report ZuP 015/001, *Konrad Zuse Internet Archive*. <http://www.zib.de/zuse/>.
- [154] K. Zuse: 1936, 'Rechenmaschine'. Patent Z 23 624 IX.
- [155] K. Zuse: 1936, 'Mechanisches Schaltglied'. Patent Z 23 189 IX.

- [156] A. A. Markov: 1906, 'Распространение закона больших чисел на величины, зависящие друг от друга (Распространение закона больших чисел на величины, зависящие друг от друга)'. *Izvestiâ Fiziko-matematičeskogo obšestva pri Kazanskom universitete (Известия Физико-математического общества при Казанском университете)*, series II 15, 135–156.
- [157] A. Kolmogoroff: 1931, 'Über die analytischen Methoden in der Wahrscheinlichkeitsrechnung'. *Mathematische Annalen* 104, 415–458.
- [158] A. Kolmogoroff: 1933, 'Zur Theorie der stetigen zufälligen Prozesse'. *Mathematische Annalen* 108, 149–160.
- [159] A. Kolmogoroff: 1936, 'Zur Theorie der Markoffschen Ketten'. *Mathematische Annalen* 112, 155–160.
- [160] R. Livi and A. Vulpiani: 2003, *The Kolmogorov Legacy in Physics*, No. 636 in Lecture Notes in Physics. Berlin – Heidelberg – New York: Springer. ISBN 3-540-20307-9.
- [161] A. N. Kolmogorov: 1941, 'Рассеяние энергии при локально изотропной турбулентности (Рассеяние энергии при локально изотропной турбулентности)'. *Doklady Akademii Nauk SSSR (Доклады Академии Наук СССР)* 32, 19–21.
- [162] A. N. Kolmogorov: 1954, 'Théorie générale des systèmes dynamiques et mécanique classique'. In: *Proceedings of the International Congress of Mathematicians 1954 in Amsterdam*. Groningen: Noordhoff, pp. 315–333.
- [163] A. N. Kolmogorov: 1965, 'Three approaches to the quantitative definition of information'. *Problems of Information Transmission* 1, 1–11.
- [164] A. N. Kolmogorov: 1940, 'О новом подтверждении законов Менделя (О новом подтверждении законов Менделя)'. *Doklady Akademii Nauk SSSR (Доклады Академии Наук СССР)* 27(1), 37–41.
- [165] T. D. Lysenko: 1940, 'По поводу статьи академика А. Н. Колмогорова (По поводу статьи академика А. Н. Колмогорова)'. *Doklady Akademii Nauk SSSR (Доклады Академии Наук СССР)* 28(9), 832–833.
- [166] F. Sánchez Garduño: 2002, 'Kolmogorov y la biología teórica'. In: F. Sánchez Garduño, P. Miramontes, and J. L. Gutiérrez Sánchez (eds.): *Clásicos de la biología matemática*. México D. F. – Buenos Aires: siglo xxi. ISBN 968-23-2361-4.
- [167] A. N. Čirâev and N. G. Himčenko: 2006, *Kolmogorov v vospominaniâh učenikov (Колмогоров в воспоминаниях учеников)*. Moscow: МСНМО (МЦНМО). ISBN 5-94057-198-0.
- [168] A. Einstein: 1939. Letter to Franklin D. Roosevelt.
- [169] C. F. von Weizsäcker: 1935, 'Zur Theorie der Kernmassen'. *Zeitschrift für Physik* 96, 431–458.
- [170] T. Mayer-Kuckuck: 1970, *Physik der Atomkerne*. Stuttgart: B. G. Teubner.

- [171] M. Volmer and A. Weber: 1926, 'Keimbildung in übersättigten Gebilden'. *Zeitschrift für physikalische Chemie (Leipzig)* **119**, 277–301.
- [172] L. Farkas: 1927, 'Keimbildungsgeschwindigkeit in übersättigten Dämpfen'. *Zeitschrift für physikalische Chemie (Leipzig)* **125**, 236.
- [173] F. Haber: 1922, 'Über amorphe Niederschläge und krystallisierte Sole'. *Berichte der Deutschen Chemischen Gesellschaft B* **55**, 1717–1733.
- [174] R. C. Tolman: 1949, 'The effect of droplet size on surface tension'. *The Journal of Chemical Physics* **17**(3), 333–337.
- [175] G. Jackson: 2010. Private communication.
- [176] C. F. von Weizsäcker: 1957, *Die Verantwortung der Wissenschaft im Atomzeitalter*. Göttingen: Vandenhoeck & Ruprecht. ISBN 3-525-33130-4.
- [177] Presse- und Informationsamt der Bundesregierung: 1982, 'Porträt Carl Friedrich Freiherr von Weizsäcker'. E. Reineke (photographer), Bundesarchiv (signature B 145 Bild-F063257-0006).
- [178] H. F. Zacher: 2007, *Jahresbericht der Max-Planck-Gesellschaft 2007 – Beilage Personalien*, pp. 23–27. Berlin: Max-Planck-Gesellschaft.
- [179] C. F. von Weizsäcker: 1933, 'Durchgang schneller Korpuskularstrahlen durch ein Ferromagnetikum'. *Annalen der Physik* **409**(8), 869–896.
- [180] S. M. Ulam: 1977, *The Scottish Book: A collection of problems*. Los Alamos: National Technical Information. ASIN B002SG5F72. The original *Księga Szkocka* was kept by *Banach* and is now available in Polish and English at <http://banach.univ.gda.pl/e-scottish-book.html>.
- [181] N. Metropolis and S. Ulam: 1949, 'The Monte Carlo method'. *Journal of the American Statistical Association* **44**(247), 335–341.
- [182] E. Fermi, J. Pasta, and S. Ulam: 1955, 'Studies of nonlinear problems'. Technical report LA-1940, Los Alamos National Laboratory, Los Alamos, New Mexico.
- [183] H. Reiss: 1952, 'Theory of the liquid drop model'. *Industrial and Engineering Chemistry* **44**(6), 1284–1288.
- [184] R. H. H. amd Robert McGraw and R. Strey: 2001, 'Biography of Howard Reiss'. *Journal of Physical Chemistry B* **105**(47), 11533–11536.
- [185] J. E. Verschaffelt: 1936. *Bulletin de l'Académie Royale de Belgique, classe de sciences* **22**(4), 373–390.
- [186] E. A. Guggenheim: 1940, 'The thermodynamics of interfaces in systems of several components'. *Transactions of the Faraday Society* **35**, 397–412.
- [187] R. C. Tolman: 1948, 'Consideration of the Gibbs theory of surface tension'. *The Journal of Chemical Physics* **16**(8), 758–774.

- [188] J. G. Kirkwood and F. P. Buff: 1949, 'The statistical mechanical theory of surface tension'. *The Journal of Chemical Physics* **17**(3), 338–343.
- [189] J. H. Irving and J. G. Kirkwood: 1950, 'The statistical mechanical theory of transport processes. 4. The equations of hydrodynamics'. *The Journal of Chemical Physics* **18**(6), 817–829.
- [190] S. Kondo: 1956, 'Thermodynamical fundamental equation for spherical interface'. *The Journal of Chemical Physics* **25**(4), 662–669.
- [191] H. Reiss: 1952, 'The statistical mechanical theory of irreversible condensation. I'. *The Journal of Chemical Physics* **20**(8), 1216–1227. Erratum: 1953, *The Journal of Chemical Physics* **21**(7): 1312.
- [192] H. Reiss: 1950, 'The kinetics of phase transitions in binary systems'. *The Journal of Chemical Physics* **18**(9), 840–848.
- [193] L. Monchick and H. Reiss: 1954, 'Studies of evaporation of small drops'. *The Journal of Chemical Physics* **22**(5), 831–836.
- [194] H. Reiss and S. W. Mayer: 1961, 'Theory of the surface tension of molten salts'. *The Journal of Chemical Physics* **34**(6), 2001–2003.
- [195] H. Reiss and S. W. Mayer: 1961, 'Law of corresponding states for fused salts'. *The Journal of Chemical Physics* **35**(3), 820–826.
- [196] H. Reiss and R. K. Bowles: 2000, 'Simulation of nanoscale density fluctuations'. *The Journal of Chemical Physics* **113**(19), 8615–8630.
- [197] P. Schaaf, B. Senger, J.-C. Voegel, R. K. Bowles, and H. Reiss: 2001, 'Simulative determination of kinetic coefficients for nucleation rates'. *The Journal of Chemical Physics* **114**(18), 8091–8104.
- [198] D. Reguera, R. K. Bowles, Y. Djikaev, and H. Reiss: 2003, 'Phase transitions in systems small enough to be clusters'. *The Journal of Chemical Physics* **118**(1), 340–353.
- [199] H. Reiss: 2001, 'Autobiographical Anecdotes'. *Journal of Physical Chemistry B* **105**(47), 11537–11541.
- [200] P. Liddy and P. Rutherford: 2001, 'Radiation survey of the Downey facility'. Engineering product document RS-00019, The Boeing Company.
- [201] J. L. Bromberg: 1999, *NASA and the space industry*, New Series in NASA History. Baltimore: Johns Hopkins University Press. ISBN 0-8018-6532-8.
- [202] H. Reiss: 1965, *Methods of thermodynamics*. New York: Blaisdell.
- [203] H. C. Andersen: 1980, 'Molecular dynamics simulations at constant pressure and/or temperature'. *The Journal of Chemical Physics* **72**(4), 2384–2393.

- [204] A. Lotfi: 1993, *Molekular-dynamische Simulationen an Fluiden: Phasengleichgewicht und Verdampfung*, No. 335 in Fortschritt-Berichte, Reihe 3: Verfahrenstechnik. Düsseldorf: VDI. ISBN 3-18-143503, Ph.D. thesis, Ruhr-Universität Bochum, Institut für Thermo- und Fluid-dynamik.
- [205] N. Metropolis, A. W. Rosenbluth, M. N. Rosenbluth, A. N. Teller, and E. Teller: 1953, 'Equation of state calculations by fast computing machines'. *The Journal of Chemical Physics* **21**(6), 1087–1092.
- [206] G. M. Torrie and J. P. Valleau: 1977, 'Nonphysical sampling distributions in Monte Carlo free-energy estimation: Umbrella sampling'. *Journal of Computational Physics* **23**(2), 187–199.
- [207] C. Valeriani, E. Sanz, and D. Frenkel: 2005, 'Rate of homogeneous crystal nucleation in molten NaCl'. *The Journal of Chemical Physics* **122**, 194501.
- [208] H. Wang, H. Gould, and W. Klein: 2007, 'Homogeneous and heterogeneous nucleation of Lennard-Jones liquids'. *Physical Review E* **76**, 031604.
- [209] B. J. Block, S. K. Das, M. Oettel, P. Virnau, and K. Binder: 2010, 'Curvature dependence of surface free energy of liquid drops and bubbles: A simulation study'. Preprint arXiv:1009.0609v1 [cond-mat.soft]. Submitted to J. Chem. Phys.
- [210] K.-C. Ng, J. P. Valleau, G. M. Torrie, and G. N. Patey: 1979, 'Liquid-vapour co-existence of dipolar hard spheres'. *Molecular Physics* **38**(3), 781–788.
- [211] I. S. Graham and J. P. Valleau: 1990, 'A Monte-Carlo study of the coexistence region of the restricted primitive model'. *Journal of Physical Chemistry* **94**(20), 7894–7898.
- [212] I. R. McDonald and K. Singer: 1967, 'Calculation of thermodynamic properties of liquid argon from Lennard-Jones parameters by a Monte Carlo method'. *Discussions of the Faraday Society* **43**, 40–49.
- [213] A. Z. Panagiotopoulos: 1987, 'Direct determination of phase coexistence properties of fluids by Monte Carlo simulation in a new ensemble'. *Molecular Physics* **61**(4), 813–826.
- [214] D. Möller and J. Fischer: 1990, 'Vapour liquid equilibrium of a pure fluid from test particle method in combination with NpT molecular dynamics simulations'. *Molecular Physics* **69**(3), 463–473.
- [215] J. Vrabec and J. Fischer: 1995, 'Vapour liquid equilibria of mixtures from the NpT plus test particle method'. *Molecular Physics* **85**(4), 781–792.
- [216] J. Vrabec: 1996, *Vorhersage thermodynamischer Stoffdaten durch molekulare Simulation*, No. 455 in Fortschritt-Berichte, Reihe 3: Verfahrenstechnik. Düsseldorf: VDI. Ph.D. thesis, Ruhr-Universität Bochum, Institut für Thermo- und Fluid-dynamik.
- [217] J. Vrabec and H. Hasse: 2002, 'Grand Equilibrium: Vapour-liquid equilibria by a new molecular simulation method'. *Molecular Physics* **100**(21), 3375–3383.
- [218] D. P. Landau and K. Binder: 2009, *A guide to Monte Carlo simulation in statistical physics*. Cambridge University Press. Third edition. ISBN 978-0-521-76848-1.

- [219] W. Krauth and O. Pluchery: 1994, 'A rapid dynamical Monte Carlo algorithm for glassy systems'. *Journal of Physics A* **27**, L715–L720.
- [220] G. Rutkai and T. Kristóf: 2010, 'Dynamic Monte Carlo simulation in mixtures'. *The Journal of Chemical Physics* **132**, 104107.
- [221] O. Redlich and J. N. S. Kwong: 1949, 'On the thermodynamics of solutions. V. An equation of state. Fugacities of gaseous solutions'. *Chemical Reviews* **44**(1), 233–244.
- [222] G. Soave: 1972, 'Equilibrium constants from a modified Redlich-Kwong equation of state'. *Chemical Engineering Science* **27**, 1197–1203.
- [223] K. S. Pitzer: 1939, 'Corresponding states for perfect liquids'. *The Journal of Chemical Physics* **7**(8), 583–590.
- [224] P. G. Debenedetti: 1996, *Metastable liquids: Concepts and principles*. Princeton, NJ: Princeton University Press. ISBN 0-691-08595-1.
- [225] H. J. C. Berendsen, J. P. M. Postma, W. F. van Gunsteren, A. Dinola, and J. R. Haak: 1984, 'Molecular-dynamics with coupling to an external bath'. *The Journal of Chemical Physics* **81**(8), 3684–3690.
- [226] S. Nosé: 1984, 'A molecular dynamics method for simulations in the canonical ensemble'. *Molecular Physics* **52**(2), 255–268.
- [227] W. G. Hoover: 1985, 'Canonical dynamics: Equilibrium phase-space distributions'. *Physical Review A* **31**(3), 1695–1697.
- [228] B. L. Holian, A. F. Voter, and R. Ravelo: 1995, 'Thermostatted molecular dynamics: How to avoid the Toda demon hidden in Nosé-Hoover dynamics'. *Physical Review E* **52**(3), 2338–2347.
- [229] M. M. Cielinski: 1985, 'Computer simulation of the Lennard-Jones fluid in the grand canonical ensemble'. M. Sc. thesis, Department of Chemistry, University of Maine, Orono.
- [230] M. Lupkowski and F. van Swol: 1991, 'Ultrathin films under shear'. *The Journal of Chemical Physics* **95**(3), 1995–1998.
- [231] T. C. Germann and K. Kadau: 2008, 'Trillion-atom molecular dynamics becomes a reality'. *International Journal of Modern Physics C* **19**(9), 1315–1319.
- [232] M. Bernreuther and J. Vrabec: 2006, 'Molecular simulation of fluids with short range potentials'. In: M. Resch et al. (eds.): *High Performance Computing on Vector Systems*. Berlin – Heidelberg – New York: Springer, pp. 187–195. ISBN 3-540-29124-5.
- [233] M. Buchholz, H.-J. Bungartz, and J. Vrabec: 2010, 'Software design for a highly parallel molecular dynamics simulation framework in chemical engineering'. *Journal of Computational Science*. Submitted.
- [234] S. Deublein, B. Eckl, J. Stoll, S. V. Lishchuk, G. Guevara Carrión, C. W. Glass, T. Merker, M. Bernreuther, H. Hasse, and J. Vrabec: 2010, '*ms2*: A molecular simulation tool for thermodynamic properties'. Technical report, Boltzmann-Zuse Society of Computational Molecular Engineering (BZS).

- [235] A. Laaksonen, V. Talanquer, and D. W. Oxtoby: 1995, 'Nucleation: Measurements, theory, and atmospheric applications'. *Annual Review of Physical Chemistry* **46**, 489–524.
- [236] S.-H. Lee, J. M. Reeves, J. C. Wilson, D. E. Hunton, A. A. Viggiano, T. M. Miller, J. O. Ballenthin, and L. R. Lait: 2003, 'Particle formation by ion nucleation in the upper troposphere and lower stratosphere'. *Science* **301**(5641), 1886–1889.
- [237] R. G. Harrison and M. H. P. Ambaum: 2008, 'Enhancement of cloud formation by droplet charging'. *Proceedings of the Royal Society A* **464**, 2561–2573.
- [238] M. Kulmala: 2003, 'How particles nucleate and grow'. *Science* **302**(5647), 1000–1001.
- [239] R. von Helmholtz: 1886, 'Untersuchungen über Dämpfe und Nebel, besonders über solche von Lösungen'. *Annalen der Physik* **263**(4), 508–543.
- [240] C. T. R. Wilson: 1897, 'Condensation of water vapour in the presence of dust-free air and other gases'. *Philosophical Transactions of the Royal Society A* **189**, 265–307.
- [241] C. F. Powell: 1928, 'Condensation phenomena at different temperatures'. *Proceedings of the Royal Society of London A* **119**, 553–577.
- [242] M. Volmer and H. Flood: 1934. *Zeitschrift für physikalische Chemie (Leipzig) A* **170**, 273.
- [243] T. Pierce, P. M. Sherman, and D. D. McBride: 1971, 'Condensation of argon in a supersonic stream'. *Astronautica Acta* **16**, 1–4.
- [244] V. A. Shneidman: 2005, 'Violation of adiabatic scaling in the distribution of particles nucleated in a rapid quench'. *Physical Review Letters* **75**(25), 4634–4637.
- [245] M. Mecke, A. Müller, J. Winkelmann, J. Vrabec, J. Fischer, R. Span, and W. Wagner: 1996, 'An accurate van der Waals-type equation of state for the Lennard-Jones fluid'. *International Journal of Thermophysics* **17**(2), 404. Erratum: 1998, *International Journal of Thermophysics* **19**(5): 1493.
- [246] A. Linhart, C.-C. Chen, J. Vrabec, and H. Hasse: 2005, 'Thermal properties of the metastable superaturated vapor of the Lennard-Jones fluid'. *The Journal of Chemical Physics* **122**, 144506.
- [247] C. Nie, J. Gend, and W. H. Marlow: 2007, 'The free energy of the supersaturated vapor via restricted ensemble simulations'. *The Journal of Chemical Physics* **127**, 154505.
- [248] C. Nie, J. Gend, and W. H. Marlow: 2008, 'Study of thermal properties of the metastable supersaturated vapor with the restricted ensemble'. *Physica A* **387**, 1433–1438.
- [249] V. G. Baidakov, S. P. Protsenko, and Z. R. Kozlova: 2008, 'Thermal and caloric equations of state for stable and metastable Lennard-Jones fluids: I. Molecular-dynamics simulations'. *Fluid Phase Equilibria* **263**(1), 55–63.
- [250] J. E. McDonald: 1963, 'Homogeneous nucleation of vapor condensation. II. Kinetic aspects'. *American Journal of Physics* **31**, 31–41.

- [251] M. Rao, B. J. Berne, and M. H. Kalos: 1978, 'Computer simulation of the nucleation and thermodynamics of microclusters'. *The Journal of Chemical Physics* **68**(4), 1325–1336.
- [252] J. H. ter Horst and D. Kashchiev: 2003, 'Determination of the nucleus size from the growth probability of clusters'. *The Journal of Chemical Physics* **119**(4), 2241–2246.
- [253] I. J. Ford: 2004, 'Statistical mechanics of nucleation: A review'. *Proceedings of the Institution of Mechanical Engineers, Part C: Journal of Mechanical Engineering Science* **218**, 883–899.
- [254] J. Wedekind, A.-P. Hyvärinen, D. Brus, and D. Reguera: 2008, 'Unraveling the «Pressure Effect» in nucleation'. *Physical Review Letters* **101**, 125703.
- [255] K. Yasuoka and M. Matsumoto: 1998, 'Molecular dynamics of homogeneous nucleation in the vapor phase. I. Lennard-Jones fluid'. *The Journal of Chemical Physics* **109**(19), 8451–8462.
- [256] T. L. Hill: 1964, *Thermodynamics of small systems*. New York: W. A. Benjamin. Dover (1994) republication, ISBN 0-486-68109-2.
- [257] V. I. Kalikmanov and M. E. H. van Dongen: 1993, 'Self-consistent cluster approach to the homogeneous kinetic nucleation theory'. *Physical Review E* **47**(5), 3532–3539.
- [258] M. Blander and J. L. Katz: 1972, 'The thermodynamics of cluster formation in nucleation theory'. *Journal of Statistical Physics* **4**(1), 55–59.
- [259] H. R. Hertz: 1882, 'Ueber die Verdunstung der Flüssigkeiten, insbesondere des Quecksilbers, im luftleeren Raume'. *Annalen der Physik und Chemie (Leipzig)* **17**(10), 177–200.
- [260] A. Kantrowitz: 1951, 'Nucleation in very rapid vapor expansions'. *The Journal of Chemical Physics* **19**(9), 1097–1100.
- [261] J. Feder, K. C. Russell, J. Lothe, and G. M. Pound: 1966, 'Homogeneous nucleation and growth of droplets in vapours'. *Advances in Physics* **15**(1), 111–178.
- [262] D. Kashchiev: 2000, *Nucleation. Basic Theory with Applications*. Oxford: Butterworth-Heinemann. ISBN 0-7506-4682.
- [263] K. Schaber: 2005, 'Skriptum Thermodynamik disperser Systeme'. Technical report, Institut für Technische Thermodynamik und Kältetechnik, Universität Karlsruhe (TH).
- [264] Â. B. Zel'dovič: 1942, 'К теории образования новой фазы. Кавитация (К теории образования новой фазы. Кавитация)'. *Žurnal Èksperimental'noj i Teoretičeskoj Fiziki (Журнал Экспериментальной и Теоретической Физики)* **12**, 525–538.
- [265] J. A. Fisk, M. M. Rudek, J. L. Katz, D. Beiersdorf, and H. Uchtmann: 1998, 'The homogeneous nucleation of cesium vapor'. *Atmospheric Research* **46**, 211–222.
- [266] F. Römer and T. Kraska: 2007, 'Homogeneous nucleation and growth in supersaturated zinc vapor investigated by molecular dynamics simulations'. *The Journal of Chemical Physics* **127**, 234509.

- [267] B. Novakowski and E. Ruckenstein: 1990, 'A kinetic approach to the theory of nucleation in gases'. *The Journal of Chemical Physics* **94**(2), 1397–1402.
- [268] J. Merikanto, E. Zapadinsky, A. Lauri, and H. Vehkamäki: 2007, 'Origin of the failure of classical nucleation theory: Incorrect description of the smallest clusters'. *Physical Review Letters* **98**, 145702.
- [269] A. Laaksonen, I. J. Ford, and M. Kulmala: 1994, 'Revised parametrization of the Dillmann-Meier theory of homogeneous nucleation'. *Physical Review E* **49**(6), 5517–5524.
- [270] M. E. Fisher: 1967, 'Theory of condensation and critical point'. *Physics (New York)* **3**(5), 255.
- [271] J. R. Morris, C. Z. Wang, K. M. Ho, and C. T. Chan: 1994, 'Melting line of aluminum from simulations of coexisting phases'. *Physical Review B* **49**(5), 3109–3115.
- [272] M. Kulmala, A. Lauri, H. Vehkamäki, A. Laaksonen, D. Petersen, and P. E. Wagner: 2001, 'Strange predictions by binary heterogeneous nucleation theory compared with a quantitative experiment'. *Journal of Physical Chemistry B* **105**(47), 11800–11808.
- [273] D. Reguera and H. Reiss: 2004, 'Fusion of the extended modified liquid drop model for nucleation and dynamical nucleation theory'. *Physical Review Letters* **93**, 165701.
- [274] R. Zandi, D. Reguera, and H. Reiss: 2006, 'Nucleation rates in a new phenomenological model'. *Journal of Physical Chemistry B* **110**(44), 22251–22260.
- [275] V. V. Slezov and J. W. P. Schmelzer: 1998, 'Comments on nucleation theory'. *Journal of Physics and Chemistry of Solids* **59**(9), 1507–1519.
- [276] R. Lovett: 2007, 'Describing phase coexistence in systems with small phases'. *Reports on Progress in Physics* **70**, 195–218.
- [277] J. K. Lee, J. A. Barker, and F. F. Abraham: 1973, 'Theory and Monte Carlo simulation of physical clusters in the imperfect vapor'. *The Journal of Chemical Physics* **58**(8), 3166–3180.
- [278] A. I. Rusanov and E. N. Brodskaya: 1977, 'The molecular dynamics simulation of a small drop'. *Journal of Colloid and Interface Science* **62**(3), 542–555.
- [279] M. Salonen, I. Napari, and H. Vehkamäki: 2007, 'Molecular dynamics simulation of atomic clusters in equilibrium with a vapour'. *Molecular Simulation* **33**(3), 245–251.
- [280] D. I. Zhukovitskii: 1995, 'Molecular dynamics study of cluster evolution in supersaturated vapor'. *The Journal of Chemical Physics* **103**(21), 9401–9407.
- [281] S. Sumardiono and J. Fischer: 2005, 'Molecular dynamics simulations of mixture droplet evaporation'. In: *Proceedings of Eurotherm Seminar 77 in Parma, June 2005 – Heat and Mass Transfer in Food Processing*.
- [282] F. P. Buff: 1955, 'Spherical interface. II. Molecular theory'. *The Journal of Chemical Physics* **23**(3), 419–427.

- [283] S. Kondo: 1955, 'A statistical-mechanical theory of surface tension of curved surface layer'. *Journal of the Physical Society of Japan* **10**(5), 381–386.
- [284] F. P. Buff: 1951, 'Spherical interface. I. Thermodynamics'. *The Journal of Chemical Physics* **19**(12), 1591–1594.
- [285] D. W. Oxtoby and D. Kashchiev: 1994, 'A general relation between the nucleation work and the size of the nucleus in multicomponent nucleation'. *The Journal of Chemical Physics* **100**(10), 7665–7671.
- [286] I. J. Ford: 1997, 'Nucleation theorems, the statistical mechanics of molecular clusters, and a revision of classical nucleation theory'. *Physical Review E* **56**(5), 5615–5629.
- [287] J. W. P. Schmelzer: 2001, 'Comments on the nucleation theorem'. *Journal of Colloid and Interface Science* **242**(2), 354–372.
- [288] J. W. P. Schmelzer: 2003, 'Some additional comments on the nucleation theorem'. *Russian Journal of Physical Chemistry* **77**, S143–S145.
- [289] H. Vehkamäki: 2006, *Classical Nucleation Theory in Multicomponent Systems*. Berlin – Heidelberg – New York: Springer. ISBN 3-540-29213-6.
- [290] J. Wedekind, J. Wölk, D. Reguera, and R. Strey: 2007, 'Nucleation rate isotherms from molecular dynamics simulations'. *The Journal of Chemical Physics* **127**, 154515.
- [291] P. R. ten Wolde and D. Frenkel: 1998, 'Computer simulation study of gas-liquid nucleation in a Lennard-Jones system'. *The Journal of Chemical Physics* **109**, 9901–9918.
- [292] I. Napari, J. Julin, and H. Vehkamäki: 2009, 'Cluster sizes in direct and indirect molecular dynamics simulations'. *The Journal of Chemical Physics* **131**, 244511.
- [293] S. M. Thompson, K. E. Gubbins, J. P. R. B. Walton, R. A. R. Chantry, and J. S. Rowlinson: 1984, 'A molecular dynamics study of liquid drops'. *The Journal of Chemical Physics* **81**(1), 530–542.
- [294] K. Koga, X. C. Zeng, and A. K. Shchekin: 1998, 'Validity of Tolman's equation: How large should a droplet be?'. *The Journal of Chemical Physics* **109**(10), 4063–4070.
- [295] T. V. Bykov and A. K. Šëkin: 1999, 'Poverhnostnoe, natâzhenie, dlina Tolmana i êf-fektivnaâ konstanta žestkosti poverhnostnogo sloâ kapli s bol'shim radiusom krivizny (По-верхностное, натяжение, длина Толмана и эффективная константа жесткости по-верхностного слоя капли с большим радиусом кривизны)'. *Neorganičeskie Materialy (Неорганические Материалы)* **35**(6), 759–763.
- [296] I. Napari and A. Laaksonen: 2007, 'Surface tension and scaling of critical nuclei in diatomic and triatomic fluids'. *The Journal of Chemical Physics* **126**, 134503.
- [297] J. R. Henderson and J. Lekner: 1978, 'Surface oscillations and the surface thickness of classical and quantum droplets'. *Molecular Physics* **36**(3), 781–789.
- [298] K. Binder: 1982, 'Monte Carlo calculation of the surface tension for two- and three-dimensional lattice-gas models'. *Physical Review A* **25**(3), 1699–1709.

- [299] S. Brunauer: 1943, *The adsorption of gases and vapors. Vol. I: Physical adsorption*. Princeton University Press. ISBN 1406750301.
- [300] L. G. Harriman: 1989, 'Sorbents and desiccants'. In: R. A. Parsons (ed.): *1989 ASHRAE Handbook – Fundamentals*. pp. 19.1–19.6. ISBN 9-910110-57-3.
- [301] W. Steele: 1993, 'Molecular interactions for physical adsorption'. *Chemical Reviews* **93**(7), 2355–2378.
- [302] I. Langmuir: 1916, 'The constitution and fundamental properties of solids and liquids. Part I. Solids'. *Journal of the American Chemical Society* **38**, 2221–2295.
- [303] S. Brunauer, P. H. Emmett, and E. Teller: 1938, 'Adsorption of gases in multimolecular layers'. *Journal of the American Chemical Society* **60**, 309–319.
- [304] T. Young: 1805, 'An essay on the cohesion of fluids'. *Philosophical Transactions of the Royal Society* **95**, 65–87.
- [305] G. F. Teletzke, L. E. Scriven, and H. T. Davis: 1982, 'Wetting transitions. II. First order or second order?'. *The Journal of Chemical Physics* **78**(3), 1431–1439.
- [306] S. Sokołowski and J. Fischer: 1993, '«Liquid-vapour» density profiles for fluids in pores from density functional theory'. *Journal of the Chemical Society, Faraday Transactions* **89**(5), 789–794.
- [307] N. Giovambattista, P. J. Rosky, and P. G. Debenedetti: 2006, 'Effect of pressure on the phase behavior and structure of water confined between nanoscale hydrophobic and hydrophilic plates'. *Physical Review E* **73**, 041604.
- [308] J. Harting, C. Kunert, and H. J. Herrmann: 2006, 'Lattice Boltzmann simulations of apparent slip in hydrophobic microchannels'. *Europhysics Letters* **75**(2), 328–334.
- [309] T. J. Spencer, A. P. Hollis, I. Halliday, and C. M. Care: 2009, 'Dynamic wetting for continuum hydrodynamics with multi-component lattice Boltzmann equation simulation method'. In: *2nd Micro and Nano Flows Conference Programme: MNF2009*. London: Brunel University. ISBN 978-1902316734.
- [310] F. A. Cotton, G. Wilkinson, and P. L. Gaus: 1994, *Basic Inorganic Chemistry*. Chichester: Wiley.
- [311] E. Kozak and S. Sokołowski: 1991, 'Wetting transitions and capillary condensation in slit-like pores'. *Journal of the Chemical Society: Faraday Transactions* **87**(20), 3415–3422.
- [312] K. Bucior, L. Yelash, and K. Binder: 2009, 'Molecular-dynamics simulation of evaporation processes of fluid bridges confined in slitlike pores'. *Physical Review E* **79**, 031604.
- [313] N. Giovambattista, P. G. Debenedetti, and P. J. Rosky: 2007, 'Effect of surface polarity on water contact angle and interfacial hydration structure'. *Journal of Physical Chemistry B* **111**, 9581–9587.
- [314] J. A. van Meel, A. J. Page, R. P. Sear, and D. Frenkel: 2008, 'Two-step vapor-crystal nucleation close below triple point'. *The Journal of Chemical Physics* **129**, 204505.

- [315] *M. E. Fisher* and *H. Nakanishi*: 1981, 'Scaling theory for the criticality of fluids between plates'. *The Journal of Chemical Physics* **75**(12), 5857–5863.
- [316] *G. J. Zarragoicoechea* and *V. A. Kuz*: 2002, 'van der Waals equation of state for a fluid in a nanopore'. *Physical Review E* **65**, 021110.
- [317] *L. Sałamacha*, *A. Patrykiewicz*, *S. Sokołowski*, and *K. Binder*: 2005, 'The structure of fluids confined in crystalline slitlike nanoscopic pores'. *The Journal of Chemical Physics* **122**, 074703.
- [318] *J. W. Cahn*: 1977, 'Critical point wetting'. *The Journal of Chemical Physics* **66**(8), 3667–3672.
- [319] *P. A. Monson*: 2008, 'Contact angles, pore condensation, and hysteresis: Insights from a simple molecular model'. *Langmuir* **24**, 12295–12302.
- [320] *K. Iland*: 2004, 'Experimente zur homogenen Keimbildung von Argon und Stickstoff'. Dissertation, Institut für Physikalische Chemie, Universität Köln, Göttingen. ISBN 3-86537-135-3.
- [321] *K. Yasuoka* and *M. Matsumoto*: 1998, 'Molecular dynamics of homogeneous nucleation in the vapor phase. II. Water'. *The Journal of Chemical Physics* **109**(19), 8463–8470.
- [322] *K. K. Tanaka*, *K. Kawamura*, *H. Tanaka*, and *K. Nakazawa*: 2005, 'Tests of the homogeneous nucleation theory with molecular-dynamics simulations. I. Lennard-Jones molecules'. *The Journal of Chemical Physics* **122**, 184514.
- [323] *T. Kraska*: 2006, 'Molecular-dynamics simulation of argon nucleation from supersaturated vapor in the NVE ensemble'. *The Journal of Chemical Physics* **124**, 054507.
- [324] *H. Matsubara*, *T. Koishi*, *T. Ebisuzaki*, and *K. Yasuoka*: 2007, 'Extended study of molecular dynamics simulation of homogeneous vapor-liquid nucleation of water'. *The Journal of Chemical Physics* **127**, 214507.
- [325] *N. Lümme* and *B. Kvamme*: 2008, 'Determination of nucleation rates of FeCl₂ in supercritical water by molecular dynamics simulations'. *Journal of Supercritical Fluids* **47**, 270–280.
- [326] *F. Römer* and *T. Kraska*: 2009, 'Molecular dynamics simulation of naphthalene particle formation by rapid expansion of a supercritical solution'. *Journal of Physical Chemistry C* **113**, 19028–19038.
- [327] *J. Wedekind*, *D. Reguera*, and *R. Strey*: 2006, 'Finite-size effects in simulation of nucleation'. *The Journal of Chemical Physics* **125**, 214505.
- [328] *J. Wedekind*, *R. Strey*, and *D. Reguera*: 2007, 'New method to analyze simulations of activated processes'. *The Journal of Chemical Physics* **126**, 134103.
- [329] *G. M. White*: 1969, 'Steady-state random walks with application to homogeneous nucleation'. *The Journal of Chemical Physics* **50**(11), 4672–4678.

- [330] W. Christen, K. Rademann, and U. Even: 2006, 'Efficient cooling in supersonic jet expansions of supercritical fluids: CO and CO₂'. *The Journal of Chemical Physics* **125**, 174307.
- [331] W. Christen and K. Rademann, 'Probing free jet expansions of supercritical fluids'. *Physica Scripta* **80**, 048127.
- [332] R. A. Zahoransky, J. Höschele, and J. Steinwandel: 1995, 'Formation of argon clusters by homogeneous nucleation in supersonic shock tube flow'. *The Journal of Chemical Physics* **103**(20), 9038–9044.
- [333] R. A. Zahoransky, J. Höschele, and J. Steinwandel: 1999, 'Homogeneous nucleation of argon in an unsteady hypersonic flow field'. *The Journal of Chemical Physics* **110**(17), 8842–8843.
- [334] K. Iland, J. Wölk, R. Strey, and D. Kashchiev: 2007, 'Argon nucleation in a cryogenic nucleation pulse chamber'. *The Journal of Chemical Physics* **127**, 154506.
- [335] H. L. Frisch and F. C. Collins: 1952, 'Diffusional processes in the growth of aerosol particles'. *The Journal of Chemical Physics* **20**(11), 1797–1803.
- [336] G. Chkonia, J. Wölk, R. Strey, and D. Reguera: 2009, 'Evaluating nucleation rates in direct simulations'. *The Journal of Chemical Physics* **130**, 064505.
- [337] L. Szilard: 1929, 'Über die Entropieverminderung in einem thermodynamischen System bei Eingriffen intelligenter Wesen'. *Zeitschrift für Physik* **53**(11–12), 840–856.
- [338] K. Maruyama, F. Nori, and V. Vedral: 2009, 'Colloquium: The physics of Maxwell's demon and information'. *Reviews of Modern Physics* **81**(1), 1–23.
- [339] W. J. Dunning: 1955, 'Theory of crystal nucleation from vapour, liquid, and solid systems'. In: W. E. Garner (ed.): *Chemistry of the Solid State*. London: Butterworth's Scientific Publications, pp. 159–183. ASIN B0000CJ717.
- [340] J. W. P. Schmelzer, G. Röpke, and F.-P. Ludwig: 1997, 'Nuclear multifragmentation processes and nucleation theory'. *Physical Review C* **55**(4), 1917–1927.
- [341] F. H. Stillinger: 1963, 'Rigorous basis of the Frenkel-Band theory of association equilibrium'. *The Journal of Chemical Physics* **38**(7), 1486–1494.
- [342] S. Toxværd: 2004, 'Molecular dynamics simulation of nucleation'. *Molecular Simulation* **30**, 179–182.
- [343] V. Talanquer: 2007, 'Nucleation of self-associating fluids: free versus activated association'. *Journal of Physical Chemistry B* **111**(13), 3438–3446.
- [344] A. Määttänen, H. Vehkamäki, A. Lauri, S. Merikallio, J. Kauhanen, H. Savijärvi, and M. Kulmala: 2005, 'Nucleation studies in the Martian atmosphere'. *Journal of Geophysical Research E – Planets* **110**, 02002.
- [345] Y.-L. Huang, J. Vrabc, and H. Hasse: 2009, 'Prediction of ternary vapor-liquid equilibria for 33 systems by molecular simulation'. *Fluid Phase Equilibria* **287**, 62–69.

- [346] J. Vrabec, G. K. Kedia, U. Buchhauser, R. Meyer-Pitroff, and H. Hasse: 2009, 'Thermodynamic models for vapor-liquid equilibria of nitrogen + oxygen + carbon dioxide at low temperatures'. *Cryogenics* **49**, 72–79.
- [347] K. Iland, J. Wedekind, J. Wölk, P. E. Wagner, and R. Strey: 2004, 'Homogeneous nucleation rates of 1-pentanol'. *The Journal of Chemical Physics* **121**(24), 12259–12264.
- [348] A.-P. Hyvärinen, D. Brus, V. Ždímal, J. Smolík, M. Kulmala, Y. Viisanen, and H. Lihavainen: 2006, 'The carrier gas pressure effect in a laminar flow diffusion chamber, homogeneous nucleation of *n*-butanol in helium'. *The Journal of Chemical Physics* **124**, 224304. Erratum: 2008, *The Journal of Chemical Physics* **128**: 109901.
- [349] D. Brus, A.-P. Hyvärinen, J. Wedekind, Y. Viisanen, M. Kulmala, V. Ždímal, J. Smolík, and H. Lihavainen: 2008, 'The homogeneous nucleation of 1-pentanol in a laminar flow diffusion chamber: The effect of pressure and kind of carrier gas'. *The Journal of Chemical Physics* **128**, 134312.
- [350] R. Strey and Y. Viisanen: 1993, 'Measurement of the molecular content of binary nuclei. Use of the nucleation rate surface for ethanol-hexanol'. *The Journal of Chemical Physics* **99**(6), 4693–4704.
- [351] Y. Viisanen, R. Strey, A. Laaksonen, and M. Kulmala: 1994, 'Measurement of the molecular content of binary nuclei. 2. Use of the nucleation rate surface for water-ethanol'. *The Journal of Chemical Physics* **100**(8), 6062–6072.
- [352] R. Strey, Y. Viisanen, and P. E. Wagner: 1995, 'Measurement of the molecular content of binary nuclei. 3. Use of the nucleation rate surfaces for the water-*n*-alcohol series'. *The Journal of Chemical Physics* **103**(10), 4333–4345.
- [353] R. B. Nellas, B. Chen, and J. I. Siepmann: 2007, 'Dumbbells and onions in ternary nucleation'. *Physical Chemistry Chemical Physics* **9**, 2779–2781.
- [354] R. Kible: 2006, 'Clusteringalgorithmen zur Keimdetektion in Gasen'. Diplomarbeit Nr. 2449, Institut für Visualisierung und Interaktive Systeme, Universität Stuttgart. Saarbrücken, 2008: VDM Verlag Dr. Müller. ISBN 3-83645-939-6.
- [355] V. G. Baidakov and G. S. Boltachev: 1999, 'Curvature dependence of the surface tension of liquid and vapor nuclei'. *Physical Review E* **59**(1), 469–475.
- [356] V. G. Baidakov, G. S. Boltachev, and J. W. P. Schmelzer: 2000, 'Comparison of different approaches to the determination of the work of critical cluster formation'. *Journal of Colloid and Interface Science* **231**, 312–321.
- [357] M. P. Moody and P. Attard: 2003, 'Curvature-dependent surface tension of a growing droplet'. *Physical Review Letters* **91**(5).
- [358] J. Julin, I. Napari, J. Merikanto, and H. Vehkamäki: 2008, 'Equilibrium sizes and formation energies of small and large Lennard-Jones clusters from molecular dynamics: A consistent comparison to Monte Carlo simulations and density functional theories'. *The Journal of Chemical Physics* **129**, 234506.

Curriculum vitæ

Name	Martin Thomas <i>Horsch</i>
Date of birth	August 13, 1982 in Stuttgart
Nationality	Federal Republic of Germany

Formal qualification	
Date	September 10, 2010
Institution	Universität Paderborn
Degree	Doktor-Ingenieur (Dr.-Ing.)
Grade	1,0 – sehr gut mit Auszeichnung (summa cum laude)
Date	July 13, 2006
Institution	Universität Stuttgart
Degree	Diplom-Informatiker (Dipl.-Inf.)
Grade	1,0 – sehr gut mit Auszeichnung (summa cum laude)
Date	June 27, 2000
Institution	Karls gymnasium Stuttgart
Degree	Abitur
Grade	1,0 – sehr gut (magna cum laude)

Academic affiliation	
Period	October 2010 – present
University, Department	Imperial College London, Chemical Engineering and Technology
Chair	Prof. George <i>Jackson</i> DPhil FRSC CChem
Period	January 2009 – present
University, Department	Universität Paderborn, Maschinenbau
Chair	Prof. Dr.-Ing. <i>Jadran Vrabec</i>
Period	January 2008 – December 2008
University, Department	Universität Stuttgart, Energie-, Verfahrens- und Biotechnik
Chair	Prof. Dr.-Ing. <i>Hans Hasse</i> Dr.-Ing. habil. <i>Jadran Vrabec</i>
Period	August 2006 – December 2007
University, Department	Universität Stuttgart, Maschinenbau
Chair	Prof. Dr.-Ing. <i>Hans Hasse</i>
Period	May 2004 – August 2005
University, Department	Universität Stuttgart, Informatik
Chair	Prof. Dr. rer. nat. <i>Volker Diekert</i> Prof. Dr. <i>Javier Esparza</i>
Period	September 2001 – March 2005
University, Department	Universität Stuttgart, Architektur und Stadtplanung
Chair	Prof. Dr. agr. <i>Giselher Kaule</i>